AD-A075 065 HONEYWELL CORPORATE TECHNOLOGY CENTER BLOOMINGTON MN F/G 20/2
GROWTH OF SINGLE CRYSTAL GALLIUM PHOSPHIDE BY LIQUID PHASE EPIT--ETC(U)
APR 79 P E PETERSEN , R G SCHULZE F33615-77-C-5043
UNCLASSIFIED HR-47108 AFML-TR-79-4049 NL

1 OF 2
AD
AD75065

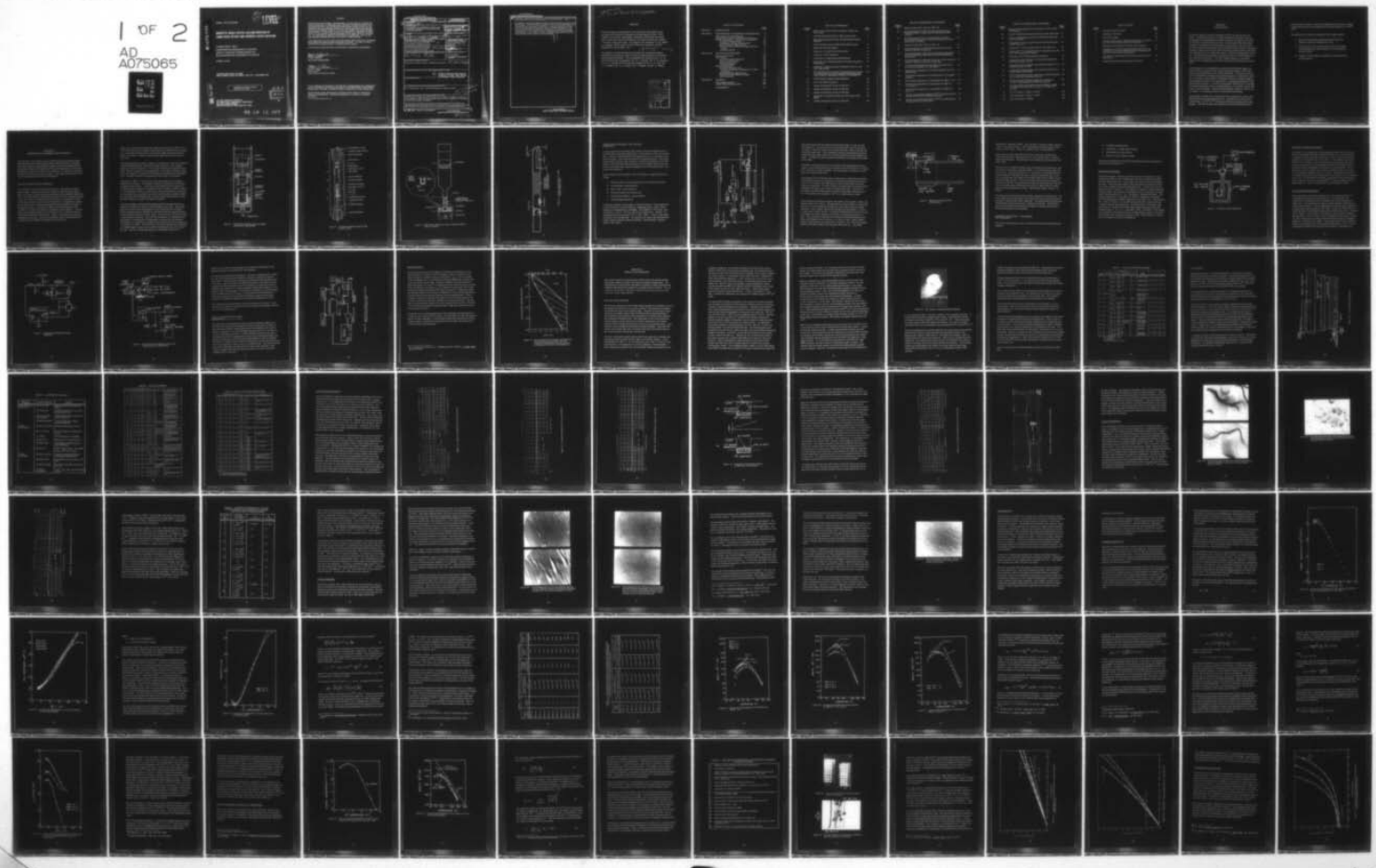

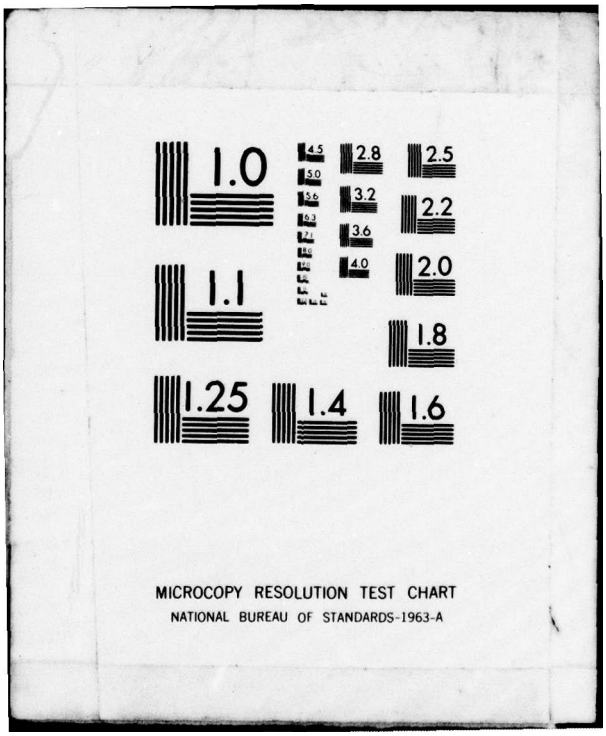
1.0
1.1
1.25
1.4
1.6
1.8
2.0
2.2
2.5
2.8
3.2
3.6
4.0
4.5
5.0
5.6
6.3
7.1
MICROCOPY RESOLUTION TEST CHART
NATIONAL BUREAU OF STANDARDS-1963-A

AFML-TR-79-4049

LEVEL II

GROWTH OF SINGLE CRYSTAL GALLIUM PHOSPHIDE BY LIQUID PHASE EPITAXY AND SYNTHESIS SOLUTE DIFFUSION

HONEYWELL INC.
CORPORATE RESEARCH CENTER
10701 LYNDALE AVENUE SOUTH
BLOOMINGTON, MINNESOTA 55420

APRIL 1979

TECHNICAL REPORT AFML-TR-79-4049
FINAL TECHNICAL REPORT FOR PERIOD 1 APRIL 1977 – 30 SEPTEMBER 1978

APPROVED FOR PUBLIC RELEASE, DISTRIBUTION LIMITED.

AIR FORCE MATERIALS LABORATORY
AIR FORCE WRIGHT AERONAUTICAL LABORATORIES
AIR FORCE SYSTEMS COMMAND
WRIGHT-PATTERSON AIR FORCE BASE, OHIO 45433

NOTICE

When Government drawings, specifications, or other data are used for any purpose other than in connection with a definitely related Government procurement operation, the United States Government thereby incurs no responsibility nor any obligation whatsoever; and the fact that the Government may have formulated, furnished, or in any way supplied the said drawings, specifications, or other data, is not to be regarded by implication or otherwise as in any manner licensing the holder or any other person or corporation, or conveying any rights or permission to manufacture, use, or sell any patented invention that may in any way be related thereto.

This report has been reviewed by the Information Office (OI) and is releasable to the National Technical Information Service (NTIS). At NTIS, it will be available to the general public, including foreign nations.

This technical report has been reviewed and is approved for publication.

Robert Hickmott

ROBERT L. HICKMOTT
Project Engineer

FOR THE COMMANDER

Melvin C. Ohmer

MELVIN C. OHMER
Acting Chief
Laser & Optical Materials Branch

If your address has changed, if you wish to be removed from our mailing list, or if the addressee is no longer employed by your organization please notify AFML/LPO, W-PAFB, OH 45433 to help us maintain a current mailing list.

Copies of this report should not be returned unless return is required by security considerations, contractual obligations, or notice on a specific document.

AIR FORCE/56780/4 September 1979 — 100

UNCLASSIFIED

SECURITY CLASSIFICATION OF THIS PAGE (When Data Entered)

REPORT DOCUMENTATION PAGE	READ INSTRUCTIONS BEFORE COMPLETING FORM
1. REPORT NUMBER: AFML-TR-79-4049	2. GOVT ACCESSION NO. / 3. RECIPIENT'S CATALOG NUMBER
4. TITLE (and Subtitle): ADVANCED DEVELOPMENT ON GALLIUM PHOSPHIDE MATERIALS FOR SATELLITE ATTITUDE SENSORS	5. TYPE OF REPORT & PERIOD COVERED: Final Technical Report, 1 Apr 77-30 Sep 78 / 6. PERFORMING ORG. REPORT NUMBER: 47108
7. AUTHOR(s): P.E. Petersen, R.G. Schulze, S.R. Peterson	8. CONTRACT OR GRANT NUMBER(s): F33615-77-C-5043
9. PERFORMING ORGANIZATION NAME AND ADDRESS: Honeywell Corporate Research Center, 10701 Lyndale Avenue South, Bloomington, Minnesota 55420	10. PROGRAM ELEMENT, PROJECT, TASK AREA & WORK UNIT NUMBERS: Program Element 62102F, Project/Task/Work Unit 2423/01/02
11. CONTROLLING OFFICE NAME AND ADDRESS: Air Force Materials Laboratory, Air Force Systems Command, Wright Patterson AFB, Ohio 45433	12. REPORT DATE: April 1979 / 13. NUMBER OF PAGES: 112
14. MONITORING AGENCY NAME & ADDRESS (if different from Controlling Office): 2423, 01	15. SECURITY CLASS. (of this report): UNCLASSIFIED / 15a. DECLASSIFICATION/DOWNGRADING SCHEDULE

16. DISTRIBUTION STATEMENT (of this Report)

Approved for public release, distribution unlimited HR-47108

17. DISTRIBUTION STATEMENT (of the abstract entered in Block 20, if different from Report)

Growth of Single Crystal Gallium Phosphide by Liquid Phase Epitaxy and Synthesis Solute Diffusion.

Correct title per Telecon

18. SUPPLEMENTARY NOTES

19. KEY WORDS (Continue on reverse side if necessary and identify by block number)

III-V Compounds, GaP, Liquid Phase Epitaxy, Solution Growth

Approximately 30 wks x 40 hrs/wk = 1200 hrs

20. ABSTRACT (Continue on reverse side if necessary and identify by block number)

The objective of this research program was to further develop the synthesis-solute-diffusion (SSD) and liquid-phase epitaxy (LPE) techniques for the growth of high-quality gallium phosphide.

This program resulted in the growth of epitaxial layers of GaP which had excellent growth morphology and carrier concentrations ~5 x 10^{15} cm^{-3}. The SSD technique was advanced so that low dislocation density bulk GaP could

DD FORM 1 JAN 73 1473 EDITION OF 1 NOV 65 IS OBSOLETE

UNCLASSIFIED

SECURITY CLASSIFICATION OF THIS PAGE (When Data Entered)

407493

20. be grown. Carbon was identified as the principal acceptor in this material which limited the carrier concentration to $\sim 2 \times 10^{16}$ cm^{-3}.

- An extensive materials evaluation program was conducted as a part of this development. The morphology of the grown material was analyzed by optical and electron-microscopic techniques. Hall and resistivity analysis was used to determine the majority carrier transport properties. The carrier concentration profiles were determined by capacitance-voltage measurements. The deep levels were investigated by photocapacitance spectroscopy, and the minority carrier diffusion lengths were measured by the Schottky-barrier photo current technique.

approximately 3 over 2 x 10 to the 16 power

PREFACE

This final report submitted March 1979, describes work performed by personnel of the Honeywell Corporate Material Sciences Center, 10701 Lyndale Avenue South, Bloomington, Minnesota 55420 during the period from 1 April 1977 through 30 September 1978 under Contract No. F33615-77-C-5043, Project No. 2423. The program was monitored by Mr. Robert L. Hickmott, (AFML/LPO) Air Force Materials Laboratory, Wright-Patterson Air Force Base, Ohio.

(513) 255-6652 - 785-6652

The program was directed toward the growth and evaluation of gallium phosphide by liquid phase epitaxy and bulk solution growth by the synthesis solute diffusion technique. The investigation was conducted by Dr. P. E. Petersen (principal investigator), Mr. R. G. Schulze, Mr. S. R. Peterson, Dr. S. A. Jamison with the technical assistance of Mr. D. W. Tuft, Mr. J. D. Hintgen, Mr. R. A. Sienko, Mr. J. Floeder, and Mr. N. Mellen.

TABLE OF CONTENTS

LIST OF ILLUSTRATIONS

LIST OF ILLUSTRATIONS--CONTINUED

LIST OF ILLUSTRATIONS--CONCLUDED

LIST OF TABLES

SECTION I
INTRODUCTION

The device potential of gallium phosphide (GaP) is of interest to the Air Force. In addition to its use as a light-emitting diode material, GaP has the potential for photodetectors for high sensitivity, for high-speed visible/UV detection in attitude control systems, for detector/junction field effect transistor combinations for self-scanned imaging arrays, for solar cells, for high-temperature electronics and for charge transfer devices. Honeywell's research, partly with the aid of USAF programs and partly with its own funds, has established GaP as a high-performance, visible/UV photodetector material. Another Honeywell program investigated using GaP in fabricating junction field effect transistors. The effort reported herein is a materials program for investigating and evaluating techniques for growing high-quality GaP.

In this program we investigated the synthesis-solute-diffusion (SSD) technique for the bulk growth of GaP and the liquid phase epitaxy (LPE) technique for growing thin layers for device fabrication. Our primary concern was to develop these techniques for growing high-purity, high-quality material. The program also involved a substantial material evaluation program. Experiments and analyses was conducted in 1) transport properties by Hall and resistivity analysis, 2) carrier concentration profiling by C-V analysis, 3) characterizing deep levels by photocapacitance, 4) minority carrier lifetime in n-type material, 5) determining dislocation density by surface etch pit studies, 6) evaluating surface and bulk growth morphology.

This program resulted in the development of the liquid-phase epitaxy techniques for the growth of high-quality GaP. Epitaxial layers with carrier concentration $\sim 5 \times 10^{15}$ cm^{-3} were grown which had excellent growth morphology. The SSD technique was advanced so that low dislocation density

bulk GaP could be grown. Carbon was identified as the primary acceptor which limited the carrier concentration in the bulk material to $\sim 2 \times 10^{16}$ cm^{-3}.

The balance of this report is contained in three major sections:

- Section II describes the experimental techniques and apparatus employed throughout this work
- Section III gives the experimental results and discusses the significance and, where possible, the interpretation of these results
- Section IV recapitulates the significant accomplishments of this program

SECTION II
EXPERIMENTAL TECHNIQUES AND APPARATUS

The objective of this program was to further develop the synthesis solute diffusion (SSD) and the liquid phase epitaxy (LPE) techniques for growing high-quality gallium phosphide (GaP) single crystals and epitaxial layers. During this program we modified both the growth apparatus and the growth techniques to improve the quality of the material. In addition, we evaluated the characteristics of the material grown. This section describes the techniques and apparatus used in this investigation.

BULK SOLUTION GROWTH APPARATUS

Two methods of crystal growth were performed: bulk growth and liquid phase epitaxy. Based on our previous experience with the bulk growth of GaP, we elected to further develop the synthesis-solute-diffusion (SSD) technique. The SSD technique uses elemental Ga and P as the starting materials. A two-zone furnace is required for this technique: the phosphorus is kept in the low-temperature zone where the temperature is regulated to approximately 400°C so as to maintain approximately one atmosphere pressure in the growth ampoule. The gallium is kept in the high-temperature zone (~1000°C) to increase the solubility of phosphorus in the gallium. The phosphorus reacts with the gallium at the surface to form a GaP film which is subsequently dissolved by the gallium. Hence, a concentration gradient is established in the melt. One end of the gallium melt is cooled and growth is initiated as the phosphorus diffuses to this cooled end.

Figure 1 is a schematic of the growth apparatus used for runs SSD C-2→C-4. The growth occurs in the graphite insert which was replaced for every growth run. The growth initiates from a rather large single-crystal seed held in place by the insert. Results of these growth experiments are described in Section III.

The growth ampoule as shown in Figure 1 is mounted in a three-zone Thermco Spartan diffusion furnace, which was mounted vertically. The complete apparatus is shown in Figure 2. The top zone controls the temperature and, hence, the over-presssure of the phosphorus. The middle and bottom zones are driven together to maintain a flat temperature profile across the gallium melt. Cooling is achieved by blowing N_2 on the bottom of the ampoule.

In growth run SSD C-6, the carbon crucible was replaced with a graphite-coated quartz crucible. The graphite coating was achieved by the pyrolysis of reagent grade acetone. In this first crystal growth with this apparatus, the seed was held in place by dimpling the quartz crucible as shown in Figure 3. The dimpling, however, proved to be a major perturbation to the growth. In succeeding runs, an attempt was made to hold the seed by surface tension. The most successful technique used a carbon-coated quartz retainer to hold the seed in place, as shown in the insert in Figure 3.

A series of random nucleated solution growth (RNS) experiments was performed to determine the source of carbon doping in the melts. The growth apparatus used for these experiments is shown schematically in Figure 4. These experiments were conducted in a horizontal Thermco Spartan furnace. A quartz growth ampoule was used, which, in some cases, was carbon coated by the pyrolysis of acetone. As in the vertical system, the phosphorus was maintained at a moderately low temperature to control the over-pressure. The gallium was contained in a pyrolytic boron nitride boat and maintained at a temperature ~1100°C. The extremity of the quartz ampoule was maintained at a slightly higher temperature to prevent transporting vapor to the end of the tube. (Results of these experiments are discussed in Section III.)

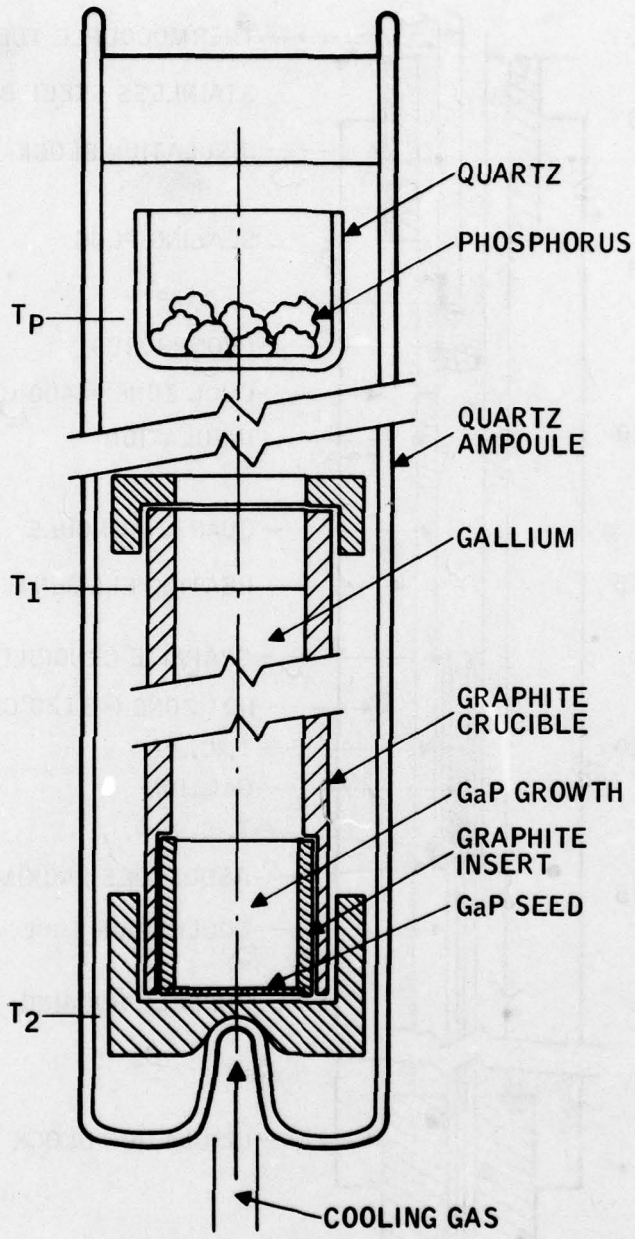

Figure 1. SSD Growth Ampoule using a Graphite Crucible and Tip Cooling

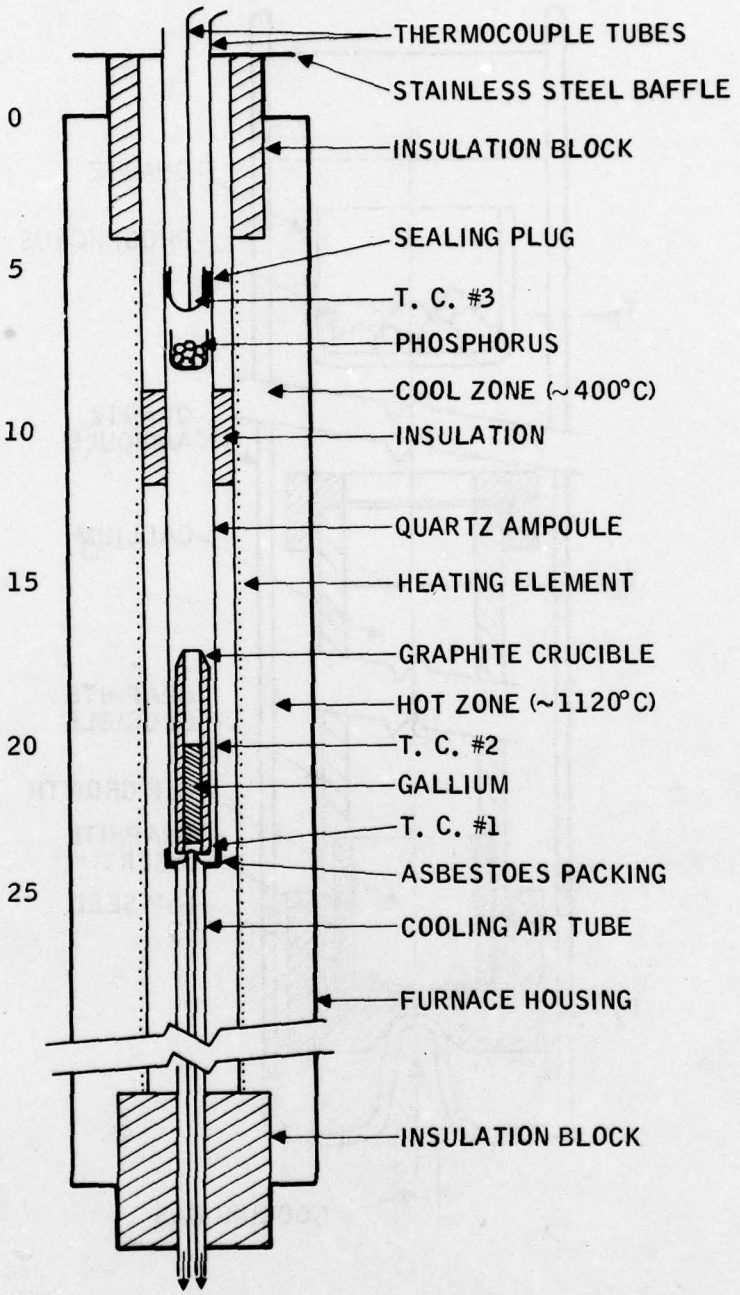

Figure 2. Complete Apparatus used for SSD Growth of GaP

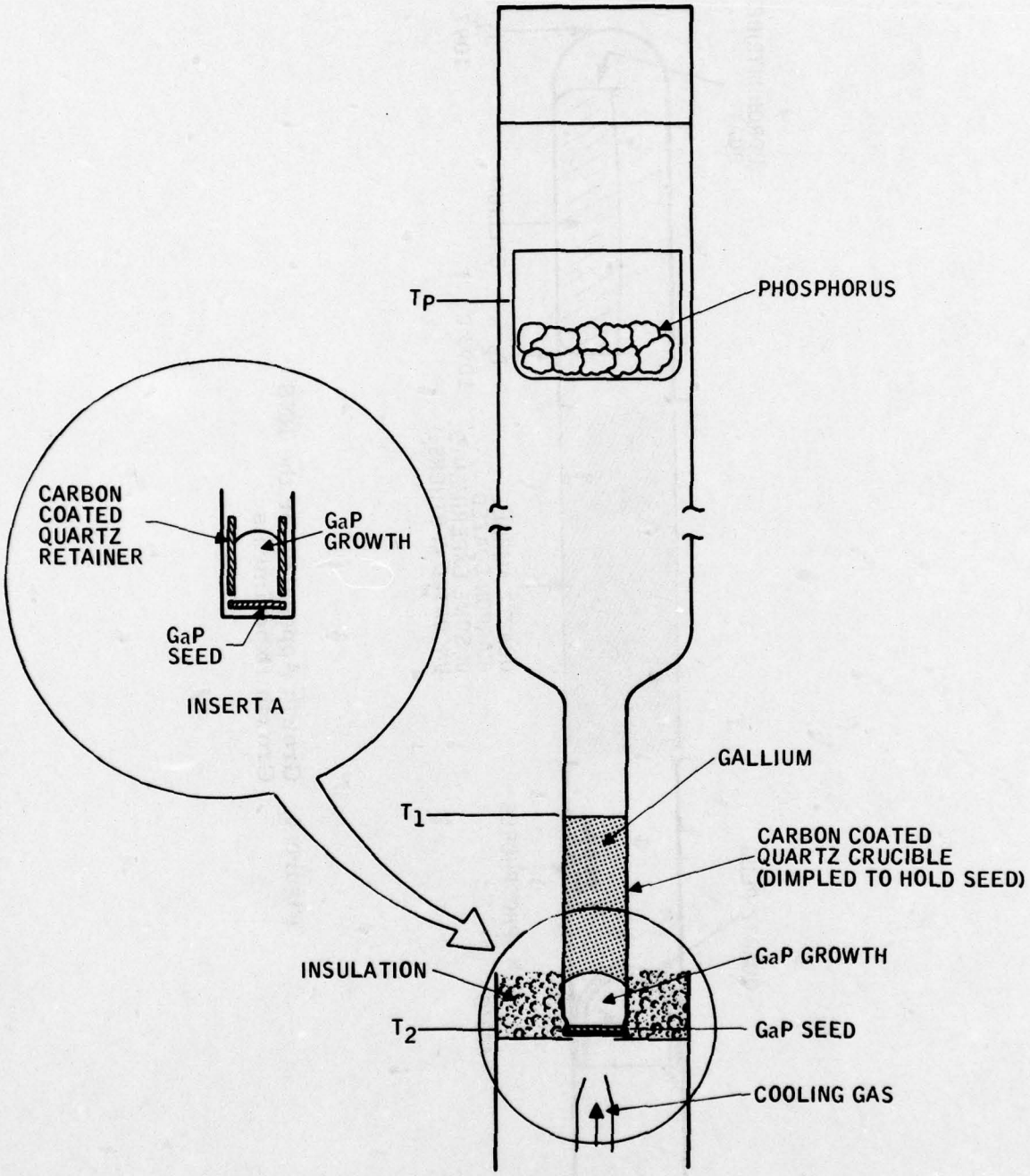

Figure 3. SSD Growth Apparatus using a Graphite-Coated Quartz Ampoule

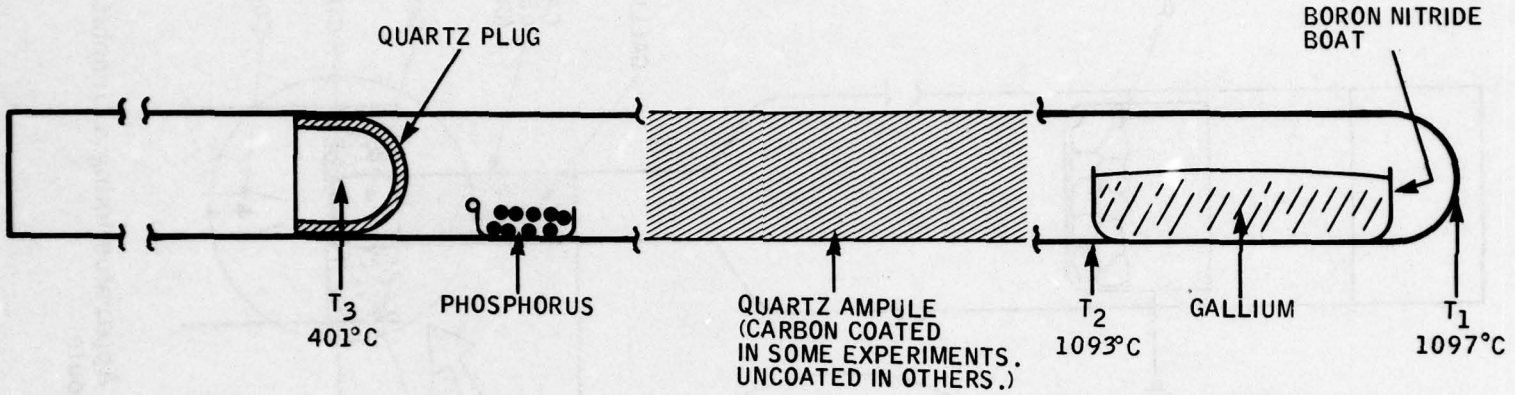

Figure 4. Growth Apparatus for the RNS Growth Experiments

LIQUID PHASE EPITAXIAL (LPE) GROWTH APPARATUS

A new apparatus for the liquid phase growth of GaP was designed and constructed under Honeywell funding prior to the inception of the work reported here. Because certain features of the apparatus are very important in the growth program, they will be described in considerable detail. The design features were arrived at as a result of our previous experience in the LPE growth of GaP and GaAs and by drawing on the scientific literature and personal contacts with other scientists engaged in the LPE growth of III-V compound semiconductors.

Certain desired characteristics of the LPE system strongly influenced the design:

- Minimum chance of contamination from construction materials
- Leak tightness, leak testability
- Ease of use => reproducibility
- Minimum growth-turn-around time
- Temperature stability, ease of control
- Overall design simplicity

A schematic diagram of the system is shown in Figure 5. The growth tube is General Electric (General Electric, Willoughby Quartz Plant, Enclid Avenue and Campbell Road, Willoughby, Ohio 44094) No. 214 quartz, with nominal O.D. and I.D. of 70 mm and 66 mm respectively. Another ~6 in. long quartz tube with a ground O.D. (2.750 + .000 in. - 010 in.) was fused to each end of the growth tube. The ground O.D. quartz tube sections were made by Quartz Scientific (Quartz Scientific, 819 East Street, Fairport Harbor, Ohio 44077).

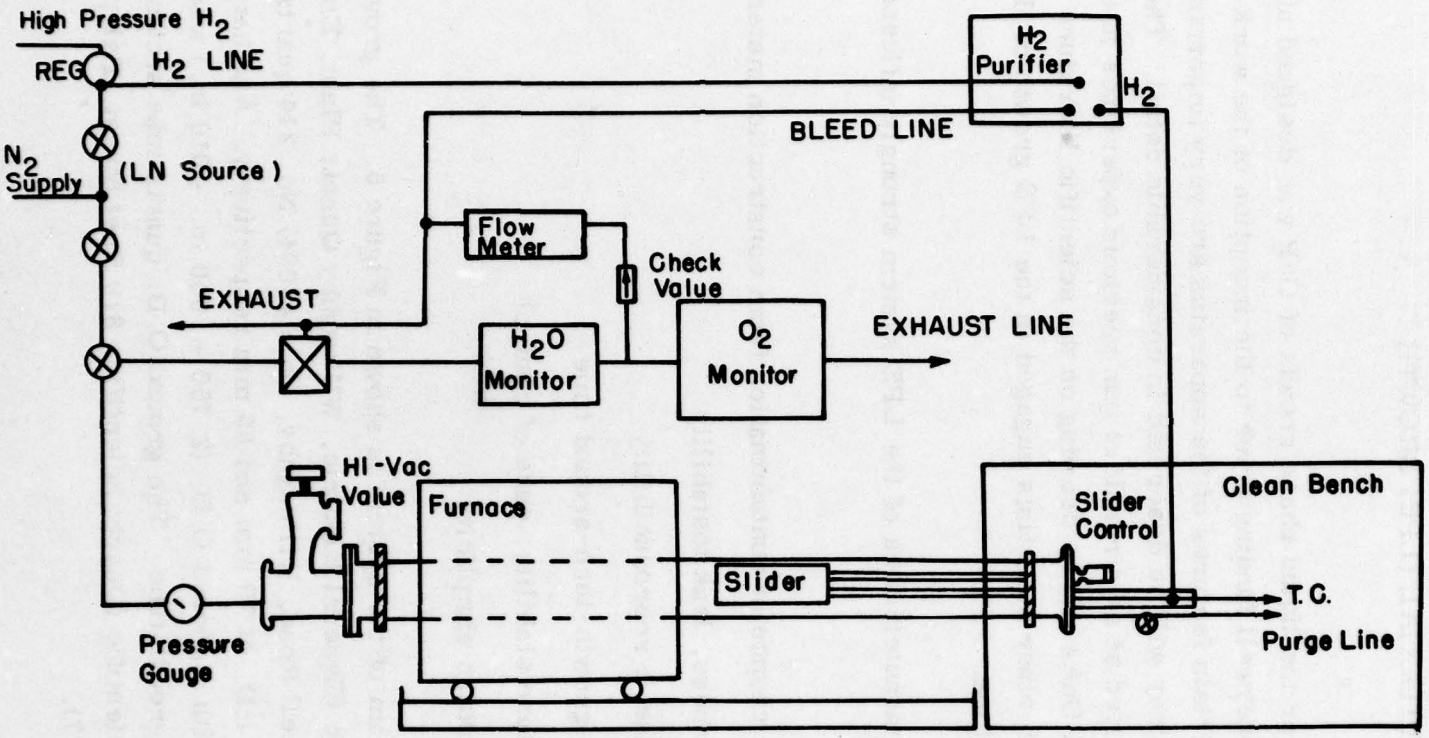

Figure 5. Schematic GaP LPE System

The ground quartz section ensured an easier leak-tight, o-ring, end-cap seal (Figure 6). The end-cap on the end of the growth tube through which the slider is inserted contains the hydrogen flow tube, which is coaxial with the thermocouple tube. This arrangement permits positioning the thermocouple inside the slider base and at various positions along the length of the slider. An additional thermocouple tube was laid in the growth tube outside of the slider.

The slider actuating mechanism is a stainless steel bellows-sealed device made by Varian Associates (Varian Associates-Vacuum Division, 611 Hansen Way, Palo Alto, California 94303). This mechanism is attached to the end plate by a Varian Conflat seal.

The opposite end of the growth tube is capped with a fitting and seal similar to that shown in Figure 6, except that it contains the exhaust gas line and a 1-3/4 in. tee section, and a high-vacuum valve through which the growth tube can be evacuated. For leak testing, the growth tube is evacuated with a cryogenic fore-pump, and a vapor-ion high vacuum pump. This type of evacuation prevents contamination from back streaming of diffusion pump oil. The system was evacuated to $<10^{-6}$ torr, while heated to 900°C.

With substrates previously prepared, the system can be opened, loaded, and closed in about five minutes. Nitrogen gas is reverse flowed (in the exhaust end and out of the loading end) through the growth tube during the loading operation. After loading, high-purity hydrogen gas was flowed at a rate of ~1 ℓpm before furnace heat up. A minimum flushing period of several hours is necessary to reduce oxygen concentration in the exhaust stream to $\lesssim 1$ ppm. Tank hydrogen is purified with a Matheson Model 8362 palladium diffusion unit (Matheson Gas Products, P. O. Box 96, Joliet, Illinois 60434). Oxygen contamination is monitored with a Research, Inc. Model 648 Oxygen Monitor with Model 648RX Range Extender (Research Inc., Box 24064,

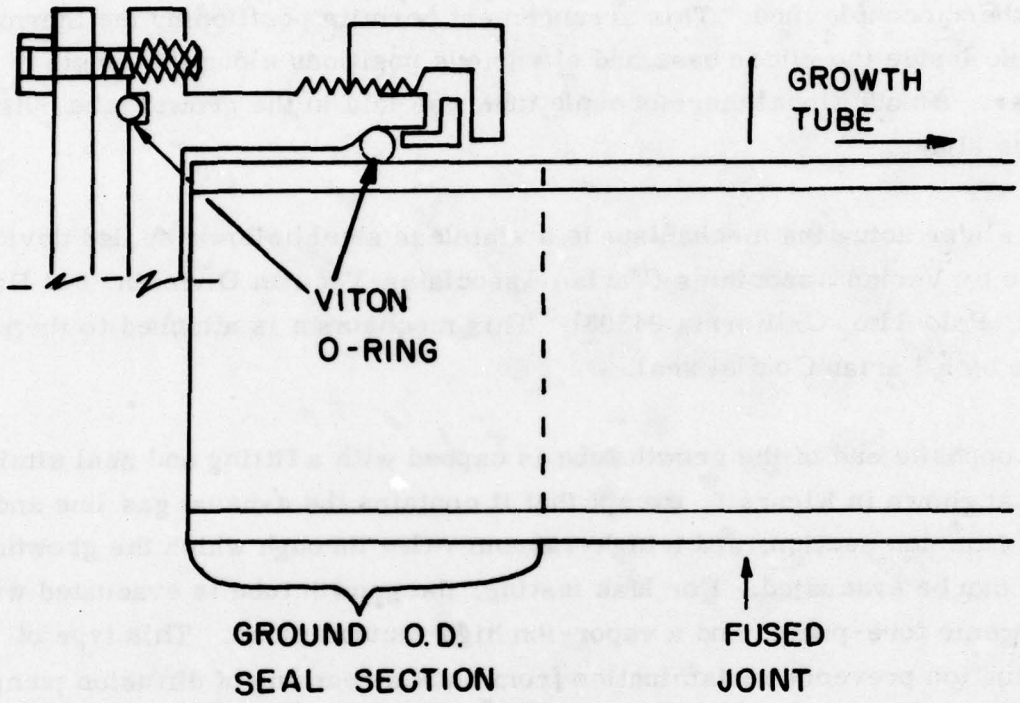

Figure 6. Schematic of Growth Tube End-Cap Seal

Minneapolis, Minnesota 55424). The instrument measures oxygen concentrations of a few ppm with ease. While measuring an absolute oxygen concentrations in the system, it also is a valuable check on leak-tightness.

Water vapor was also measured from time to time with a Panametrics Model 600 hygrometer (Panametrics Inc., 221 Crescent Street, Waltham, Massachusetts 02154). The dewpoint of the exhaust gas was measured to be below -80°C.

The furnace is a Lindbergh Omega Junior (Tempress Microelectronics, 304 Hart Street, Watertown, Wisconsin 53094). It is a three-zone furnace with a 3-inch I.D., low-thermal mass core. The furnace is somewhat less than half the length of the growth tube and is mounted on wheels so that, at the end of a growth run, the furnace can be rolled away from the slider to minimize the cooling off time. The two end zones of the furnace are slaved to the center controller. Temperature cool-down during growth was controlled with a Eurotherm Type 120 Programmer placed in series with the center zone thermocouple (Eurotherm Corp., Isaac Newton Center, Reston, VA 22070).

The loading end of the growth tube is inside a laminar flow clean bench. All of the quartz parts of the system were cleaned with aqua regia and rinsed in deionized, distilled water before assembly. The stainless steel fittings were ultrasonically cleaned with acetone, toluene and methanol. Polyethylene gloves were worn during assembly and loading or unloading procedures to prevent contamination from handling.

MATERIAL EVALUATION - TECHNIQUES AND APPARATUS

Four major techniques were used to evaluate the material grown during this program:

- Transport measurements
- Capacitance - voltage measurements
- Photocapacitance spectroscopy
- Minority carrier diffusion length

This section discusses the techniques and apparatus generally employed in each of these measurements.

Transport Measurements

During this program, Hall and resistivity data were obtained from representatives samples of all the SSD growth runs and from selected samples from the LPE growth runs. In all cases, the van der Pauw Hall technique was used. This technique enables measuring samples of arbitrary shapes and, hence, reduces the sample preparation time. A schematic of the apparatus is shown in Figure 7. The sample is mounted in a Janis Model 8DT research dewar, which allows measuring down to the temperature of liquid helium (Janis Research Co., Inc., 22 Spencer, Stoneham MA 02180). The sample temperature is controlled to 0.1K with a Lakeshore Cryotronics DT-500 temperature controller (Lakeshore Cryotronics, Inc., 9629 Sandrock TR., Eden, NY 14057). The current is measured with a Keithly 602 electrometer (Keithly Instruments Inc., 28775 Aurora Rd., Cleveland, Ohio 44139) and the voltages with a Fluke 8300A digital voltmeter (John Fluke Manufacturing Co., Inc., P.O. Box 7428, Seattle, WA 98133). This apparatus is capable of Hall measurements on bridge-shaped samples and can measure samples with resistances as great as $10^9\Omega$. These features, however, were not required during this investigation.

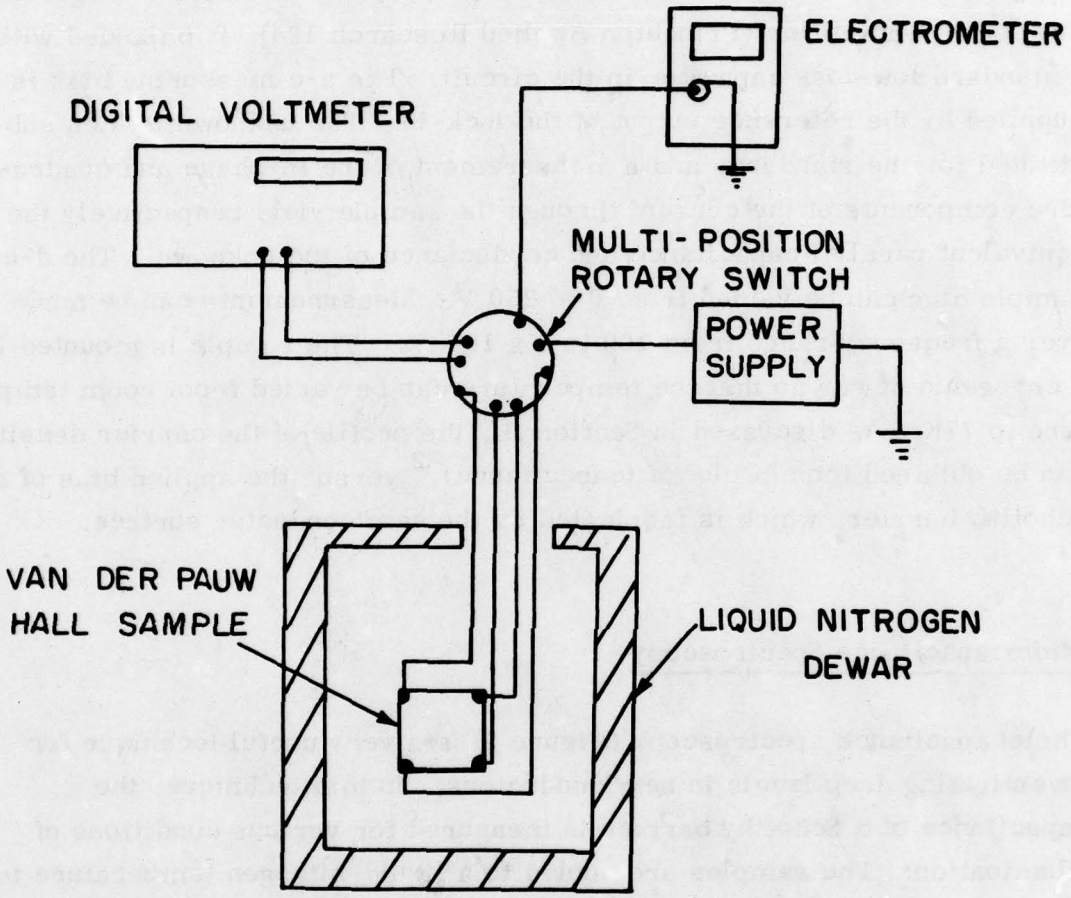

Figure 7. Schematic of Hall Apparatus

Capacitance-Voltage Measurements

A schematic of the capacitance measuring apparatus is shown in Figure 8. The lock-in amplifier (Princeton Applied Research 124), is balanced with a standard low-loss capacitor in the circuit. The a-c measuring bias is supplied by the reference output of the lock-in. The unknown is then substituted for the standard, and a measurement of the in-phase and quadrature components of the current through the sample yield respectively the equivalent parallel capacitance and conductance of the unknown. The d-c sample bias can be varied from 0 to 250 V. Measurements can be made over a frequency range from 100 to 2×10^5 Hz. The sample is mounted in a cryogenic dewar so that the temperature can be varied from room temperature to 77K. As discussed in Section III, the profile of the carrier density can be obtained from a plot of $(\text{capacitance})^{-2}$ versus the applied bias of a Schottky barrier, which is fabricated on the semiconductor surface.

Photocapacitance Spectroscopy

Photocapacitance spectroscopy (Figure 9) is a very useful technique for investigating deep levels in semiconductors. In this technique, the capacitance of a Schottky barrier is measured for various conditions of illumination. The samples are cooled to a liquid-nitrogen temperature to reduce thermal effects. With this apparatus, the sample can be illuminated simultaneously with two sources. The "prime" source is a Hg-Xe lamp in conjunction with a small Oriel monochromator (Oriel Optics Corp., 1 Market Street, Stanford, Conn. 06902). This source is held constant throughout the experiment. For the "probe" source a tungsten lamp is used in conjunction with a Perkin Elmer monochromator (The Perkin Elmer Corporation, Main Ave., Norwalk, Conn. 06851). The energy of the "prime" radiation incident on the sample is varied during the measurement. In fact, as will be discussed in Section III, measuring the variation in capacitance as a

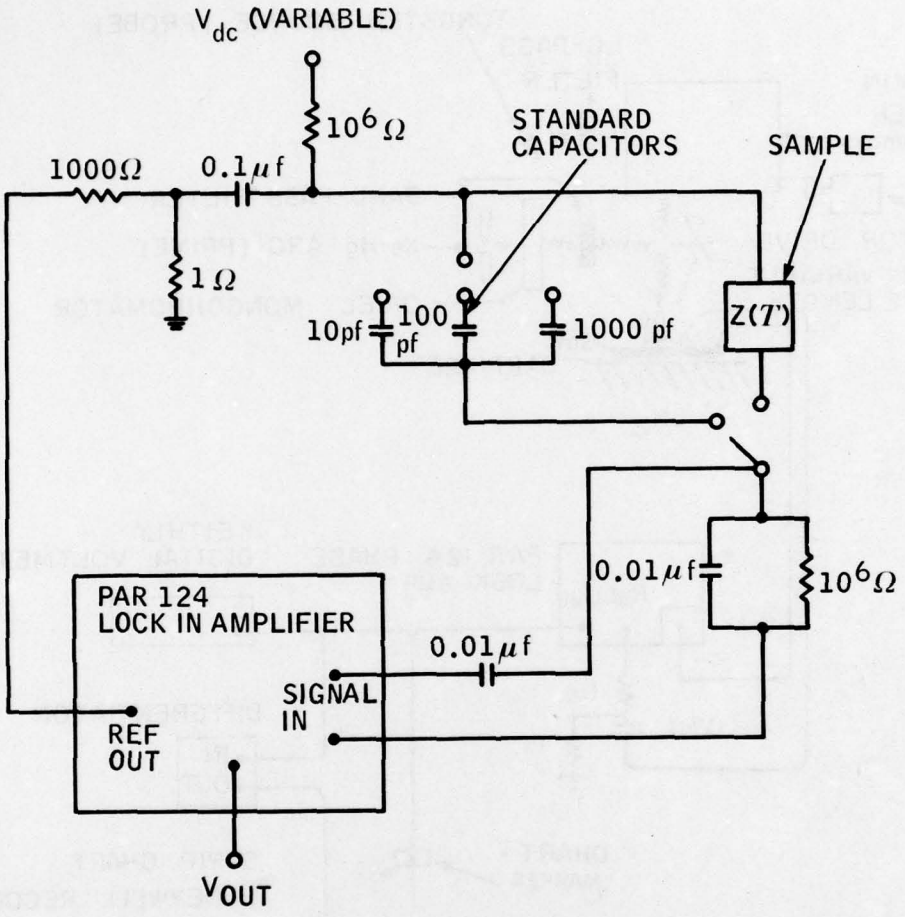

Figure 8. Capacitance-Voltage Measuring Apparatus

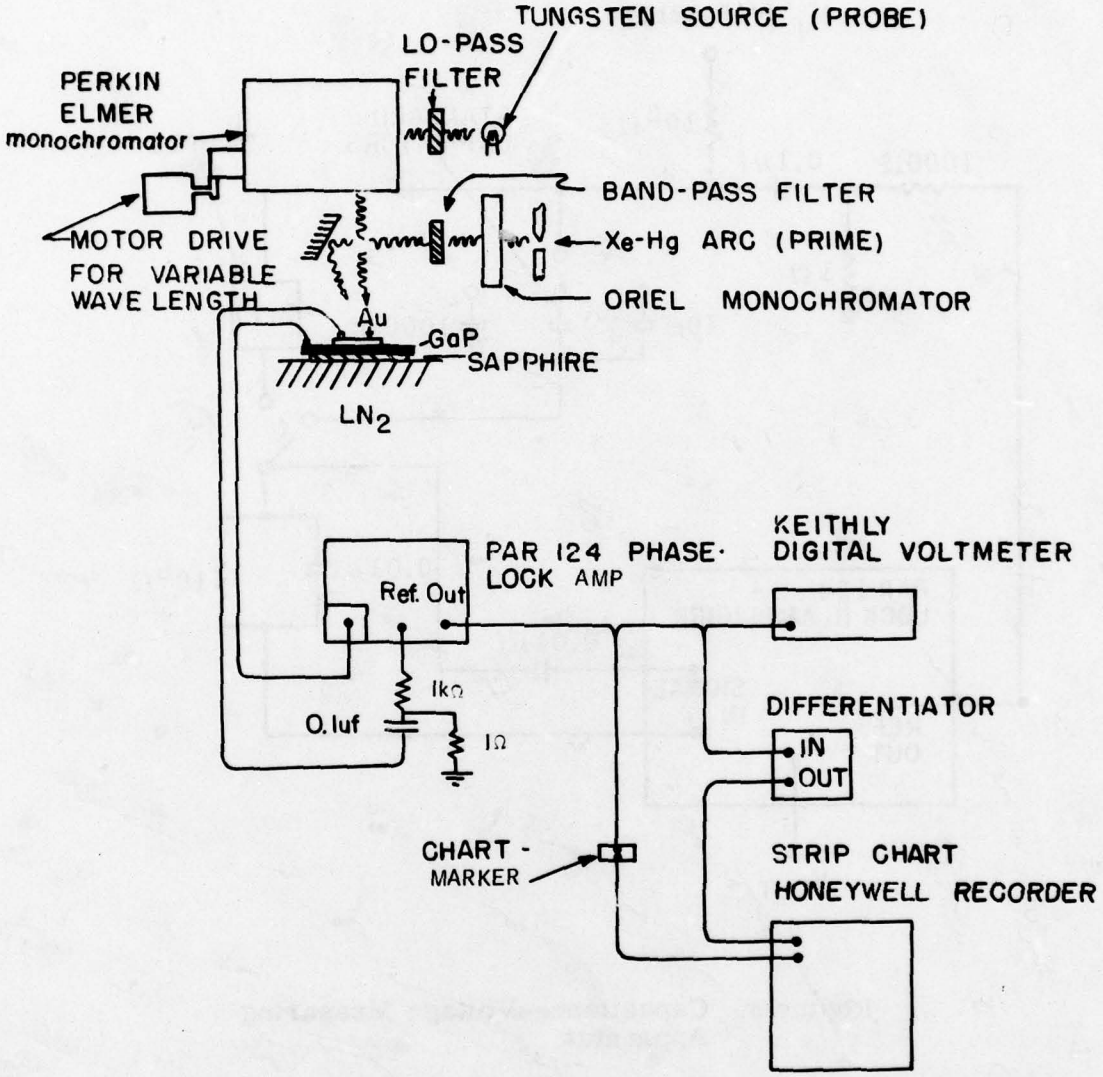

Figure 9. Schematic of the Apparatus used in the Photocapacitance Experiments

function of the "prime" energy allows one to determine the position of the deep levels within the band gap of the semiconductor.

A Princeton Applied Research Model No. 124 lock-in amplifier with a Model No. 184 current sensitive preamplifier was used to measure the junction capacitance. This instrument provided a measurement reproducibility within 0.5 pf at a signal-to-noise ratio greater than 30 dB. The effects of stray capacitances and conductances were circumvented by balancing the lock-in amplifier with reference to a standard capacitor which was temporarily connected in place of the sample. To increase the resolution, the output capacitance is differentiated in real time. To accomplish this differentiation, a two-stage op amp circuit was constructed using an integrator and linear amplifier with feedback instead of the conventional differentiator circuit.

The capacitance and its derivative are then recorded as the "prime" radiation energy is varied as a function of time by driving the wavelength selection drum on the monochromator.

Minority-Carrier Diffusion Length Measurements

The apparatus for measuring the minority carrier diffusion length by the Schottky diode photocurrent technique is schematically shown in Figure 10. This technique requires measuring the short circuit photocurrent and the depletion capacitance of a reverse-biased Schottky barrier for various conditions of illumination and bias. An Exact function generator was used to simultaneously drive the galvanometer in the General Scanning chopper and provide the reference to the Princeton Applied Research lock-in amplifier. The lock-in is used to measure both the capacitance and the short-circuit current in a way similar to that for the C-V measurements. The monochromator plus source illuminates the back side of the wafer with radiation, whose energy is slightly less than the band gap energy of the GaP on which the Schottky barrier is formed.

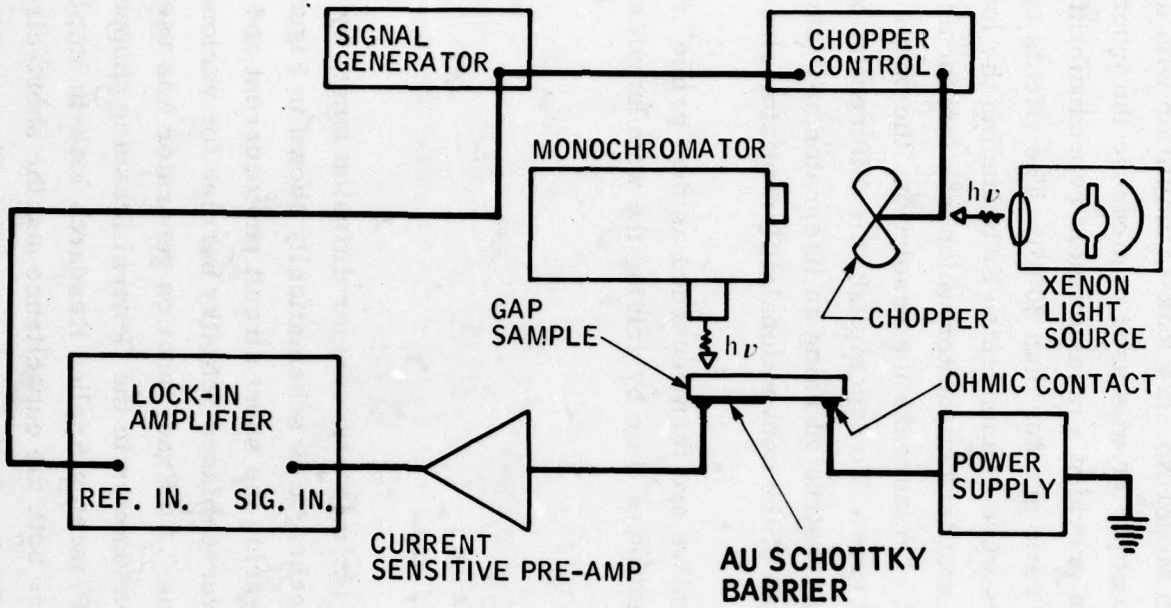

Figure 10. Schematic of Apparatus used for Minority Carrier Lifetime Experiments

Annealing Studies

Annealing experiments were designed to determine the dependence of the photoconductive and minority carrier lifetimes, and the minority carrier diffusion length on gallium vacancy concentration, V_{Ga}. From the outset, it was recognized that the probability of obtaining unambivalent results from such experiments was not high. However, because of the thermodynamic phase calculations of Jordan,[1] the experiments were relatively easy to design. Their calculations, which give V_{Ga} as a function of temperature for various equilibrium phosphorus isobars, are shown in Figure 11. These data show that anneals carried out at the same temperature, but at different phosphorus pressures should yield different gallium vacancy concentrations. The assumption is made of course that the anneal is continued long enough for the crystal to reach thermodynamic equilibrium with its environment. The purpose of performing the anneals at the same temperature is to try to eliminate other temperature-dependent processes which might also influence the parameters being measured.

The design of the annealing experiments then consisted of measuring photoconductive and minority carrier lifetime of Czochralski and LPE GaP samples before and after annealing. A correlation between these parameters and the gallium vacancy concentration determined from the phase data would serve to identify the controlling center.

[1] A. S. Jordan, R. Caruso, A. R. VonNeida and M. E. Weiner, J. Appl. Phys. 45, 3472 (1974).

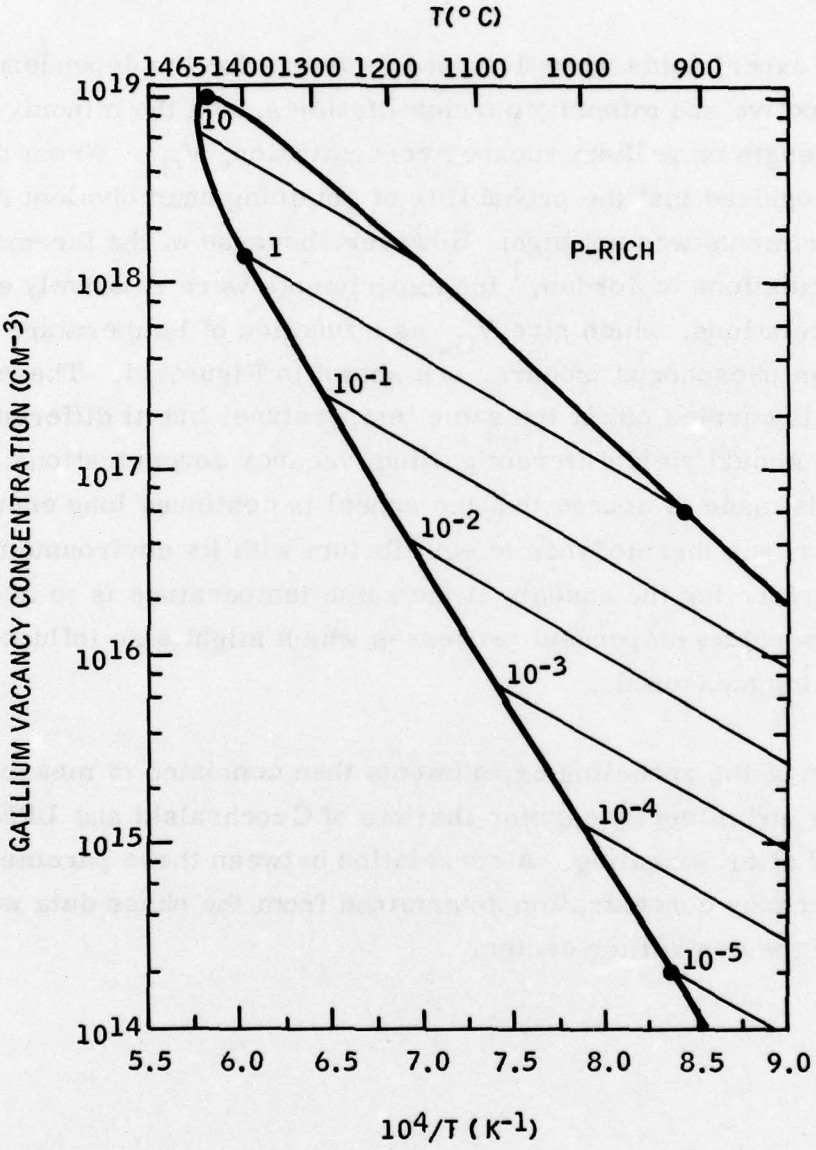

Figure 11. The Variation of Ga-Vacancy Concentration with Reciprocal Temperature for GaP Crystals in Equilibrium with Fixed Values of Phosphorus Pressure in Atmospheres

SECTION III
RESULTS AND DISCUSSION

This section reports the experimental results of the bulk solution growth, liquid phase epitaxial growth, and material evaluation experiments. The development of crystal growth procedures necessary to obtain material with specified state-of-the-art properties is a highly iterative process. The discussion of the results is therefore combined with the report of the results to present a more logical picture.

BULK SOLUTION GROWTH

Our previous experience with the bulk solution growth of GaP showed that when the growth was carried out in a sealed ampoule, in the presence of graphite the conductivity type was invariably p-type. That this is not simply a direct result of the graphite being in physical contact with the growth solution is demonstrated by the fact that n-type conductivity is almost always obtained from undoped LPE growth runs. The conclusion is that in the closed bulk growth ampoule, water vapor from one of the components of the system, interacts with the graphite and carries carbon into the growth solution. This probably occurs through the formation of carbon monoxide. Since the LPE system uses an open flow tube, any water vapor that evolved from parts of the system would be continuously carried away.

The first bulk solution growth experiments of this work were to identify and eliminate possible sources of water vapor in the growth ampoule. In the first growth run, SSD C-1, the following steps were taken to minimize water contamination: 1) the phosphorus used was packaged in nitrogen filled, 5 gram ampoules (one growth run); 2) the growth ampoule was loaded in a dry

nitrogen atmosphere; 3) the growth ampoule and crucible were vacuum-baked at 1180°C for two hours prior to loading; and 4) the loaded ampoule was baked at 400°C for four hours during evacuation with an oil-free sputter ion vacuum system. A Czochralski seed crystal was used. Although the seed crystal partially dissolved, a large enough growth occurred to permit Hall evaluation: the crystal was p-type. Two similar growth runs were performed. SSD C-2 used a new graphite crucible designed for easier crystal extraction and SSD C-3 employed an 850°C preloading vacuum bake of the gallium to remove water vapor and Ga_2O_3. Good single-crystal boules were grown in each of these runs, ~1.2 cm in diameter x 0.5 cm long, but again the conductivity was p-type, in the middle to upper 10^{16} cm^{-3} range.

To unequivocally identify the graphite as the source of the carbon acceptor, even if unable to eliminate the incorporation mechanism for the time being, a random nucleated SSD growth was designed. A pyrolytic boron nitride, PBN, boat containing gallium was placed in one end of a quartz ampoule and a quartz boat containing phosphorus was placed in the other end. The gallium end was held at ~1100°C and the phosphorus end at ~375°C. The first growth run of this type, RNS C-2, evidently had sufficient temperature gradient along the length of the gallium boat and beyond to vapor-transport most of the GaP out of the boat onto the ampoule walls. An appropriate temperature gradient leveling during the next run, RNS C-2, produced the desired growth in the gallium filled PBN boat. The starting gallium and phosphorus were the same as used in the SSD runs and the loading procedures, nitrogen atmosphere, and 850°C vacuum bake of the gallium were similar to those used for the SSD runs. Enough GaP was recovered from RNS C-1 and ample crystals were available from RNS C-2 to measure n-type conductivity. Thus, the graphite is clearly identified as the source of the carbon in the SSD runs and the sealed ampoule is related to the carbon incorporation method. As an additional proof, another run was made identical to RNS C-2 except that the interior of the quartz ampoule was coated with

carbon (pyrolized acetone). The resulting crystals were p-type, thus providing very strong proof that elemental carbon (graphite) was the source of the acceptor, and that the incorporation method was something other than physical contact of the carbon with the growth solution.

With this understanding, the continued SSD runs were used to study other important crystal properties. To minimize dislocation density, the seed crystal for SSD-4 was very carefully etched on both sides in aqua regia. Work damage on the back side could conceivably propagate through the seed into the growing crystal. Also, the wall of the graphite insert which surrounds the growing crystal was roughened to prevent sticking and transmission of strain which can also generate dislocations. A single crystal boule of GaP (Figure 12) was grown, nearly inclusion free and $\sim$1.25 cm diameter x 0.5 cm long. The interface between the GaP crystal and the gallium melt was convex, demonstrating the proper heat flow pattern. The roughened graphite insert did not prevent the boule from sticking, however. Hall measurements showed the usual mid-10^{16} cm^{-3} hole concentration. Standard etch and reveal techniques revealed none of the previously identified saucer pits, but did show an average density of small etch pits of $\sim 10^5$ cm^{-2}. Some regions had zero etch pits, while others had higher densities than 10^5 cm^{-2}.

SSD C-6 was designed to determine if strains induced by the sticking of GaP to the graphite crucible were contributing to the dislocation density, Instead of using the graphite crucible, a carbon-coated quartz crucible was used. In this case, the crucible was also the ampoule since it could itself be sealed. The purpose of the carbon coating was to prevent sticking since our experience had shown that the growing GaP boule will stick very tightly to a clean quartz surface. A 1.25 cm-diameter seed crystal, oriented in the usual $\langle\bar{1}\bar{1}\bar{1}\rangle$ direction, was held in place by dimpling the quartz crucible. The dimples upset the growth pattern and caused some polycrystalline growth near the dimples. However, the boule was quite large (1.25 cm diameter x

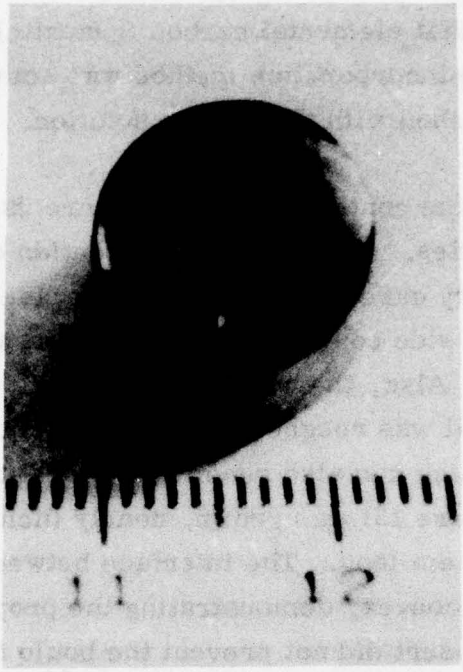

Figure 12. GaP Grown by Synthesis Solute Diffusion

0.5 cm long) and showed a desirable, slightly convex up growth interface. It did not stick to the carbon coated crucible walls. The dislocation density was found to vary from mid-10^3 cm^{-2} to mid-10^4 cm^{-2}. This represented an improvement but was still higher than desired. As usual the material was p-type with a room temperature hole concentration in the mid-10^{16} cm^{-3}.

Since the dimpling of the crucible of SSD C-6 has caused some polycrystalline growth which may have in turn influenced the dislocation density, two attempts were made to repeat SSD C-6, but without the dimpling. SSD C-7 failed because of a leak in the quartz seal. SSD C-8 was a partial test of the hypothesis. The seed failed to remain in place at the bottom of the gallium column, held there only by the surface tension of the gallium. The resulting growth was polycrystalline but some of the larger single-crystal areas showed etch pit densities < 100 cm^{-2} on x-ray diffraction verified $<\bar{1}\bar{1}\bar{1}>$ surfaces.

Another comparison was attempted with SSD C-8. Canyonlands 21st Century Company phosphorus was used instead of phosphorus from Atomergic Chemetals Company which had been used in all preceeding runs.

The hole concentration for the GaP from SSD C-8 was somewhat higher ($\sim 10^{17}$ cm^{-3}) than normal. On the basis of this limited but discouraging result, no more experiments were performed with Canyonlands 21st Century Company phosphorus.

The crucible used for SSD C-9 was modified to accommodate a much larger diameter seed crystal (3.2 cm). The seed was held in place with a quartz liner ring rather than with dimples in the crucible wall. The resulting growth was quite polycrystalline and no EPD studies were possible.

The crucible for SSD C-10 was scaled down to accommodate a 1.4 cm ϕ seed crystal, which was held in place with the same method as SSD C-9. Unfortunately, the seed crystal dissolved and the growth was again very polycrystalline.

The final bulk solution growth run of the program was designed to determine the effect of presaturating the gallium with phosphorus. This was done in the sealed crucible under normal growth conditions before loading the seed crystal in place. The experiment required opening the crucible, installing the seed and a new charge of phosphorus and resealing the crucible. The latter part of the growth period was disrupted by interruption of the crucible tip cooling. However, the first several millimeters of the boule were single-crystal, showing that dissolving the seed can be eliminated by presaturating the gallium with phosphorus. Hall measurements showed this run to have the usual mid-10^{16} range acceptor concentration resulting from the carbonized crucible wall.

Table 1 summarizes the growth conditions used in all of the RNS and SSD runs.

TABLE 1. GaP BULK GROWTH SUMMARY

Run Number	Time (days)	Starting Materials				Growth Container	T_1	T_2	T_p
		Gallium	Phosphorus	GaP to Saturate Melt	GaP Seed				
SSD C-1	7	E. P. 7-9's R-331-I	At. Ch. 6-9's D60633	Im. No. 2 Cz.	Im. No. 4 Cz.	Graphite crucible in quartz ampule	1124°C	1090°C	398°C
SSD C-2	14	E. P. 7-9's R-331-I	At. Ch. 6-9's D60633	Im. No. 4 Cz.	Im. No. 4 Cz.	Graphite crucible in quartz ampule	1084°C	1045°C	395°C
SSD C-3	10	E. P. 7-9's R-941-G	At. Ch. 6-9's D60633	Im. No. 4 Cz.	Im. No. 4 Cz.	Graphite crucible in quartz ampule	1083°C	1036°C	396°C
SSD C-4	9	E. P. 7-9's R-475-E	At. Ch. 6-9's D60633	As above	As above	Graphite crucible in quartz ampule	1080°C	1044°C	401°C
SSD C-5	Aborted	E. P. 7-9's R-475-E				Quartz crucible in quartz ampule, both carbonized			
SSD C-6	12	E. P. 7-9's R-475-E	Same as C-4	Same as C-4	Same as C-4	Quartz crucible in quartz ampule, carbonized	1040°C	1003°C	400°C
SSD C-7	13	E. P. 7-9's R-475E	Cnlds. 21 6-9's P46-977	Im. No. 4 Cz.	Im. No. 4 Cz.	Carbon-coated quartz	1054°C	840°C	420°C
SSD C-8	11	E. P. 7-9's R-475-E	Cnlds. 21 6-9's P46-977	Im. No. 4 Cz.	Im. No. 4 Cz.	Carbon-coated quartz	1030°C	996°C	414°C
SSD C-9	13	E. P. 7-9's R-475-E	At. Ch. 6-9's D60633	Im. No. 4 Cz.	Im. No. 4 Cz.	Carbon-coated quartz container and seed holder	1035°C	1003°C	408°C
SSD C-10	9	E. P. 7-9's F-6-75	At. Ch. 6-9's E2238	Im. No. 4 Cz.	Im. No. 4 Cz.	Carbon-coated quartz - quartz seed holder	1057°C	950°C	406°C
SSD C-11	4	E. P. 7-9's R-33-I	At. Ch. 6-9's E2238	Synthesized by us in a separate run	Im. No. 4 Cz.	Carbon-coated quartz container and seed holder	1070°C	890°C	410°C
RNS C-1	10	E. P. 7-9's	At. Ch. 6-9's	n. a.	n. a.	BN crucible quartz ampule	1070°C	1040°C	375°C
RNS C-2	11	E. P. 7-9's R-475-E	At. Ch. 6-9's D60633	n. a.	n. a.	Bn crucible quartz ampule	1097°C	1093°C	401°C
RNS C-3	12	E. P. 7-9's R-475-E	Cnlds. 21 6-9's P46-977	n. a.	n. a.	BN crucible carbon coated quartz ampule	1095°C	1093°C	415°C

Note: E. P. - Eagle Picher
At. Ch. - Atomergic Chemetals
Im. - Imanco
Cz. - Czochralski
Cnlds. 21 - Canyonlands 21st Century

LPE GROWTH

Liquid phase epitaxy is the solution growth of a relatively thin epitaxial layer of material onto a suitable substrate. Previous Honeywell LPE work was applied in preparing GaP pn-junctions and copper-doped GaP for photodetector devices. The objective of the work reported here is to grow high-purity ($\leq 5 \times 10^{15}$ cm^{-3}), low-dislocation-density (≤ 200 cm^{-2}), GaP LPE layers of controlled thicknesses and smooth surface morphology.

To accomplish this, a systematic program of LPE-growth experiments was performed involving the preparation of approximately 115 LPE layers. Each of 40 growth runs was designed to study the influence of some particular grow parameter upon the properties of the LPE layer.

All of the LPE runs were performed using the apparatus previously described in Section II. The LPE slider (Figure 13) works in the following way: Ga and GaP are put in the growth charge bins; lapped and polished GaP substrates are placed in the substrate slots. The sliding member (top) is positioned so that the growth charge columns are not over the substrates. The assembly is raised to about 950°C in a palladium-diffused H_2 atmosphere. After the system has reached thermal equilibrium, the slider is moved to position the growth charge over the substrate. The furnace temperature is reduced for a ΔT corresponding to the desired layer thickness. After the growth, the slider is returned to the starting position, and the furnace cooled to room temperature to remove the LPE layers.

A synopsis of all the LPE runs performed is shown in Table 2. The growth runs will not be described chronologically, but will be referenced to support findings on the influence of various growth parameters on the LPE layer properties. The potential relationships explored and a summary of the results obtained are given in Table 3.

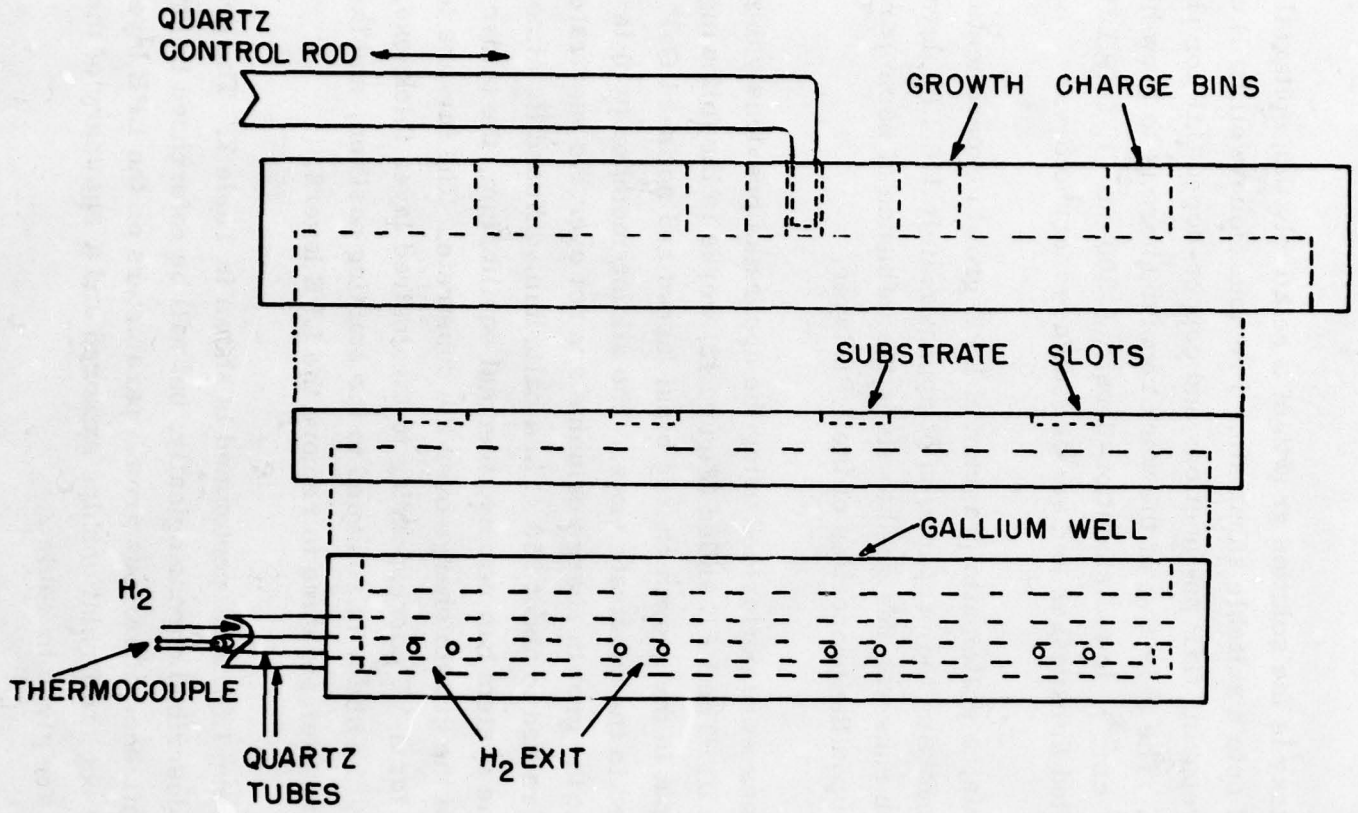

Figure 13. GaP LPE Slider Apparatus

TABLE 2. SYNOPSIS OF LPE RUNS

LPE Layer Property	Potential Influence	Results
Layer thickness uniformity	Use of Ga well	Not required for this furnace/slider
	Melt thickness	Critical parameter; 2 mm much better than 10 mm
	Furnace temperature profile	Critical parameter; must determine empirically
	Isothermal growth	Unsuccessful with existing vertical gradient
Carrier concentration	Growth temperature	Substrate degradation $\geq 970°C$
	Bake out cycles	No advantages for experiments tried.
	Ga vendor	Three found to be acceptable
	H_2 flow rate	Flow rate ≥ 1.0 ℓpm preferred
	Substrate type	Czochralski and SSD tried; no clear difference
	Source type	RNS, PDI and Czoch. all yielded some $< 10^{16}$ cm^{-3} layers.
Surface morphology	Substrate surface	Bromine-methanol chemical-mechanical polishing best
	Cool down rate	Not critical up to at least 0.5°C/min.
	Substrate cooling	No effect for H_2 flow rates up to 3.5 ℓpm
	Substrate orientation	<111> and <100> gave equivalent results

TABLE 3. GaP LPE SYNOPSIS

Sample No.	Growth Cycle Temperature °C				Substrate	Source	Purpose/Features
	Upper	Start	Stop	Rate			
1A	955	950	925	20°/hr	IM No. 4	PDI	First run - system check out. System evacuated to 10^{-6} Torr.
2A	960	950	930	20°/hr	IM No. 4	PDI	New H_2 purifier installed. Vac Ion pump before H_2 flow.
3A	960	950	930	20°/hr	IM No. 4	PDI	New slider retainer. Vac Sorb pump before H_2 flow.
4A 4B	960	950	930	20°/hr	IM No. 4	PDI	N_2 flush only after loading and before growth.
5A 5B	960	950	930	20°/hr	IM No. 4	RNS RNS	N_2 flush only. Substrate not in good condition.
6A 6B	960	950	930	20°/hr	IM No. 4	RNS RNS	Baked approximately 21 hrs at 950° in flowing H_2 after loading before growth for improved temperature stability. N_2 flush only. Increased H_2 flow from 1.5 lpm to 3.5 lpm
7A 7B	958	950.7	930	20°/hr	IM p-type IM p-type	PDI RNS	Grow samples on p-substrates for Hall analysis to compare PDI and RNS source material
8A 8B	958	950.3	929.3	20°/hr	IM No. 4 IM No. 4	PDI PDI	Test results of Al_2O_3 stone abrading of bottom of bin section and 1000°C vacuum bake out.
9A 9B	961	950.2	930	20°/hr	IM No. 4 IM No. 4	PDI PDI	Cooling H_2 flow rate reduced to 0.5 lpm
10A 10B	959.7	950.3	930	20°/hr	IM No. 4 IM No. 4	Both sources left in place from No. 9	Check repeated use of growth charge for reproducibility. Improved substrate handling
11A 11B	963	950.5	930	20°/hr	IM No. 4 IM No. 4	PDI PDI	20 hr. H_2 flow before heat up. Furnace profile adjusted with new longer tc. and tube.
12A 12B	961	951	930	20°/hr	IM No. 4 IM No. 4	Both sources left in place from No. 11	Substrate not etched before loading 21.5 hr H_2 flush.
13A 13B	959.2	949.9	930.0	20°/hr	IM No. 4 IM No. 4	Both sources left in place from No. 11 and 12	Test effect of bringing H_2 in end cap instead of into slider base, i.e., no cooling of the substrate.
14A 14B 14C	959	950	930	20°/hr	IM No. 4 IM No. 4 IM No. 4	PDI PDI PDI	H_2 in end cap. Empty Ga well. Leak discovered during pump down.
15A 15B 15C 15D	959	950	930	20°/hr	IM No. 4 IM No. 4 IM No. 4 IM No. 4	PDI PDI PDI PDI	First run after leak test to 10^{-6} Torr. 950° bake out. 15D: First "thin" melt.
16A	960	951	929	20°/hr	IM No. 4	IM No. 4	Test thin melt again but with graphite "flattening" plug. Melt approximately 2 mm high.
17A	960	950	930	20°/hr	IM No. 4	Left in place from 16	Same as 16 but baked 72 hrs at 850°C after loading before growth.
18A 18B 18C	960	950	930	20°/hr	IM-p IM-p IM-p	PDI PDI IM No. 4 (thin)	Grow layers on p-substrates for Hall measurements.
19A 19B 19C	960	950	930	20°/hr	IM No. 4 IM No. 4 IM No. 4	IM No. 4 (thin) PDI PDI	Back to n-substrates to check surface morphology
20A 20B 20C	960	950	930	20°/hr	IM No. 4 IM No. 4 IM No. 4	(Same as No. 19)	Same as No. 19 but with long bake out of growth charges also Ga well refilled
21A 21B	999.1	993.1	950	20°/hr	IM No. 4	Left in place from No. 19 and No. 20 and added PDI to thin melt	Grow thick layers
22A 22B 22C	968	960	922	35°/hr	IM No. 4 IM No. 4 IM No. 4	PDI (thin) PDI PDI	No excess source and double cool down rate
23A 23B 23C	960	955	919	35°/hr	IM No. 4 IM No. 4 IM No. 4	IM No. 4 PDI PDI	Repeat No. 20 but new growth tube and faster cool down rate as in No. 21

TABLE 3. GaP LEP SYNOPSIS (CONCLUDED)

Sample No.	Growth Cycle Temperature °C				Substrate	Source	Purpose/Features
	Upper	Start	Stop	Rate			
24A	962	955	915	35°/hr	IM No. 4	IM No. 4 (thin)	Repeat 23 - control rod repaired
24B					IM No. 4	PDI	
24C					IM No. 4	PDI	
25A	955	950	950	0	IM No. 4	IM No. 4	All thin melts. No temperature cool down.
25B					IM No. 4	PDI	
25C					IM No. 4	PDI	
26A	955	950	911	35°/hr	IM No. 4	PDI	3 thin melts - similar to LPE 23.
26B					IM No. 4	PDI	
26C					IM No. 4	PDI	
27A	957	952	910	35°/hr	IM No. 4	PDI	3 thin melts similar to 23 and 26. Rt end zone dropped 10° to attempt decreasing convection.
27B					IM No. 4	PDI	
27C					IM No. 4	PDI	
28A	957	952	930	35°/hr	IM No. 4	Left in place from LPE 27	3 thin melts simlar to 27. Rt end zone dropped 2° 1.0 lpm H_2 instead of 0.5.
28B					IM No. 4		
28C					IM No. 4		
29A	957	952	922	30°/hr	IM-p	Left in place from 27-28	p-substrate for Hall analysis, n-substrate for morphology check.
29B					IM No. 4		
29C					IM-p		
30A	956	951	922	35°/hr	IM No. 4	PDI	First trial of Canyonlands Ga
30B					IM No. 4	PDI	
30C					IM No. 4	PDI	
31A	957	952	917	35°/hr	IM No. 4	Left in place from LPE 30	Second trial of Canyonlands Ga
31B					IM No. 4		
31C					IM No. 4		
32A	956	951	917	35°/hr	IM-p	PDI	Hi-temp preload bake out. Back to Eagle-Picher Ga.
32B					IM No. 4	PDI	
32C					IM-p	PDI	
33A	955	950	915	35°/hr	IM-p	RNS-C2	
33B					IM No. 4	RNS-C2	
33C					Im-p	RNS-C2	
34A	955	950	917	35°/hr	(100)	RNS-C2	Use of (100) substrates.
34B					(100)	RNS-C2	
34C					(100)	RNS-C2	
35A	957	952	916	35°/hr	SSDC-4	RNS-C2	Use of SSD substrates
35B					SSDC-4	RNS-C2	
35C					SSDC-4	RNS-C2	
36A	956	949	915	35°/hr	IM No. 4	RNS-C2	
36B					IM No. 4	RNS-C2	
36C					IM No. 4	RNS-C2	
37A	955	955	915	35°/hr	IM No. 4	RNS-C2	Thick melt to grow wedge layer
37B					IM No. 4	RNS-C2	Johnson-Matthey Ga all runs through 40
38A	960	950	915	35°/hr	IM No. 4	RNS-C2	Thick melt to grow wedge layer
38B					IM No. 4	RNS-C2	
38C					IM No. 4	RNS-C2	
39A	960	950	915	35°/hr	IM No. 4	RNS-C2	Thin melt to grow wedge layer
39B					IM No. 4	RNS-C2	
39C					IM No. 4	RNS-C2	
40A	961	950	917	35°/hr	IM No. 4	RNS-C2	Thin melt and furnace set for flat layer
40B					IM No. 4	RNS-C2	
40C					IM No. 4	RNS-C2	

Abbreviation Key:

IM - *Czochralski GaP from Cambridge-IMANCO*
PDI - Polycrystalline dense ingot GaP from Cambridge-IMANCO
RNS - Random nucleated solution grown GaP from Honeywell
SSD - Synthesis-solute-diffusion grown GaP from Honeywell

Layer Thickness Uniformity

The layer thickness uniformity (as well as surface morphology which will be discussed later) was routinely evaluated on all LPE layers with a surface profilometer. The configuration of the layers was deliberately chosen to be a circular layer area 0.433-inch on a 0.375-inch square substrate. The layer was profiled along diagonals of the substrate so that the uncovered corners provided a substrate surface reference. Our previous LPE growth work had shown the advantage of incorporating a Ga well in the slider under the substrates to reduce lateral temperature differences. Thus, such a well was also included in the slider used in this work. The Ga well was filled for all growth runs except LPE 14 through 19. Although some other parameters were varied during this series of runs, the results, taken together, show no evidence for any significant effect of the Ga well. It appears that at least for this particular slider - furnace configuration, the feature of a Ga well provides little, if any advantage.

Melt thickness proved to be a very important parameter in achieving uniform layer thickness and layer flatness. Figure 14 of LPE 15A shows a typical surface profile when a layer was grown from a growth charge approximately 10 mm thick and after the temperature profile effects (discussed next) were minimized. Starting with LPE 15, a number of growths were performed in which some, or all of the growth charges were reduced to $\sim$2 mm thickness. Figure 15 of LPE 20A illustrates the results of the change as does Figure 16 of LPE 29B (29B is thicker than 20A due to a larger growth temperature interval). The difference is based on a consideration of likely convection patterns. If the dimensions of the growth charge are roughly equal in all directions, then it is obvious that a temperature gradient can produce a convection cell of about the same dimensions as the growth charge (see Figure 17). If such a cell exists, it will effectively pick up GaP on that end of the substrate. The Ga rises on the hotter end and the cycle continues. That convection is involved at all is clearly evident from the much greater average thickness of

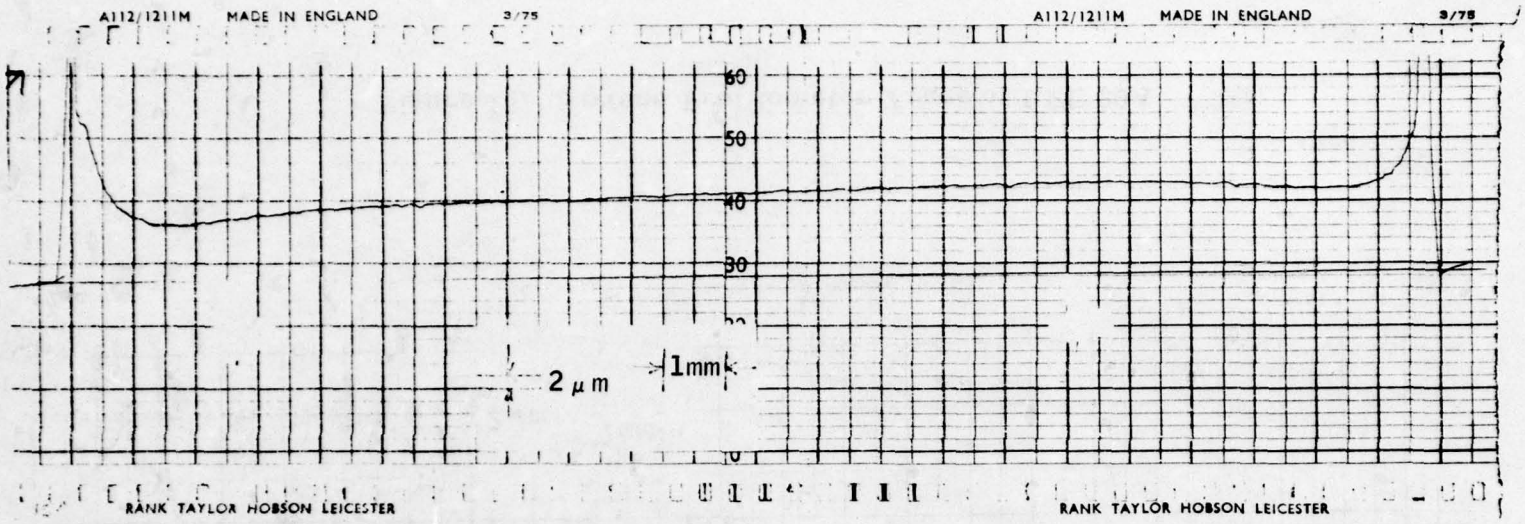

Figure 14. Surface Profilometer Trace of LPE 15A

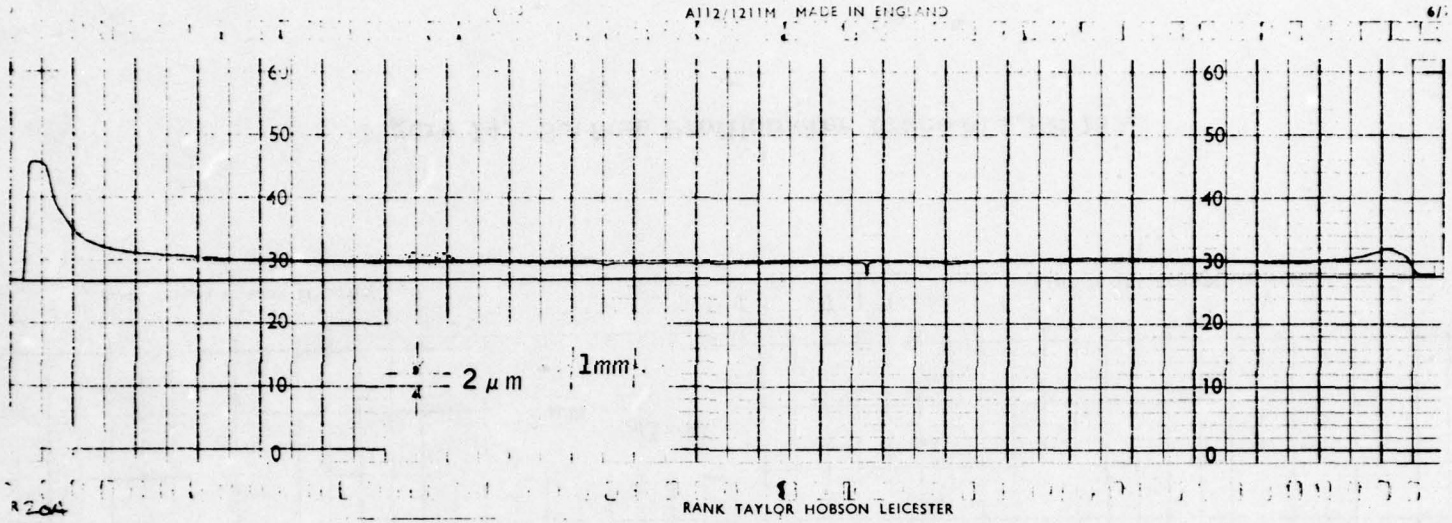

Figure 15. Surface Profilometer Trace of LPE 20A

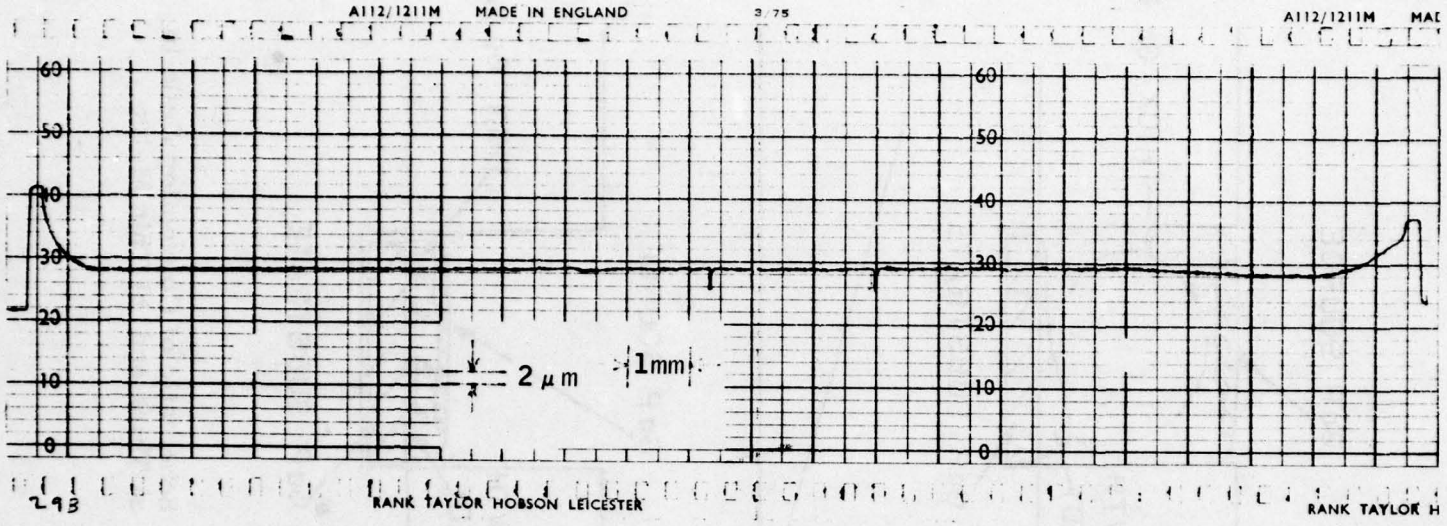

Figure 16. Surface Profilometer Trace of LPE 29B

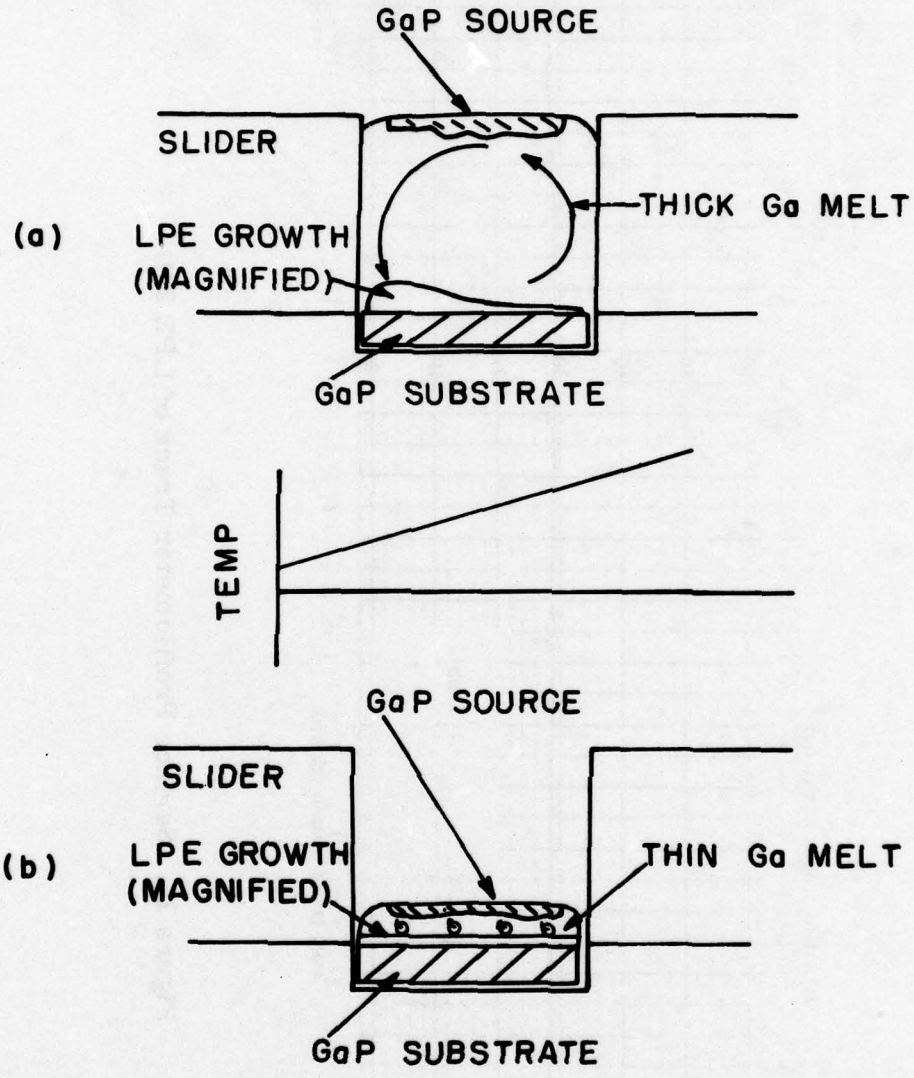

Figure 17. Schematic of Convection Cells in a) Thick and b) Thin Melts

LPE 15A, compared to LPE 20A or LPE 29B (thin melts). For, if only diffusion were involved, the average thickness of these layers would be very similar, since the diffusion length of phosphorus in Ga is less than the height of the thin melt.

Since the convection that was just discussed is driven by lateral temperature gradients, minimizing such gradients is another way of improving layer thickness uniformity. Before any growth runs were started, the temperature was measured inside and along the length of the slider using the thermocouple shown in Figure 5. By adjusting the end zones of the furnace, temperature differences along the length of the slider were reduced to $\sim 0.3°C$. Therefore, it was a surprise to find systematic layer thickness variations along the layer parallel to the length of the furnace. On the basis of the convection analysis previously described, the end zones of the furnace were adjusted in the sense necessary to reduce a temperature gradient that would cause the nonuniformity of layer thickness. Figure 18 shows the profile of a layer grown with the furnace as originally adjusted. Figures 19 and 14 show the profiles of layers grown after several empirical adjustments of the furnace profile. It is clear that the resulting temperature profile in the Ga melt must have been much flatter after these adjustments. The temperature, as measured with a thermocouple in the slider base, varied by several degrees after these adjustments. One might be tempted to offer the explanation that the H_2 gas, which flows into the slider base coaxially around the thermocouple tube is responsible for the discrepancy. However, if the assumption is made that the incoming H_2 would tend to give a low reading on the inlet end, then the furnace adjustment required turns out to be in the opposite direction of that actually used. The conclusion is that the furnace temperature profile must be adjusted empirically for the best uniformity of layer thickness.

A temperature cool-down was used to drive the growth process for all but one experiment. If a temperature gradient were to be established with the top of the melt hotter and the substrate cooler, growth should occur as in

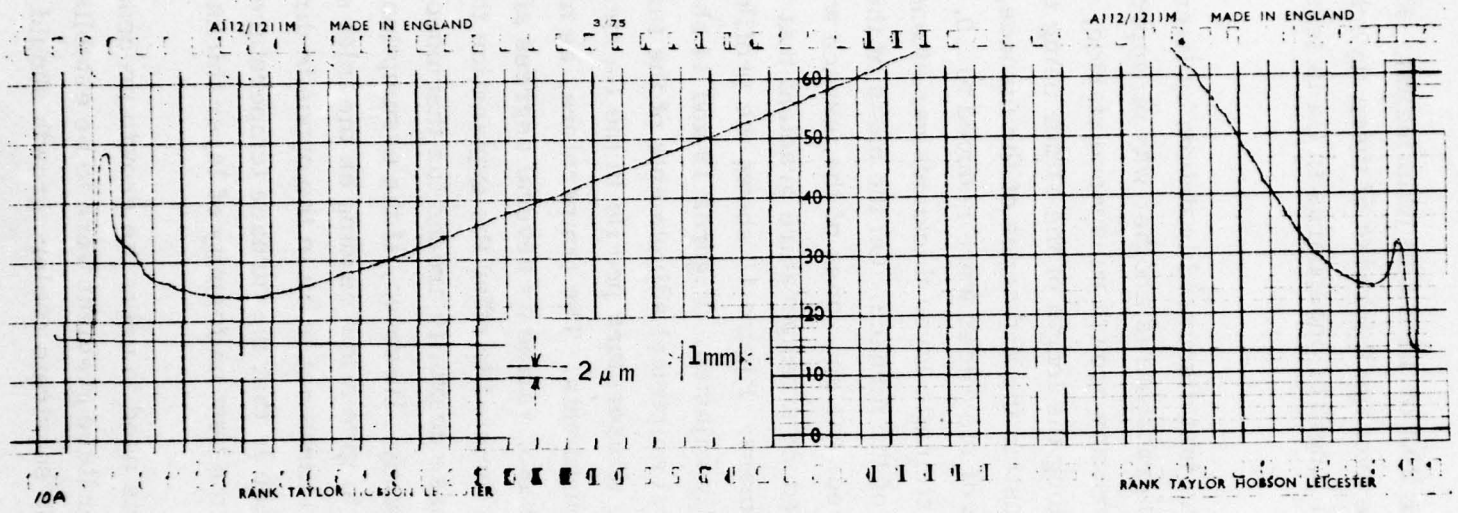

Figure 18. Surface Profilometer Trace of LPE 10A

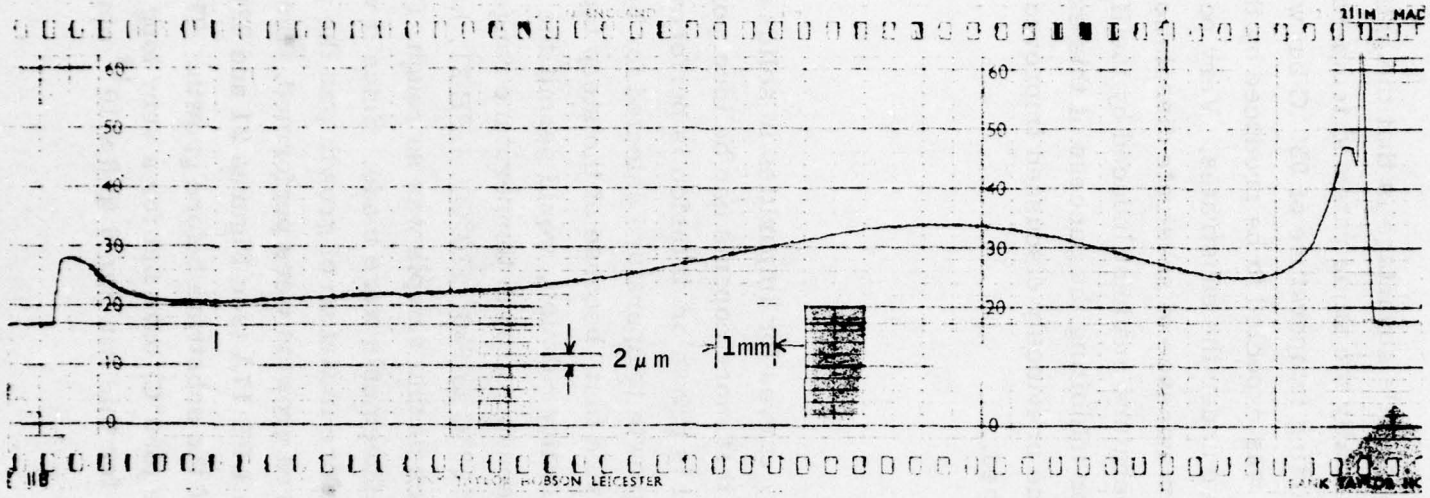

Figure 19. Surface Profilometer Trace of LPE 11B

the BSG technique. The concept's advantage is that the entire thickness of the layer is grown at essentially the same rate and temperature. LPE 25 was grown at the usual starting temperature of 950°C but with no cool down. The temperature gradient was expected to be produced by the H_2 gas flow of 1.0 lpm into the slider base under the substrates. Very poor surface morphology resulted with clear evidence of substrate dissolution on many areas. It was clear that any temperature gradient induced by the H_2 gas was inadequate. An additional factor inhibiting the success of this experiment is that it was performed before the previously discussed improved furnace temperature profile was established.

Carrier Concentration

While retrograde solubility curves for impurities in solids are known to exist, it is generally true that more dopants can be incorporated into a semiconductor when the crystal is grown or diffusion is performed at a higher temperature. Thus, the growth temperature selected for beginning experiments was the minimum value that, because of the steep temperature dependence of the GaP - Ga solubility relation, would permit the growth of adequate layer thickness with a reasonable growth temperature range. That growth temperature interval was 950°C to 920° ±10°C. LPE 21, however, ran from 993° to 950°C. The surface of this sample was so rough, (Figure 20) that no carrier concentration measurements were made. Since it was felt that thermal erosion of the substrate before initiation of growth was the probable cause, no further high temperatures growths were performed. Similar very poor surfaces which resulted in LPE 17A (see Figures 21 and 22) were also attributed to thermal erosion of the substrate before growth. This run used a relatively low temperature (850°C) bake but for a very long time (72 hours). The carrier concentration for this run was 6 to 8 x 10^{16} cm^{-3}, which showed no benefit for such a bake.

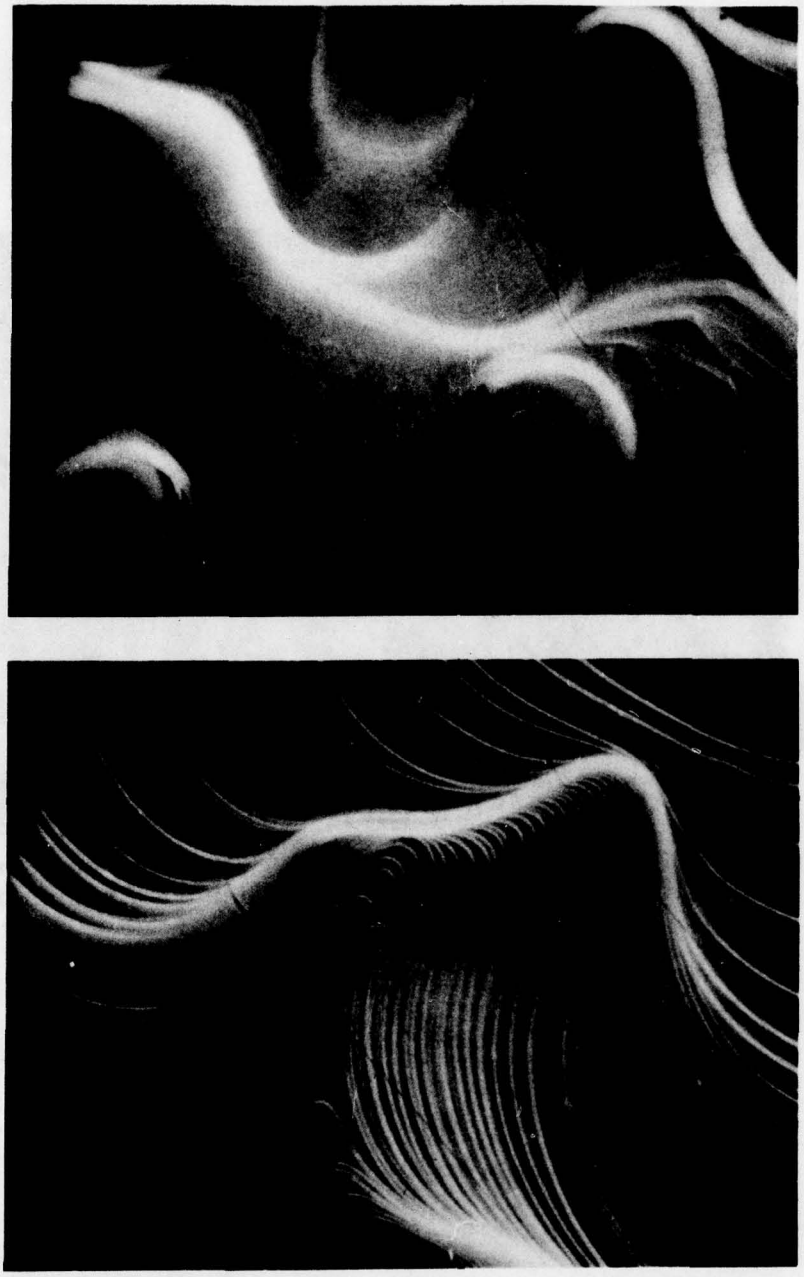

Figure 20. Microphotographs of LPE 21A and 21B Showing Poor Surfaces Related to High-Growth Temperatures (993°C to 950°C)

Figure 21. Microphotograph of LPE 17A Showing Poor Surface Morphology Resulting from Thermal Erosion of the Substrate Prior to Growth

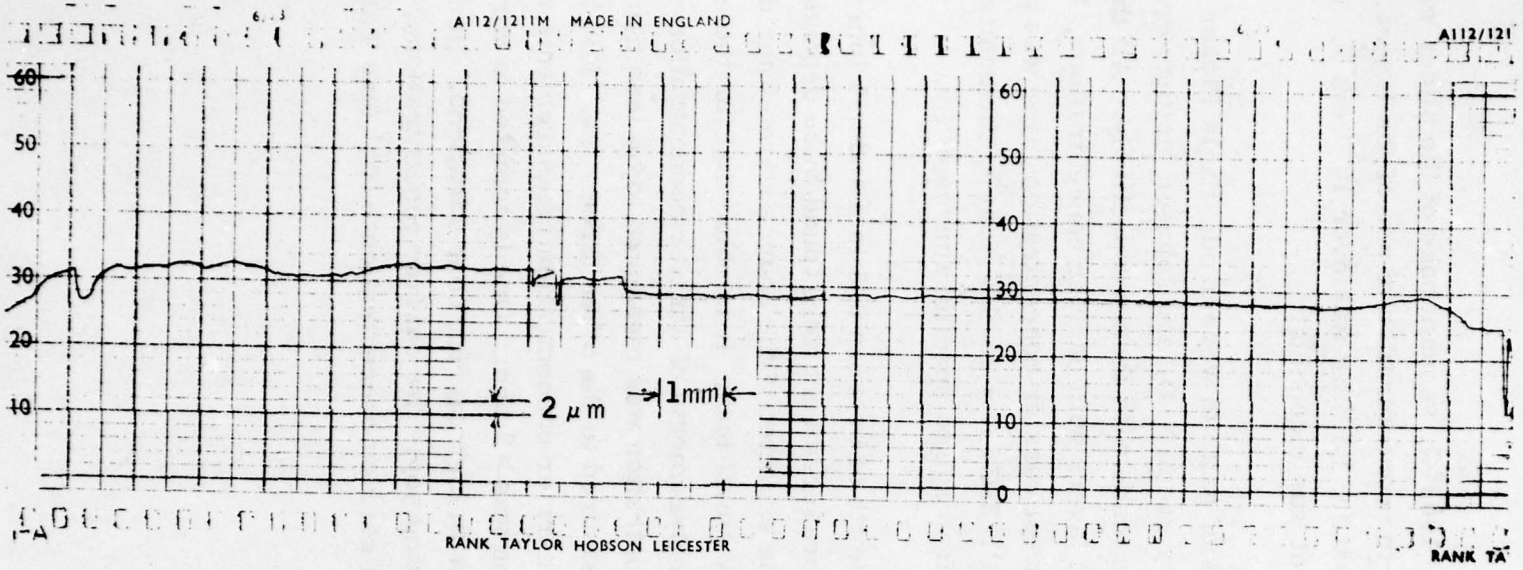

Figure 22. Surface Profilometer Trace of LPE 17A

A preloading, 12-hour, 1000°C, vacuum bake of the slider was tried with LPE 8. While the carrier concentration of one of the layers, LPE 8A was in the mid-10^{15} cm^{-3} range, LPE 8B was over 10^{16} cm^{-3}. Consequently, the effect of the bake-out was inconclusive.

Three different sources of gallium were used: Eagle Picher grade 7-9's, Canyonlands 21st Centry grade N.D. and Johnson Matthey grade A1. Thirty-four, 2 and 6 runs were made with them respectively. All three sources of Ga produced some LPE layers with carrier concentrations, $10^{15} < n < 10^{16}$ cm^{-3}. Although the lowest carrier concentration layer was grown with Johnson Matthey Ga (LPE 39C, $N = 2 \times 10^{15}$ cm^3), the scatter in data precludes assigning any advantage to specific source of Ga.

H_2 flow rates during growth of between 0.5 lpm and 3.5 lpm were used. Oxygen concentration measurements were found to be dependent upon the H_2 flow rate as would be expected if the source were either degassing of internal parts or a very small leak. It is noted that for the eight runs in which at least some measurements of carrier concentration $<10^{16}$ were made, the oxygen concentration was measured to be less than 1 ppm in five of them. It was not measured in the other three runs. For the two runs in which a majority of the carrier concentration measurements were $>10^{17}$ cm^{-3}, the oxygen concentration was >2 ppm. One is tempted to correlate high oxygen concentrations with high carrier concentrations. However, note that, even in the runs producing some low carrier concentrations, there were also some measurements of carrier concentration $>10^{17}$ (see Table 4).

TABLE 4. CARRIER CONCENTRATION, OXYGEN CONCENTRATION AND HYDROGEN FLOWRATE FOR SELECTED LPE GROWTH RUNS

LPE Run and Layer #	Carrier Concentration N, cm^{-3}	O_2 Concentration	H_2 Flow Rate
4A	$6 - 30 \times 10^{15}$	0.2 ppm	3.5 lpm
B	5×10^{15}		
8A	$2 - 7 \times 10^{15}$	0.4	3.5
B	$10^{16} - 10^{17}$		
19A	$3 - 10 \times 10^{15}$		
B	$8 - 12 \times 10^{16}$	0.6	1.0
C	$8 - 12 \times 10^{16}$		
22A	$6 - 8 \times 10^{15}$		
B	$5 - 70 \times 10^{16}$	---	0.5
C			
26A	$8 - 24 \times 10^{15}$		
B	$1 - 3 \times 10^{16}$	---	0.5
C	$9 - 20 \times 10^{15}$		
30A	$8 - 20 \times 10^{15}$		
B	---	0.6	1.0
C	---		
33A	---		
B	$5 - 6 \times 10^{15}$	0.4	1.0
C	3×10^{15}		
39A	---		
B	$1 - 7 \times 10^{15}$	---	1.0
C	$2 - 7 \times 10^{17}$		
15A	$5 - 7 \times 10^{17}$		
B	2×10^{17}	2.4 ppm	1.2
C	$1 - 3 \times 10^{17}$		
D	$7 - 8 \times 10^{16}$		
20A	1×10^{17}		
B	2×10^{17}	2.2	0.5
C	5×10^{17}		

Most of the LPE growth runs were made on Czochralski-grown GaP substrates that were purchased from Cambridge IMANCO. (Cambridge IMANCO Division, Cambridge Instrument Inc., 40 Robert Pitt Drive, Monsey, N. Y.) Both n-type and p-type substrates were used. One growth run, LPE 35, used the SSD GaP grown in this program. There was no indiciation that the conductivity type of the substrate played a role in the carrier concentration of the LPE layer. If any substrate dissolution had occurred, there may have been an effect. The carrier concentration of the LPE layers grown on substrates prepared from SSDC-4 was 1 - 2 x 10^{16} cm^{-3}. This value is toward the low end of range for all the layers grown but is by no means the best (see Table 4).

Three types of GaP were used to saturate the gallium melt and act as source material for the LPE layer growth: polycrystalline dense ingot (PDI) GaP; Czochralski single-crystal GaP; and random-nucleated-solution (RNS) grown GaP. The first two were obtained from Cambridge-IMANCO and the third was prepared in this program and described in the section on "Bulk Solution Growth." The PDI GaP was nominally undoped, as described by the supplier. The carrier concentration could not be determined by either Hall or C-V measurements because of its polycrystalline nature. The Czochralski GaP was the same as the nominally undoped (but n-type) single-crystal material used for most of the substrates. Its carrier concentration was mid-10^{16} cm^{-3}. The RNS material had a carrier concentration of 4 x 10^{16} cm^{-3}. LPE layers with carrier concentration < 10^{16} cm^{-3} were grown with all three types of source material. No systematic differences were observed.

Surface Morphology

The ability to produce flat, highly polished and etched substrate surfaces, which is essential for the growth of smooth flat LPE layers, was found to depend not only on the polishing and etching techniques employed, but upon the particular substrate material used, n-type and p-type Czochralski GaP from several ingots was used, as well as SSD single-crystal GaP.

The polishing and etching procedure that was found to be most successful and was used with some slight modifications for all LPE runs was performed as follows: GaP wafers approximately 0.022 inch thick were mounted on a lapping block with bees wax and were hand lapped using 3.0 μm alumina abrasive on a glass lap. The wafer thickness was reduced to ~ 0.015 inch. The wafer was then chemically polished to ~ 0.013 inch by machine on a polyurethane lap using a 1 to 3 percent bromine-methanol solution. It was found essential to flood the wafer with clean methanol when removing it from the bromine-methanol solution in order to avoid permanent stains. The wafers were then removed from the lapping block and coated with beeswax. The beeswax protected the polished surface of the wafer as it was wire-sawed to correct substrate dimensions. Just before loading the substrates into the slider for a run, the beeswax was removed with chloroform. An attempt was made to use fumed silica to jell the bromine-methanol solution. This proved very difficult to work with and gave no advantage.

Additional, short, bromine-methanol polishes immediately prior to loading gave no advantage in better LPE layer surface morphology.

The effects of substrate condition on the LPE layer surface morphology is shown in Figure 23. LPE 35B was grown on a substrate with a substantial number of pits and scratches apparent in the substrate. Many of these features are carried through the LPE layer growth. Figure 24 shows dramatically better surface resulting from much more highly polished and etched substrates.

Previous experience had shown that one particular boule of Czochralski GaP had yielded excellent surfaces when free-etched from a lapped surface in a potassium ferricyanide etch. That etch and three acid etches were tried on the Czochralski GaP that served as the substrate material for most of the runs performed. Aqua regia (nitric acid and hydrochloric acid) hydrofluoric acid and sulfuric acid were the three acid etches tried. In all the cases, the acid etches produced pits on the surface of the sample. Variations in the concentration of etches were also examined, but in each case the results were the same.

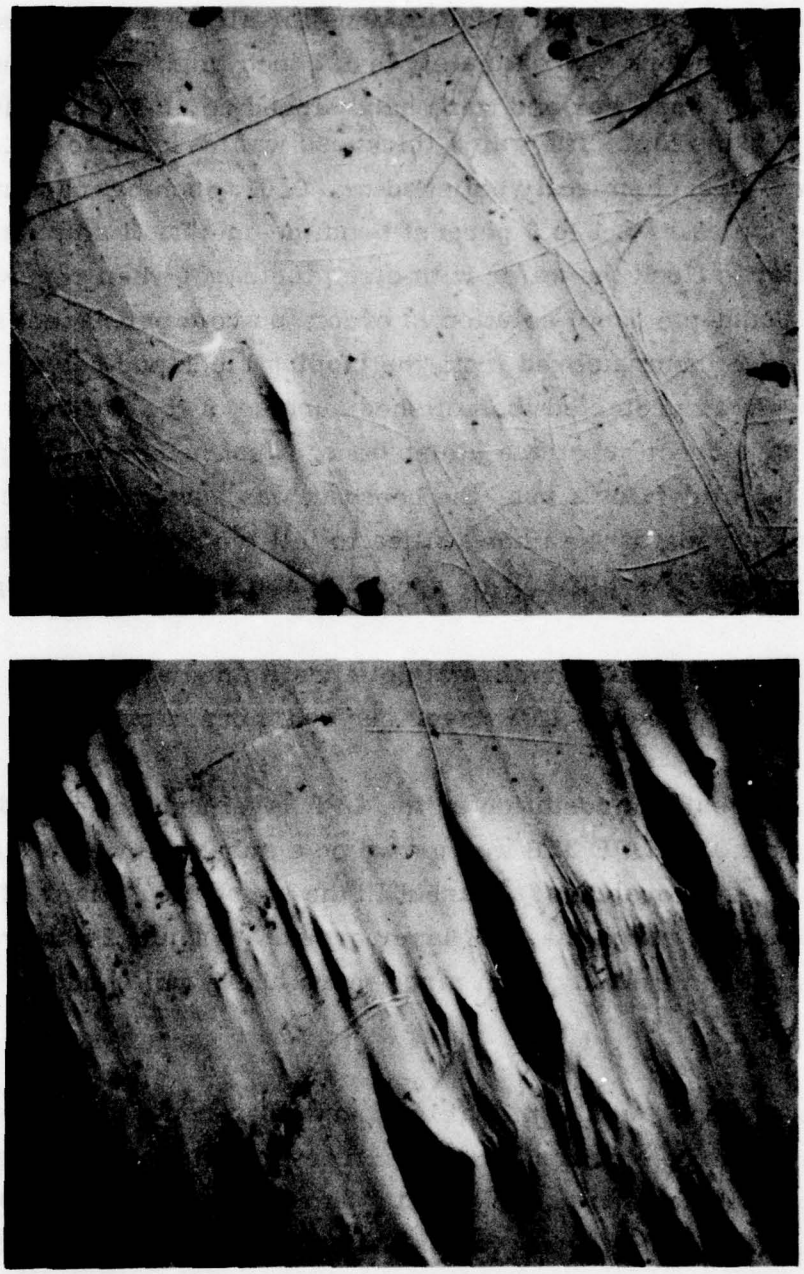

Figure 23. Microphotographs of LPE 35B Showing Results of Poor Substrate Surface Preparation (Scratches and pits have been carried through LPE layer)

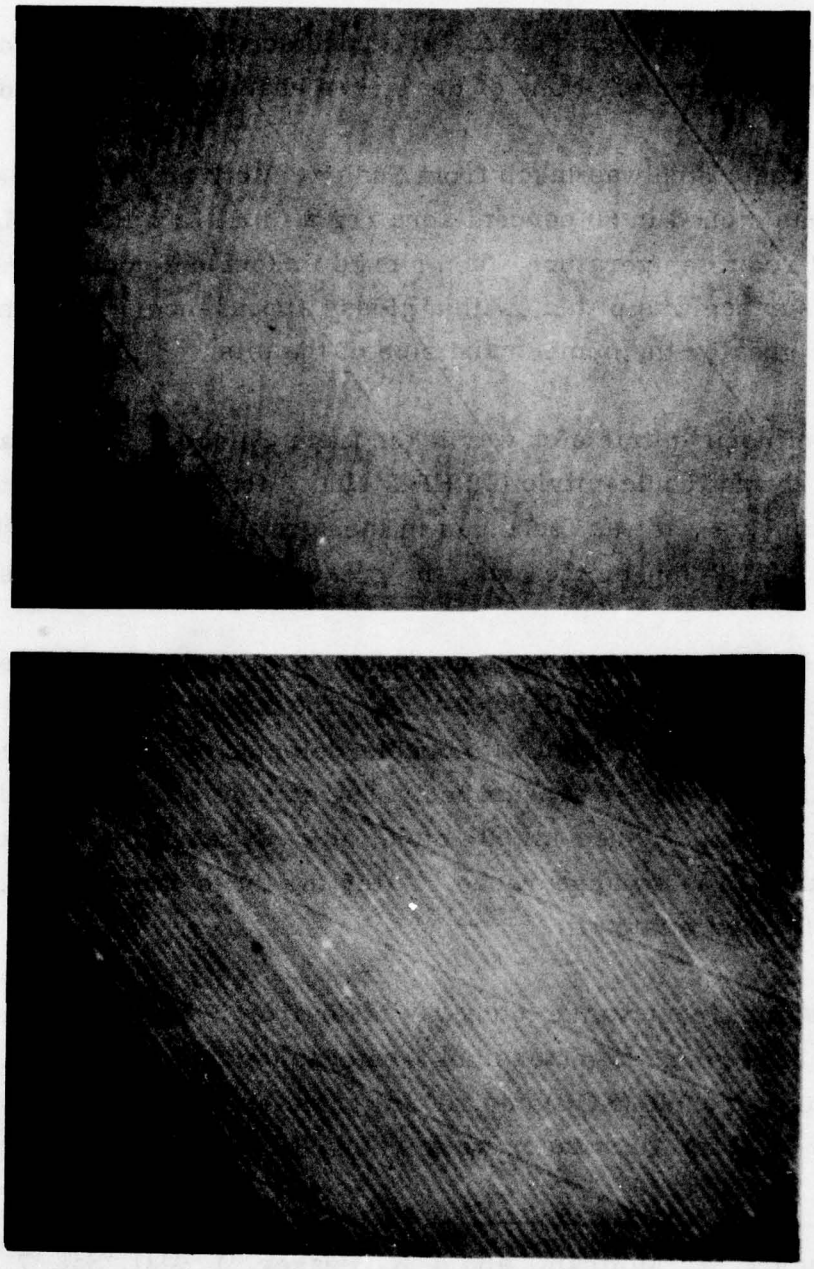

Figure 24. Microphotographs of LPE 20A and 44A Showing Excellent Surface Morphology Associated with Optimal Substrate Preparation (Closely spaced lines are very shallow growth terraces, other parallel lines are result of slide-off)

The potassium ferricyanide etch, produced scratch-like features on the surface of the sample. None of the etches examined were found usable.

The aqua regia etch was taken from Sudlow, Mottram, and Peaker[2]. The sample was etched in 50 percent aqua regia (3 HCL: 1 HNO_3:4H_2O) for one minute at room temperature, then rinsed in double deionized water. The polished surface was pitted, with a glossy appearance. The longer the etch time, the greater the number and size of the pits.

The hydrofluoric-nitric etch was taken from Chicotka[3]. The sample was etched in hydrofluoric-nitric (18 HF:2 NHO_3) for 30 seconds and then again for two minutes. It was found, as in the aqua regia etch, that the surface was pitted. The longer the etch, the greater the number of pits.

The hydrochloric-sulfuric etch was taken from Hajkova and Fremunt[4]. The etch consisted of HNO_3:2 H_2SO: 2 H_2O. The sample was placed in the etch for 30 seconds, then rinsed with double-deionized water. The surface was rough, but had a glossy appearance. The sample was examined again after a two-minute and a three-minute etch. In each case, the surface remained rough with the glossy appearance. After the three-minute etch, the surface had also formed pits on it.

The potassium ferricyanide etch was taken from Plauger[5]. The etch consisted of 32.9 grams of potassium ferricyanide ($K_3Fe(CN)_6$), 2.8 grams potassium hydroxide (KOH) and 100 ml of water. The sample was first etched at 60°C for 10 minutes while being stirred. The sample was then

---

[2]P. D. Sudlow, A. Mottram, and A. R. Peaker, J. Mat. Sci. 7, 168 (1972).

[3]R. J. Chicotka, Method of Polishing GaP, U. S. Patent 3,679,501.

[4]E. Hajkova and Fremunt, R., Phys. Stat. Sol. (a) 10, K35 (1972)

[5]L. R. Plauger, J. Electrochem Soc., 121, 455 (1974).

rinsed in double deionized water and blown dry. The polished surface was covered with scratches. The sample was then etched at 40°C in a stirred solution for 30 minutes. Additional scratches were produced.

The cool-down rate during growth was 20°C/hour for the first 21 growth runs. For the succeeding runs it was increased to 35°C/hour. There was no evidence of any difference in surface morphology (or layer thickness uniformity) due to this change in the cool-down rate. An unintentional test of a much higher (but unmeasured) cool-down rate also showed no adverse effects on either of these layer properties. In LPE 2, the slider became disconnected from the H_2 flow tube and as a result the growth bin remained on the substrate during the rapid cool down after the furnace is rolled away from the slider.

The purpose for bringing the H_2 gas into the base of the slider (Figure 13) was to produce a small temperature difference across the growth interface. Maintaining the substrate at a lower temperature than the melt is intended to eliminate constitutional super cooling and a resultant unstable growth interface. As previously discussed, bringing the H_2 into the base of the slider must have produced a very small, if any, temperature gradient since no growth occurred under isothermal conditions. Several experiments were performed in which the H_2 gas was brought in the end cap of the growth tube instead of into the base of the slider. No deleterious effect on surface morphology was noted.

One growth run, LPE 34, was performed on substrates oriented in the <100> direction. All others were oriented in the $<\bar{1}\bar{1}\bar{1}>$ direction. The surface morphology of LPE 34 was similar to other runs grown under the same conditions. Figure 25, a microphotograph of LPE 34C, shows a relatively small density of surface features. The long parallel lines resulted from small streaks of gallium left behind after slide-off.

Figure 25. Microphotograph of LPE 34C, Grown on a <100> Oriented Substrate Shows Good Surface Morphology

Annealing Studies

The first series of anneals was to determine a useable temperature range and phosphorus pressure. The anneals were carried out in evacuated sealed quartz ampules with the GaP samples placed in a pyrolytic boron nitride boat inside the ampule. The phosphorous was placed in the ampoule outside of the boat. Prior to annealing, the samples were lapped and then polished with bromine-methanol in a manner very similar to that used for LPE substrate preparation. The results of these experiments showed that excessive thermal decomposition occurred over 950°C when the annealing times were several days. In fact, anneals over 1000°C resulted in complete disappearance of the samples. At 900°C the surfaces remained sufficiently smooth to permit evaluation. The anneals were performed on groups of undoped Czochralski-grown GaP samples and sections of LPE-grown samples. The Czochralski crystals were from the same boule which provided most of the LPE substrates.

In each case, neighboring samples from the same Czochralski wafer or LPE layer were saved for evaluating the unannealed condition. Enough phosphorus was placed in the ampule to give a pressure of 1 atm. The anneals were carried out at 900°C for from 3 to 5 days.

Both the Czochralski and LPE samples converted from n-type conductivity to p-type conductivity. This was an unexpected result, since the stoichiometric defeats in GaP are not known to be shallow donors or acceptors. The gallium vacancies are suspected of being active in complex centers involving other impurities, but the interaction producing the conversion from n-type conductivity to p-type is unknown. Such change, of course, prohibited any meaningful comparisons of minority carrier lifetime or photoconductive lifetime before and after annealing since the type of carrier changed.

MATERIAL EVALUATION

A comprehensive material evaluation program was carried out in parallel with the materials growth program. The principal techniques which were used to evaluate the material were: Hall and resistivity, capacitance-voltage characteristics of Schottky barriers, photocapacitance for deep-level characterization, minority carrier lifetime, and etch-pit density. This section discusses the results of these measurements on the material which was grown during this program.

Transport Measurements

Hall-effect measurements are a primary means of identifying and quantitatively measuring the impurities in a semiconductor. We have used this technique to evaluate samples from all of the bulk (SSD and RNS) growth runs which produced useable boules. We also performed Hall analysis on n-type LPE layers which were grown on p-type substrates and hence amenable to Hall measurements. All of the Hall and resistivity data were taken using the van der Pauw technique.

For the bulk grown material, the Hall samples were cut from the boule using a wire saw and lapped flat with 1 μm abrasive on cloth. The work damage was removed by a chemical polish in a hot potassium ferricyanide etch. For the p-type samples ohmic contacts were achieved by alloying (at 420°C) small dots of In:1% Zn at the periphery of the sample. Ohmic contacts to the n-type samples were made by alloying small dots of In:1% Te at 680°C. All of the contact anneals were done in a hydrogen atmosphere. Prior to measurement the contact linearity was checked by measuring the I-V characteristic.

The Hall samples for the LPE samples were fabricated by placing a clover-leaf mask over the layer and sandblasting or etching away the epitaxial material outside the boundaries of the mask. The epitaxial layers were typically less than 10 μm thick so this technique was easy to implement. Ohmic contacts were made in a similar manner to that described for the bulk material.

The material parameters which are readily available from Hall and resistivity analysis are: 1) majority carrier type and concentration, 2) majority carrier activation energy, 3) concentration of the principal donor and acceptor and 4) the temperature dependence of the resistivity and the majority carrier mobility. In this subsection, we will present and discuss the Hall data first for the SSD material, next for the RNS material, and finally for the LPE material. The implications of these results to the material growth are discussed at the beginning of Section III.

To investigate the uniformity of the material grown by the SSD technique, two Hall samples were cut from the SSD C-6 boule: one sample was near the tip, and the other near the tail of the boule. The carrier concentration versus $10^3/T$ for both of these samples is plotted in Figure 26. Note that the majority carriers freeze-out in this p-type material as the temperature is lowered. This behavior is due to the primary acceptor level in this case being several KT from the valence band edge at $T \lesssim 100$ K. Note also that the carrier concentrations for these two undoped samples are within ±10% of each other. This demonstrates that the SSD technique can, in fact, be used to grow rather uniform boules of GaP.

In Figure 27, the Hall coefficient for four SSD grown samples is plotted as a function of reciprocal temperature. The Hall coefficient is approximately given by

$$R_H = \frac{1}{pe} , \qquad (1)$$

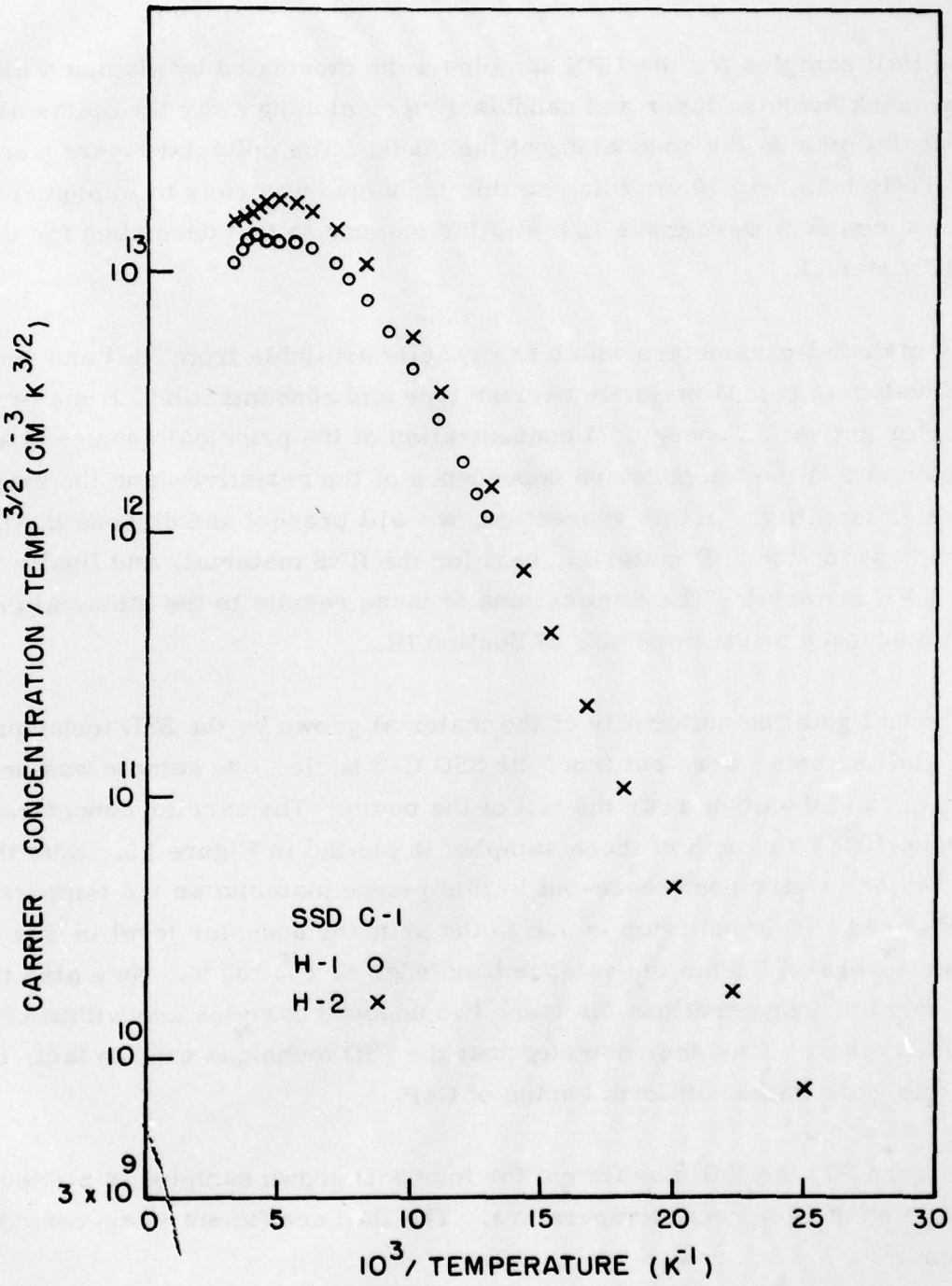

Figure 26. Temperature Dependence of the Carrier Concentration for Two Hall Samples From Run SSD C-1

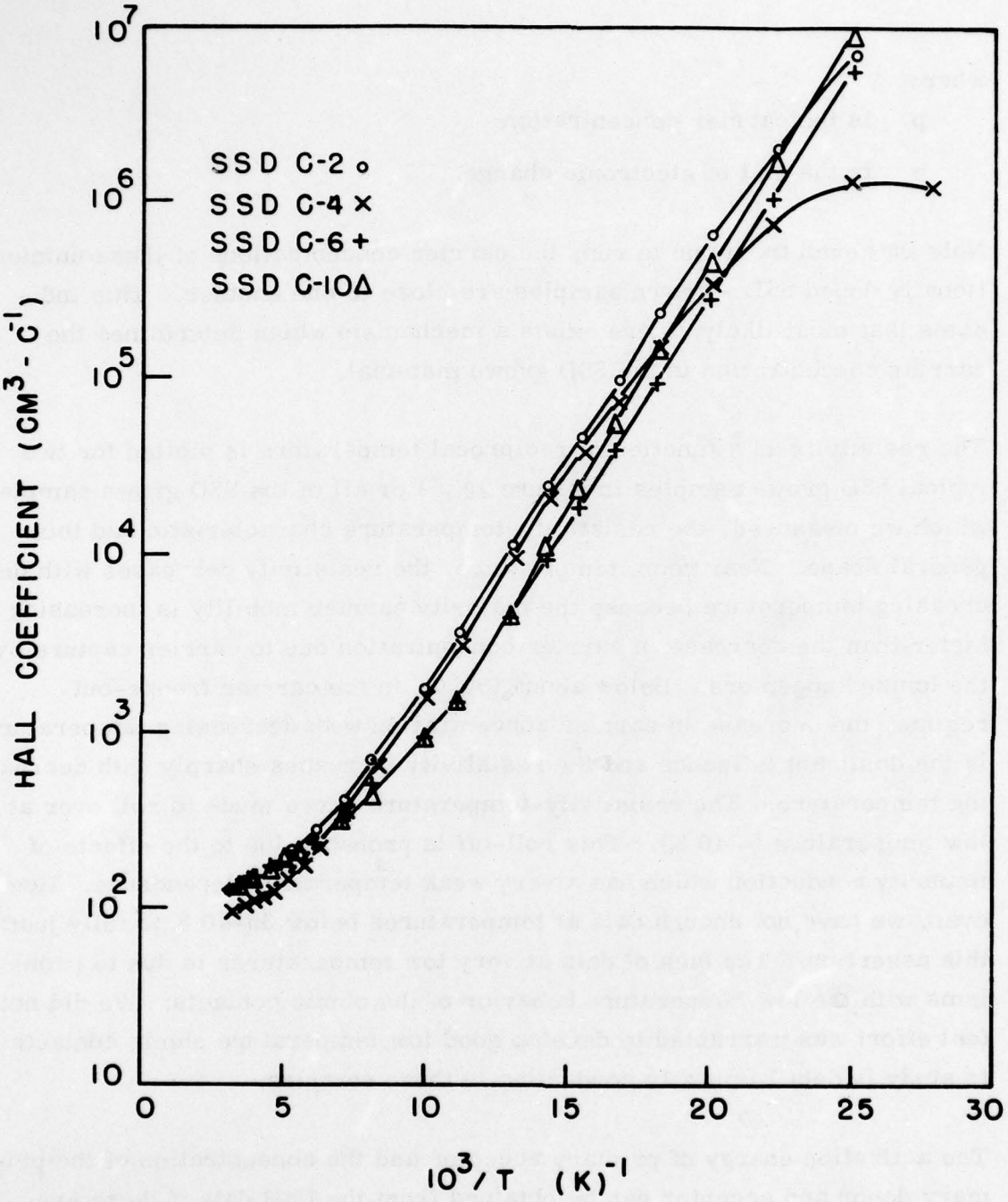

Figure 27. Temperature Dependence of the Hall Coefficient for Four SSD Samples

where

p is the carrier concentration

e is the unit of electronic charge.

Note that even from run to run, the carrier concentrations of these unintentionally doped SSD - grown samples are close to one another. This indicates that most likely, there exists a mechanism which determines the carrier concentration in the SSD grown material.

The resistivity as a function of reciprocal temperature is plotted for two typical SSD grown samples in Figure 28. For all of the SSD grown samples which we measured, the resistivity-temperature characteristic had this general shape. Near room temperature, the resistivity decreases with decreasing temperature because the majority carrier mobility is increasing faster than the decrease in carrier concentration due to carrier capture by the ionized acceptors. Below about 150°C, in the carrier freeze-out regime, the decrease in carrier concentration with decreasing temperature is the dominant influence and the resistivity increases sharply with decreasing temperature. The resistivity-temperature curve tends to roll over at low temperature ($\sim$ 40 K). This roll-off is probably due to the effects of impurity conduction which has a very weak temperature dependence. However, we have not enough data at temperatures below 35-40 K to fully justify this assertion. The lack of data at very low temperatures is due to problems with the low temperature behavior of the ohmic contacts. We did not feel effort was warranted to develop good low temperature ohmic contacts to study in detail impurity conduction in these samples.

The activation energy of primary acceptor and the concentration of the primary donor and acceptor can be obtained from the Hall data if there are single dominant donor and acceptor species, and if the carrier densities are low enough that the carrier statistics are nondegenerate. For the

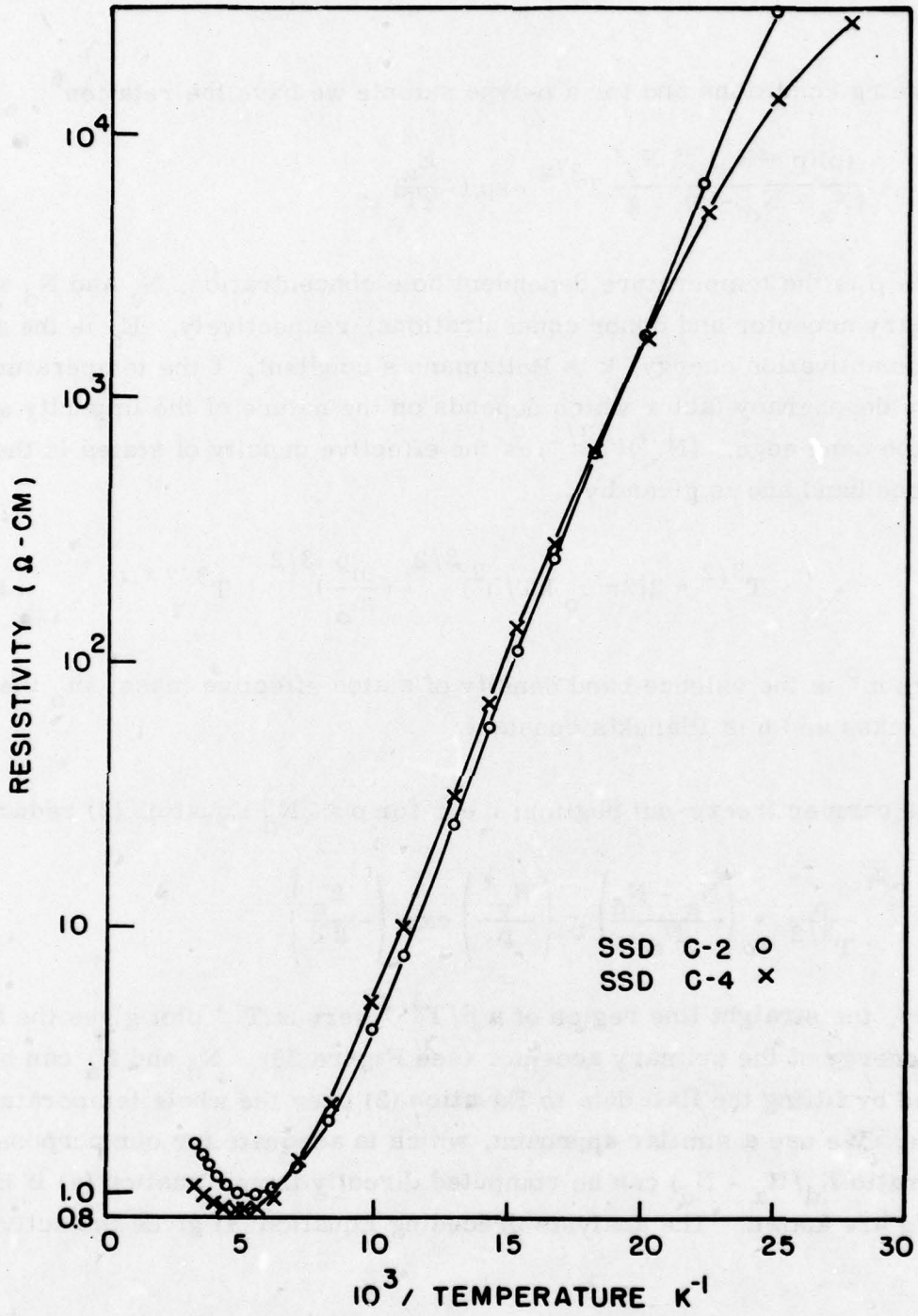

Figure 28. Temperature Dependence of the Resistivity for Two SSD-Samples

foregoing conditions and for a p-type sample we have the relation[6]

$$\frac{(p)(p + N_d)}{(N_a - N_d - p)} = \frac{N_v'}{g} T^{3/2} \exp\left(-\frac{E_a}{kT}\right) , \tag{2}$$

where p is the temperature dependent hole concentration, N_a and N_d are the primary acceptor and donor concentrations, respectively. E_a is the acceptor activation energy, k is Boltzmann's constant, T the temperature and g is a degeneracy factor which depends on the nature of the impurity state and the band edge. $(N_v')(T^{3/2})$ is the effective density of states in the valence band and is given by

$$N_v' \cdot T^{3/2} = 2(2\pi m_o kT/h^2)^{3/2} \cdot \left(\frac{m^p}{m_o}\right)^{3/2} \cdot T^{3/2} \tag{3}$$

where m^p is the valence band density of states effective mass, m_o the electron mass and h is Planck's constant.

In the carrier freeze-out regime; i. e., for $p \ll N_d$ Equation (2) reduces to

$$\frac{p}{T^{3/2}} = \left(\frac{N_a - N_d}{N_d}\right) \cdot \left(\frac{N_v'}{g}\right) \exp\left(-\frac{E_a}{kT}\right) \tag{4}$$

Hence, the straight line region of a $p/T^{3/2}$ versus T^{-1} plot gives the activation energy of the primary acceptor (see Figure 26). N_d and N_a can be obtained by fitting the Hall data to Equation (2) over the whole temperature range. We use a similar approach, which is adequate for our purpose. The ratio $N_d/N_a - N_d)$ can be computed directly from Equation (4) if E_a and N_v'/g are known. The analysis preceding Equation (4) gives the activation

---

[6] J. S. Blakemore, Semiconductor Statistics, Pergamon Press, New York (1962).

energy. The work of van der Does de Bye and Peters[7] gives $4.2 \times 10^{14} \leq N_v'/g \leq 1.1 \times 10^{15}$. $N_a - N_d$ can be obtained by extrapolating the Hall coefficient versus reciprocal temperature characteristics to zero (see Figure 27). Hence, N_a and N_d are obtained to better than factor of two. The values of E_a, N_d and N_a, so calculated for two BSG runs and four SSD runs are tabulated in Tables 5 and 6.

From the data in Table 5, we see that all of the SSD-growth runs were p-type with an activation energy around 40 meV, which is the activation energy for carbon in p-type GaP.[8] We conclude that all of the SSD-grown GaP was carbon-doped. The reason for this behavior was thoroughly investigated during this program and is discussed in some detail earlier in Section III.

Turning now to the mobility in the SSD-grown p-type material, there are three scattering mechanisms most prevalent which limit the mobility in a semiconductor: 1) lattice scattering, 2) impurity scattering, and 3) scattering due to inhomogeneities or local space charge regions. We will examine each of these mechanisms to determine its influence on the mobility in the p-type material.

The experimentally determined mobility of Hall samples from nine different SSD growth runs is plotted as a function of temperature in Figures 29 through 31. (Note that each of these plots has a similar characteristic shape.) As temperature is decreased from room temperature, the mobility increases with a power dependence $\sim T^{-2.4}$. Around 100 K, the mobility rolls over and begins to decrease as the temperature is further decreased. Then, for temperatures lower than ~ 40 K, the mobility drops precipitously with decreasing temperature.

---

[7] J. A. W. van der Does de Bye and R. C. Peters, Phillips Res. Repts. 24, 210 (1969).

[8] M. Neuberger III-V Semiconducting Compounds IFI/Plenum (1971).

TABLE 5. TABULATION OF HALL DATA FROM BULK GROWN MATERIAL

Growth Run Number	Carrier Type	Room Temperature Carrier Concentration (cm^{-3})	Principal Acceptor Activation Energy (meV)	Mobility at 300 °C cm^2/V-sec	Mobility at 77°C cm^2/V-sec
SSD C-1	p	8.00×10^{16}	42.2	84.2	416
SSD C-2	p	4.5×10^{16}	42.2	90.1	440
SSD C-3	p	1.01×10^{17}	39.7	92.1	382
SSD C-4	p	6.28×10^{16}	37.5	94.4	314
SSD C-6	p	4.46×10^{16}	44.1	106.0	1251
SSD C-8	p	1.34×10^{17}	41.8	86.8	854
SSD C-9	p	9.46×10^{16}	40.5	93.5	1429
SSD C-10	p	4.32×10^{16}	47.2	87.0	1040
SSD C-11	p	5.42×10^{16}	46.7	83.6	948
RNS C-1	n	8.02×10^{17}	38.4	61.9	101.9
RNS C-2	n	3.53×10^{16}	74	155.0	585
RNS C-3	p	1.17×10^{17}	--	68.3	--

TABLE 6. COMPARISON OF IMPURITY DENSITIES DETERMINED FROM THE HALL DATA AND FROM THE IONIZED IMPURITY EXPRESSION FOR MOBILITY FOR THE SSD GROWN MATERIAL

Growth Run Number	Donor Density (cm^{-3})		Acceptor Density (cm^{-3})	
	Hall Data	Mobility Expression	Hall Data	Mobility Expression
SSD C-1	7.16×10^{16}	1.15×10^{17}	2.02×10^{17}	2.45×10^{17}
SSD C-2	5.72×10^{16}	6.06×10^{16}	1.23×10^{17}	1.31×10^{17}
SSD C-3	1.31×10^{17}	1.15×10^{17}	2.11×10^{17}	1.95×10^{17}
SSD C-4	1.82×10^{17}	1.5×10^{17}	2.92×10^{17}	2.15×10^{17}
SSD C-6	1.86×10^{16}	1.6×10^{16}	9.26×10^{16}	7.6×10^{16}
SSD C-8	3.78×10^{16}	3.0×10^{16}	2.38×10^{17}	2.3×10^{17}
SSD C-9	2.8×10^{16}	1.7×10^{16}	1.58×10^{17}	1.47×10^{17}
SSD C-10	1.79×10^{16}	2.2×10^{16}	7.59×10^{16}	8.0×10^{16}
SSD C-11	1.74×10^{16}	2.9×10^{16}	1.05×10^{17}	1.17×10^{17}

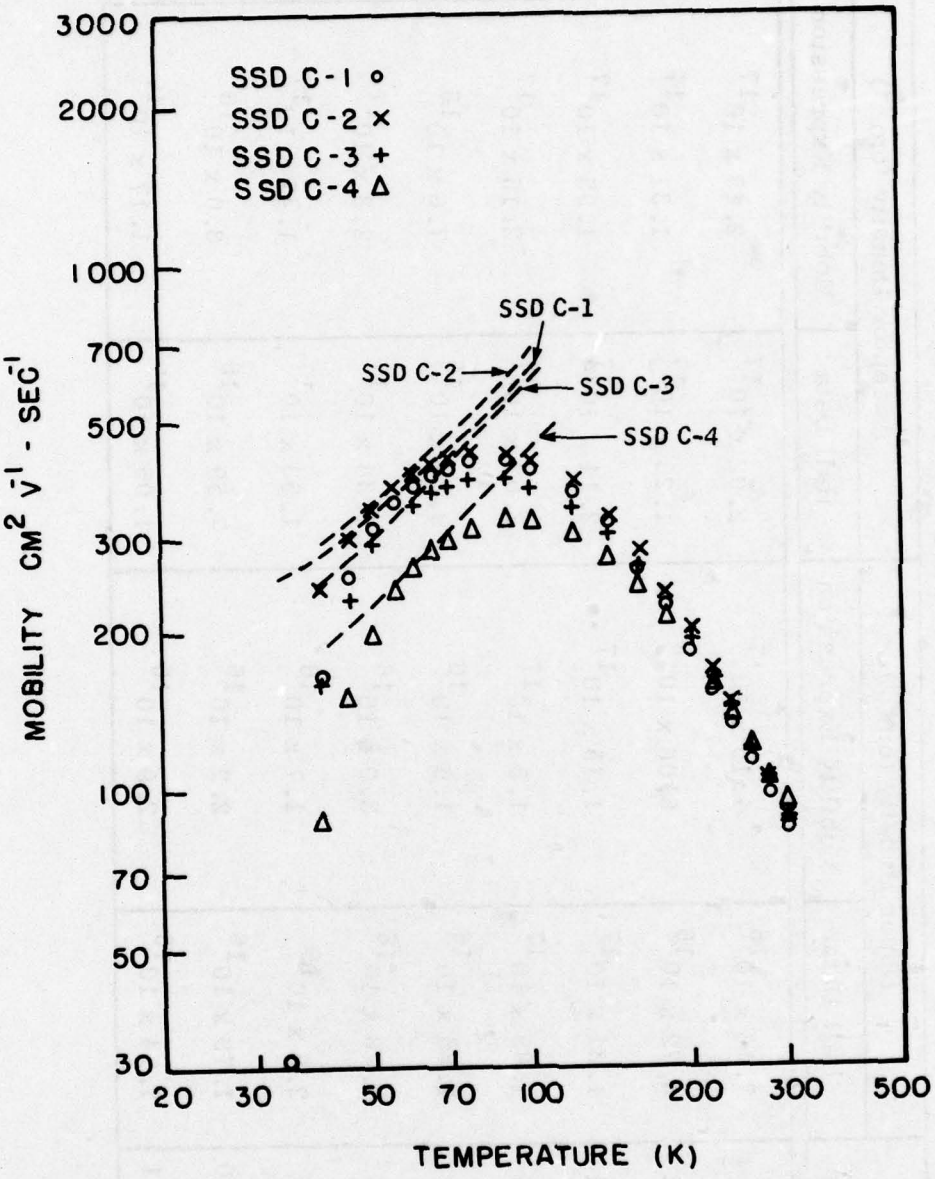

Figure 29. Temperature Dependence of the Mobility for SSD C1 → C4

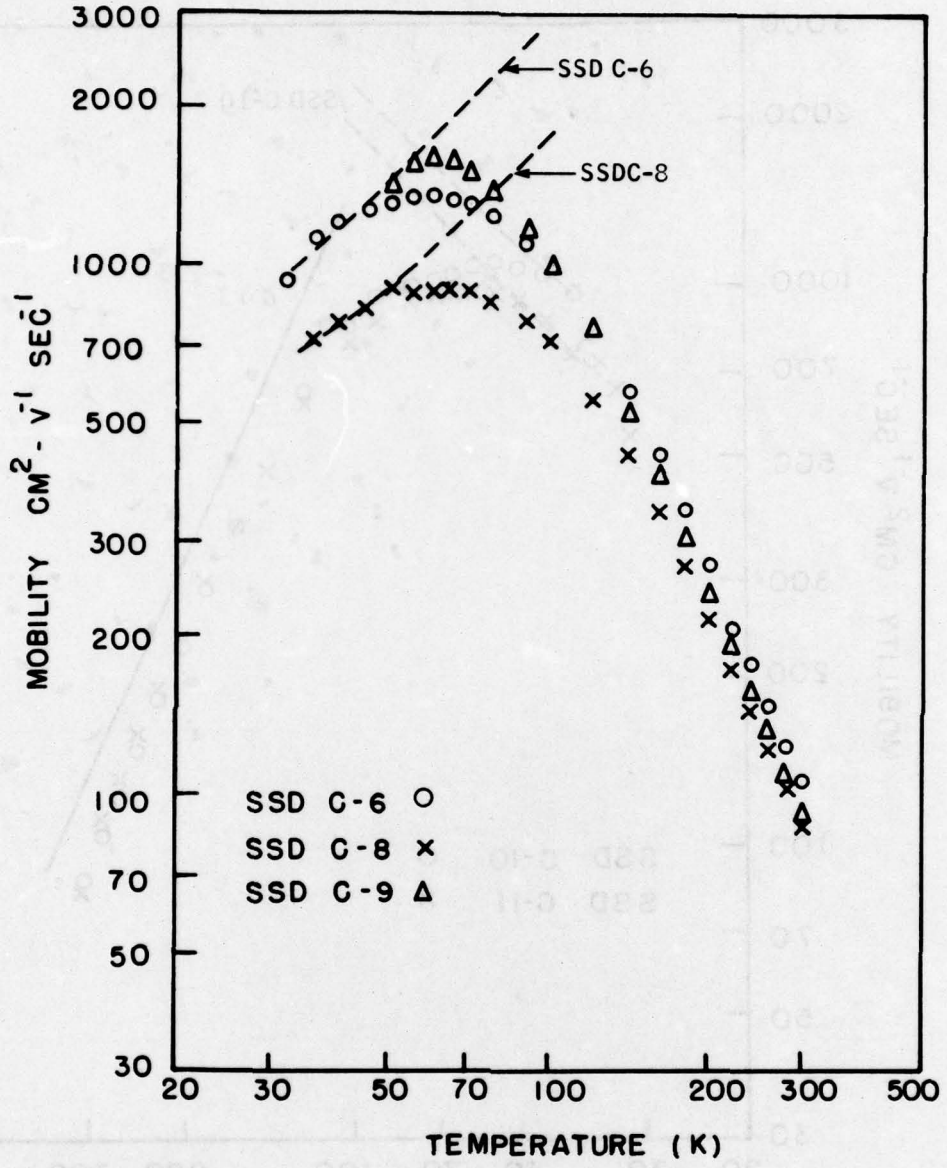

Figure 30. Temperature Dependence of the Mobility for SSD C-6, C-8, and C-9

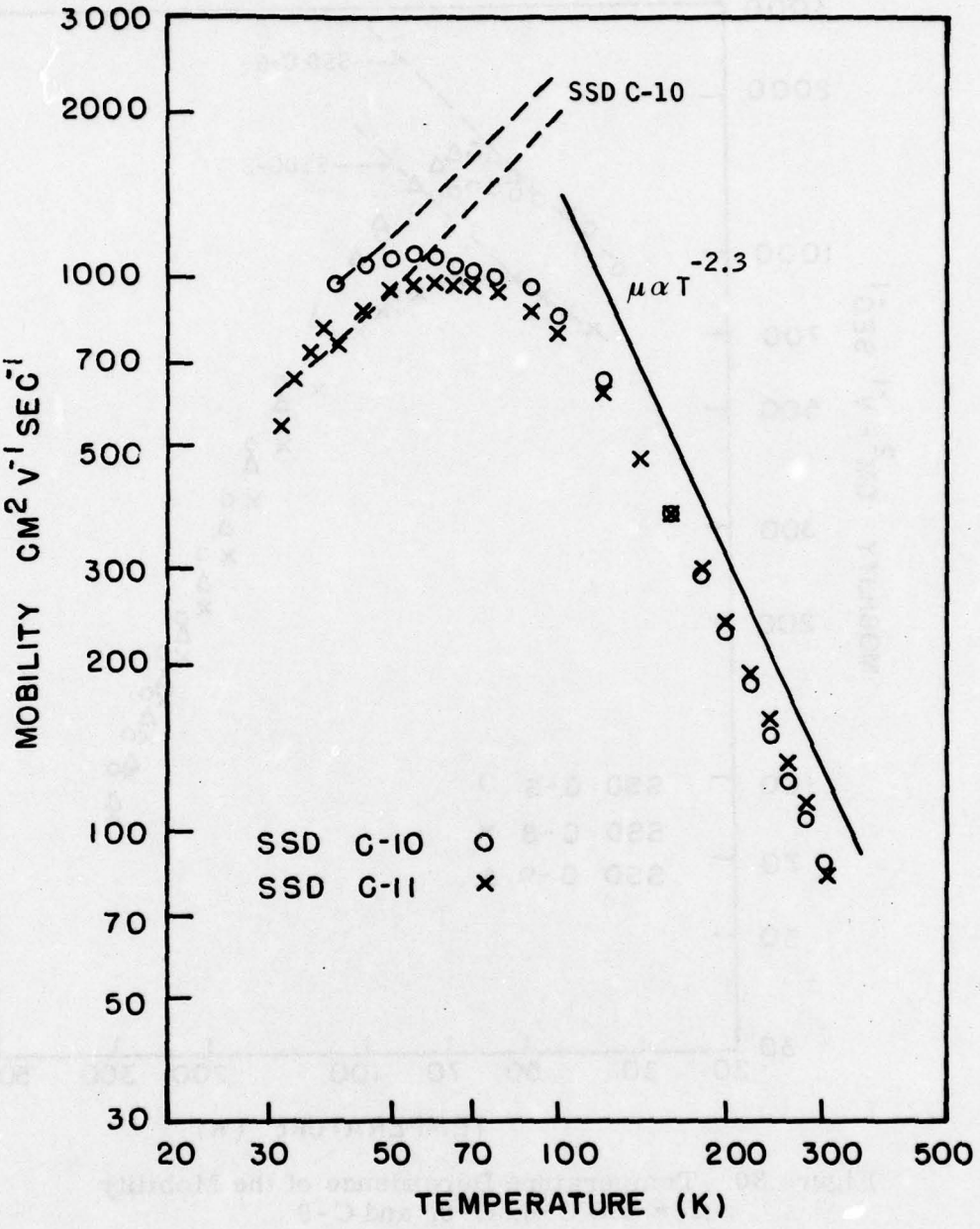

Figure 31. Temperature Dependence of the Mobility for SSD C-10 and C-11

To interpret the temperature dependence of the mobility plots of these data, we first consider the effects of lattice scattering. Casey, et al.,[9] evaluated the familiar $T^{-3/2}$ expression of Bardeen and Shockley[10] for the mobility when limited by acoustic phonon scattering and found the following expression for GaP:

$$\mu_{AC} = 5.6 \times 10^7 / [(\frac{m^*}{m_o})^{5/2} E_1^2 T^{3/2}] \text{ cm}^2/\text{Vsec} . \quad (5)$$

Here, E_1 is the volume deformation potential in eV and m* the effective mass. (Note that the temperature dependence of μ_{AC} goes as $T^{-3/2}$.) However, for the experimentally determined mobility (see Figures 29 through 31), the temperature dependence goes as $T^{-2.3}$ in the region from 300 K to ~ 120 K. Hence, the mobility around room temperature cannot be solely accounted for by acoustic mode scattering.

Ehrenreich[11] has calculated the mobility when polar optical phonons are the dominant scattering mechanism. He finds the following expression for polar mode limited mobility:

$$\mu_{pop} = 2.4 \, T^{1/2} (\frac{m_o}{m^*})^{3/2} [\exp(\frac{\theta}{T}) - 1] \, F(\frac{\theta}{T}) \text{ cm}^2/\text{Vsec} , \quad (6)$$

where ω_1 = longitudinal optical phonon frequency, $\theta = h\omega_1/k$ and F is a complicated function described in Ehrenreich's paper. It can be shown that Equation (6) gives a fair fit to the mobility near room temperature in

---

[9] H. C. Casey Jr., F. Ermanis and K. B. Wolfstirn, J. Appl. Phys. 40, 2945.

[10] J. Bardeen and W. Shockley, Phys. Rev. 80, 72 (1950).

[11] H. Ehrenreich, J. Phys. Chem. Solids, 8, 130 (1959).

p-type GaP.[12] However, Wiley and Di Domenico[13] have very convincingly argued that the agreement between experiment and the theory of polar mode scattering is fortuitous and that the mobility can be accounted for by a combination of acoustic mode scattering and nonpolar mode scattering. They showed that, when nonpolar optic scattering and acoustic mode scattering are combined, the resulting expression for the mobility is

$$\mu_{NPO+AC} = \frac{r + r^{3/2}}{1 + r^{3/2}} S(\theta, \eta, T)\, \mu_{AC} \qquad (7)$$

where $r = m_1^*/m_2^*$ is the ratio of the light to the heavy hole effective mass, θ is the Debye temperature defined above, η is the ratio of the energies of the nonpolar optical phonon to the acoustic phonon and μ_{AC} was defined in Equation (5). In Figure 31 we plot the theoretical expression of Wiley and DiDomenico and find good agreement for temperatures above 120 K. Note that above 120 K, the mobilities for all of the SSD samples are approximately equal. We conclude that, in the temperature range from 120 K to 300 K, the mobility is limited by lattice scattering and that, most likely, the limiting mechanism is a combination of acoustic and nonpolar optical phonon scattering.

At low temperatures, ionized impurity scattering is frequently found to be the limiting scattering mechanism in semiconductors. The mobility, when limited by impurity scattering, has been discussed by Blatt[14] and is given by the expression

---

[12] Technical Report AFML-TR-77-37.

[13] J. D. Wiley, M. DiDomenico, Jr. Phys. Rev. B., 2, 427 (1970).

[14] F. J. Blatt, Solid State Phys., 4, 344 (1957).

$$\mu_I = 3.3 \times 10^{15} \frac{T^{3/2}}{N_I} \left(\frac{m_o}{m^*}\right)^{1/2} \left(\frac{\kappa}{\epsilon_o}\right)^2 \ln\left[1.2 \times 10^{14} \left(\frac{T^2}{n^1}\right) \left(\frac{\kappa}{\epsilon_o}\right) \left(\frac{m^*}{m_o}\right) - 1\right]^{-1} \quad (8)$$

where κ is the dielectric constant, $N_I = p + 2N_d$ is the concentration of ionized impurities and

$$n^1 = p + (p + N_D)\left[1 + (p + N_D)/N_A\right] .$$

By fitting this expression to the low-temperature mobility, one is able to determine the impurity densities in the material. Figures 28 through 30 show the calculated plot of the mobility as a function of temperature for all of the SSD-grown samples. Table 6 shows the values of the donor and acceptor impurity densities which were used in calculating μ_I. To determine N_D and N_A, we used values for $N_D - N_A$ from the Hall data and adjusted N_D to obtain the best fit to the experimental data. Table 6 also presents the values of N_D and N_A which were determined strictly from analyzing the Hall data, as discussed earlier. Note that the agreement between these methods of determining N_D and N_A is fairly good, hence, one can have a good deal of confidence in the values listed in Table 6.

Note that the mobility for the SSD-grown material begins to drop rapidly with decreasing temperatures as the sample temperature drops below about 40 K. Such low values of the mobility are characteristic of conduction by the phonon assisted hopping of holes from neutral to ionized acceptors. We have not investigated in detail the mobility at these low temperatures. However, all samples investigated did exhibit this rapid decrease in mobility and it is fairly safe to assume it is the result of the onset of phonon assisted hopping as the valence band holes are frozen out.

Thus far, we have neglected the effects of scattering by neutral impurities on the mobility. We now present a brief analysis to show this neglect was, in fact, warranted. Erginsoy[15] derived the following expression for the mobility when limited by neutral impurity scattering:

$$\mu_N = \frac{1.4 \times 10^{22}}{N_N} \left(\frac{m^*}{m_o}\right) \left(\frac{\epsilon_o}{\kappa}\right) \text{ cm}^2/\text{Vsec} , \qquad (9)$$

where

$$N_N = N_A - (p + N_D)$$

is the neutral impurity concentration. According to Equation (9), μ_N will be most dominant at low temperatures where $p \ll N_A - N_D$. For this condition,

$$\mu_N \approx \text{constant} = \frac{7 \times 10^{20}}{N_A - N_D} \qquad (10)$$

Hence, only for rather heavily doped samples ($\gtrsim 10^{18}$ cm^{-3}) will neutral impurity scattering play a role in limiting the mobility in p-type GaP. None of the samples which we have grown had carrier concentrations in this regime.

Hall analysis was also performed on the three random-nucleated-solution (RNS) growth runs. These growth runs, described earlier in Section III, were made to isolate the source of carbon in the SSD-growth experiments. The carrier concentration divided by (temperature)$^{3/2}$ is plotted for each of these runs in Figure 32.

---

[15] C. Erginsoy, Phys. Rev. 79, 1013 (1950).

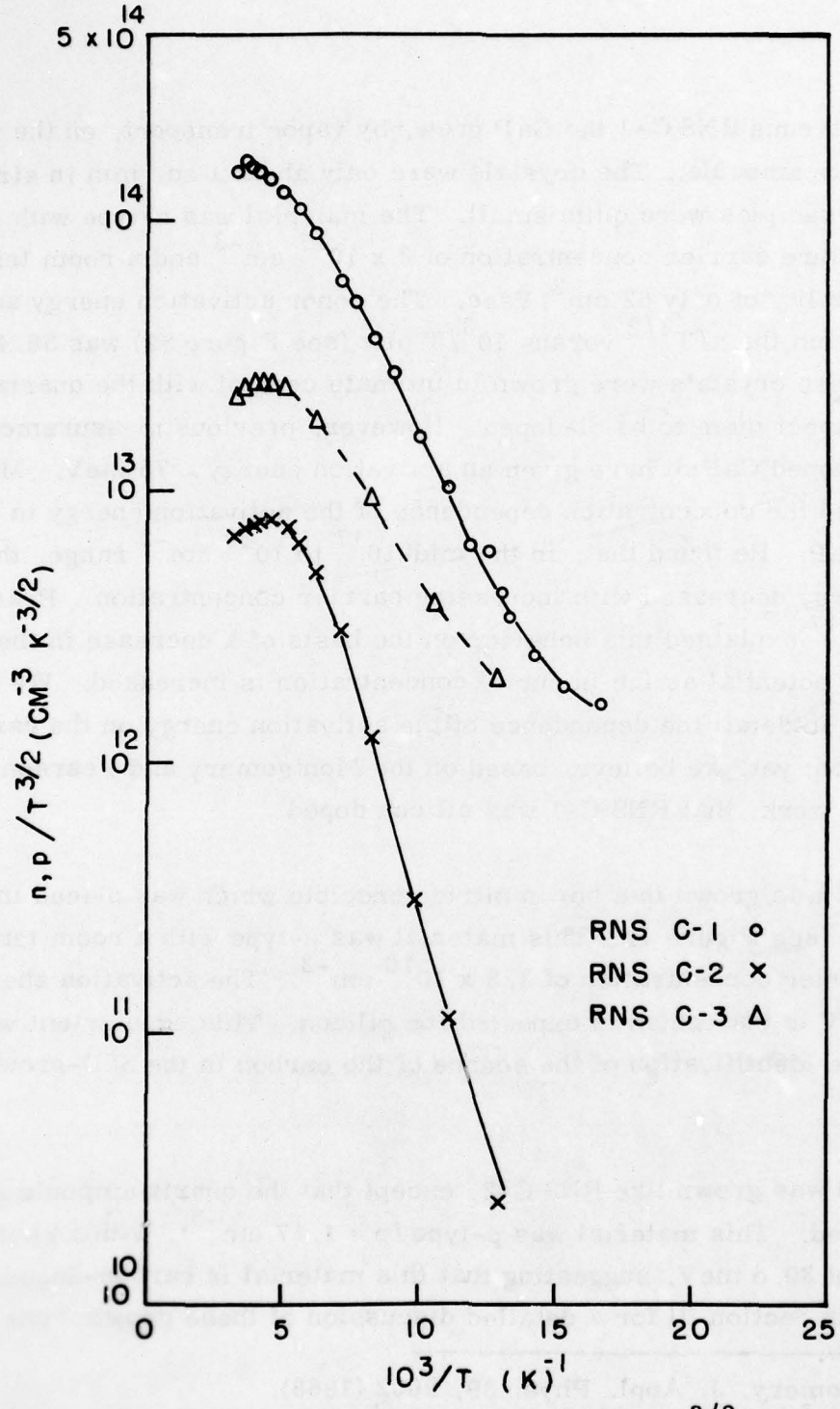

Figure 32. Carrier Concentration Divided by $T^{3/2}$ versus Reciprocal Temperature for Three RNS Growth Runs

In growth runs RNS C-1 the GaP grew, by vapor transport, on the walls of the quartz ampoule. The crystals were only about 1 sq. mm in size, so the Hall samples were quite small. The material was n-type with a room temperature carrier concentration of 8×10^{17} cm^{-3} and a room temperature mobility of only 62 $cm^2/Vsec$. The donor activation energy as determined from the $n/T^{3/2}$ versus $10^3/T$ plot (see Figure 32) was 38.4 meV. Since these crystals were grown in intimate contact with the quartz, we would expect them to be Si-doped. However, previous measurements on lighter doped GaP:Si have given an activation energy $\sim$ 75 meV. Montgomery[16] measured the concentration dependence of the activation energy in tellurium doped GaP. He found that, in the mid-10^{17} to 10^{19} cm^{-3} range, the activation energy decreased with increasing carrier concentration. Pearson and Bardeen[17] explained this behavior on the basis of a decrease in the average electron potential as the impurity concentration is increased. We did not examine in detail the dependence of the activation energy on the carrier concentration; yet, we believe, based on the Montgomery and Pearson and Bardeen work, that RNS C-1 was silicon doped.

RSN C-2 was grown in a boron nitride crucible which was placed in a quartz ampoule (see Figure 4). This material was n-type with a room temperature carrier concentration of 3.5×10^{16} cm^{-3}. The activation energy of 73.5 meV is that which is expected for silicon. This experiment was critical to the identification of the source of the carbon in the SSD-growth experiments.

RNS C-3 was grown like RNS C-2, except that the quartz ampoule was carbon coated. This material was p-type ($p = 1.17$ cm^{-3}), with an activation energy of 30.5 meV, suggesting that this material is carbon-doped. (see earlier in Section III for a detailed discussion of these growth runs.)

---

[16] Montgomery, J. Appl. Phys. 39, 2002 (1968).

[17] Pearson and Bardeen, Phys. Rev. 75, 865 (1949).

The majority of the LPE material grown during this project used n-type GaP substrates. Since the LPE material was itself n-type, Hall measurements could not be made on these layers, so C-V analysis was used to determine the carrier concentrations. Some of the LPE layers, however, were grown on p-type substrates to facilitate the fabrication of Hall samples. Figure 33 is a plot of the carrier concentration divided by (temperature)$^{3/2}$ versus reciprocal temperature for a typical LPE layer grown on a p-type substrate. This data gives a donor activation energy of 68 meV, which indicates that silicon was the primary donor in the LPE grown material.

In Figure 34, we plot the temperature dependence of the mobility for two n-type LPE grown samples. Since the mobility in n-type GaP has been well discussed by us[18] and others[19], we will not discuss in detail the mobility -- temperature characteristic for the LPE material. Note, however, that in the temperature range from 150K to 300K, the mobility varies as $T^{-3/2}$ which is the temperature dependence predicted by theory for the mobility when limited by combined intervalley and acoustic-mode scattering.

Carrier Concentration Profiles by C-V Measurement

Many of the LPE layers were grown on n-type substrates. Since the epilayers themselves were generally n-type, Hall data could not be obtained from these samples. Consequently, we used the Schottky diode capacitance technique to determine the carrier concentration in much of the LPE grown material.

---

[18] Technical Report AFML TR-77-37

[19] M. Toyama, M. Naito, A. Kasami Japanese Journal of Applied Physics 8 358 (1969)

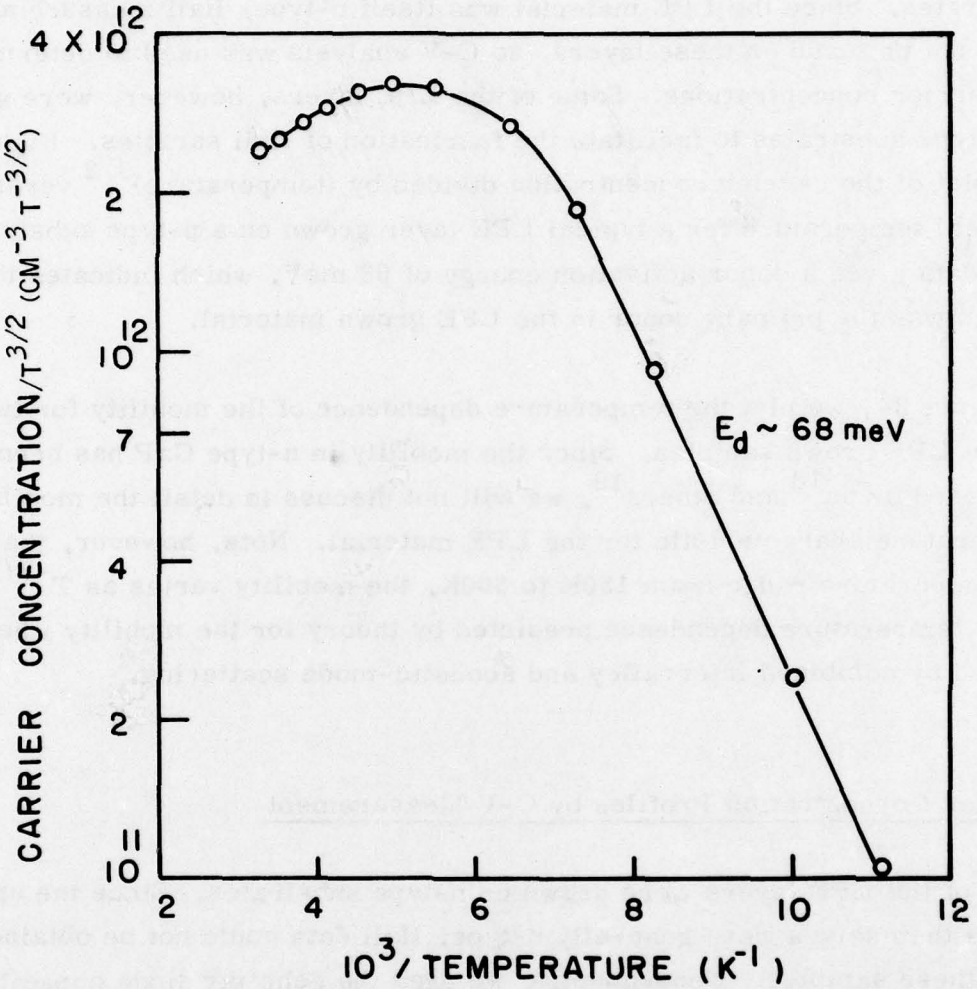

Figure 33. Carrier Concentration Divided by $T^{3/2}$ versus Reciprocal Temperature for an LPE Layer

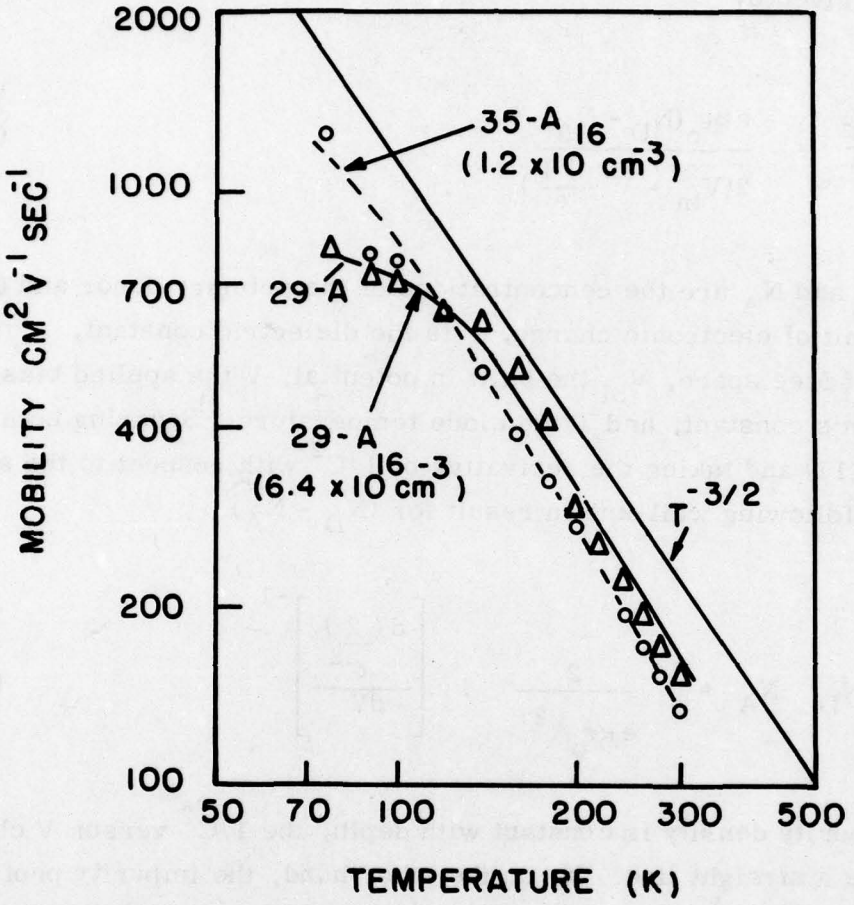

Figure 34. Temperature Dependence of the Mobility for Two n-Type LPE Samples

The capacitance C of the depletion layer of a metal semiconductor junction of area A is given by[20]

$$\frac{C}{A} = \frac{e\kappa\varepsilon_o(N_D - N_A)}{2(V_{bi} - V - \frac{kT}{e})} \quad , \tag{11}$$

where N_D and N_A are the concentrations of the primary donor and acceptors, e is the unit of electronic charge, κ is the dielectric constant, ε_o the permitivity of free space, V_{bi} the built in potential, V the applied bias, k is Boltzmann's constant, and T the diode temperature. Squaring both sides of Equation (11) and taking the derivative of $1/C^2$ with respect to the applied bias gives the following well-known result for $(N_D - N_A)$:

$$N_D - N_A = \frac{2}{e\kappa\varepsilon_o A^2} \cdot \left[\frac{d(\frac{2}{C^2})}{dV}\right]^{-1} . \tag{12}$$

If the impurity density is constant with depth, the $1/C^2$ versus V characteristic will be a straight line. If, on the other hand, the impurity profile varies with depth the $1/C^2$ - V characteristic will be curved. The profile as a function of depth is then obtained from the slope of the $1/C^2$ - V characteristic as a function of the applied bias, V. The corresponding depth (of the depletion layer) is determined from the relation

$$w = \frac{2\kappa\varepsilon_o}{e(N_D - N_A)} (V_{bi} - V - \frac{kT}{e}) . \tag{13}$$

---

[20] S. M. Sze, Physics of Semiconductor Devices, John Wiley, New York, 1969

To evaluate the impurity concentrations of the LPE layers using the Schottky barrier C-V technique, an array of Au Schottky barriers must be fabricated on the surface of the epitaxial layer. This was done using the process defined in Table 7. Figure 35 shows an LPE layer on which ohmic contacts and Schottky barriers have been fabricated. The sample is then mounted on a seven-pin header and five of the Schottky barriers and two of the ohmic contacts are connected to the header pins with 0.002 inch gold wire and silver epoxy. The header, with sample is then placed in a totally shielded circuit for measuring the I-V and C-V characteristics.

Before measuring the C-V characteristics, the I-V characteristics of each diode is measured. Figure 36 shows the curve tracer plots of the forward and reverse characteristics of a typical set of GaP/Au Schottky diodes.

Note that, for all of these diodes, the knee in the forward direction occurs at approximately the same bias voltage. This demonstrates that the saturation current is the same for all diodes, and, hence, that the surface is uniform. The reverse breakdown characteristic is also shown on Figure 36. Note that the breakdown voltages vary from 20 to 40 volts. Since we did not fabricate a guard ring structure for these diodes, we believe the breakdown is due to a premature breakdown at the periphery of the diode. We have proved this is the mode for some diodes by observing the location of the light emission when the diode is driven hard in the reverse direction. For the desired C-V measurements, a reverse bias of 10 volts was generally sufficient, so we did not work to improve the reverse breakdown characteristic.

In Section II, we described the apparatus used to make the C-V measurements and in Section III we discussed the influence of various growth parameters on the carrier concentration. Here, we will describe some of the general features of the C-V data which was used to determine the impurity profile.

TABLE 7. PROCESS FOR FABRICATING GOLD SCHOTTKY BARRIERS ON GaP EPI-LAYERS

1.	Measure surface flatness with surface profilometer
2.	Cut sample into thirds
3.	Clean mounting jig, ohmic contact mask, and Schottky barrier mask toluene, acetone, and methonal followed by d. i. H_2O rinse
4.	Clean samples in equal parts of toluene, acetone, and methonal followed by d. i. H_2O rinse
5.	Mount samples and ohmic contact mask on jig
6.	Evaporate 600Å Ag:1%Te and 300Å Ni in a vacuum of $<10^{-6}$ Torr
7.	Anneal for 15 minutes at 680°C
8.	Characterize ohmic contact -- if I-V characteristic linear go to step 9 -- if not redo the above steps
9.	Protect ohmic contacts with stop-off laquer
10.	Etch surface in dilute aqua regia ($2HC\ell:2H_2O:1HNO_3$) at 50° C.
11.	Rinse sample in d. i. H_2O
12.	Remove stop-off laquer in MEK
13.	Wash sample in two successive baths of methanol
14.	Blow dry with clean N_2 gas
15.	Mount sample and Schottky barrier mask in jig
16.	Evaporate 800Å (75Å if transparent contacts are required) Au to form Schottky barrier
17.	Measure I-V and C-V characteristic of Schottky diodes.

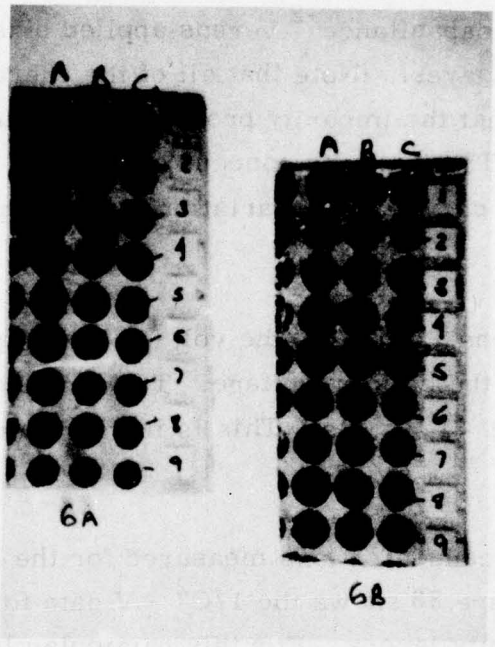

Figure 35. Layout of Gold Schottky Barrier Diodes on GaP LPE Layer

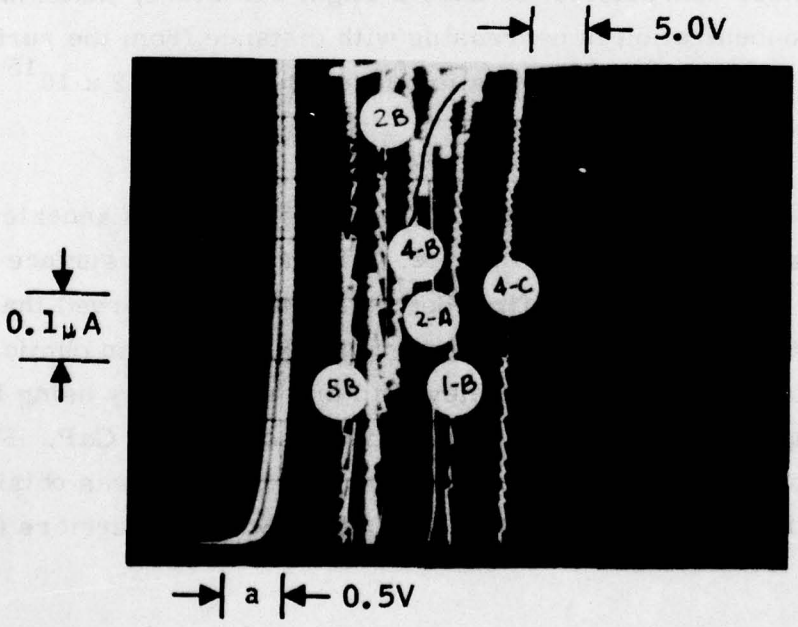

Figure 36. Current Voltage Characteristics of GaP/Au Schottky Barriers on LPE-26A

Figure 37 shows the capacitance^{-2} versus applied bias characteristic for a typical undoped LPE layer. (Note that all of the characteristics are straight lines. This shows that the impurity profile is constant with distance from the layer surface.) The impurity concentrations, for this sample varied by about 50 percent, as shown by the variation in the slope of the $1/C^2$ - V characteristics.

According to Equations 12 and 13, the voltage intercept of the $1/C^2$ - V characteristic gives the built-in voltage. The data plotted in Figure 37 yields a built-in potential of ~1.2 volts. This is in agreement with values reported in the literature.[21]

The lowest impurity concentrations measured for the LPE samples were ~ $5 \times 10^{15} cm^{-3}$. Figure 38 shows the $1/C^2$ - V data for Schottky diodes from one of these high-purity layers. For this particular layer, the impurity concentration at the surface varied from $6.2 \times 10^{15} cm^{-3}$ to $7.7 \times 10^{15} cm^{-3}$. Note that these characteristics have a slight curvature, indicating that the impurity concentration is decreasing with distance from the surface. Under one diode, the carrier concentration decreased from $6.2 \times 10^{15} \rightarrow 4.2 \times 10^{15}$ in a distance ~ 0.2 μm.

As discussed earlier in Section III, most of the samples annealed in a gallium atmosphere converted to p-type. The fact that the surface conductivity had converted to p-type was first detected when we observed that the Ag:Te contact to the annealed surface was rectifying rather than ohmic. Linear ohmic contacts could only be achieved to this material by using In:Zn solder and alloying at 480°C. Zn, of course, is an acceptor in GaP. Further confirmation of the p-type nature of the annealed material was obtained by examining the direction of rectification of Au Schottky barriers fabricated on

---

[21] M. Cowley and H. Heffner, J. Appl. Phys., 35, 255 (1964)

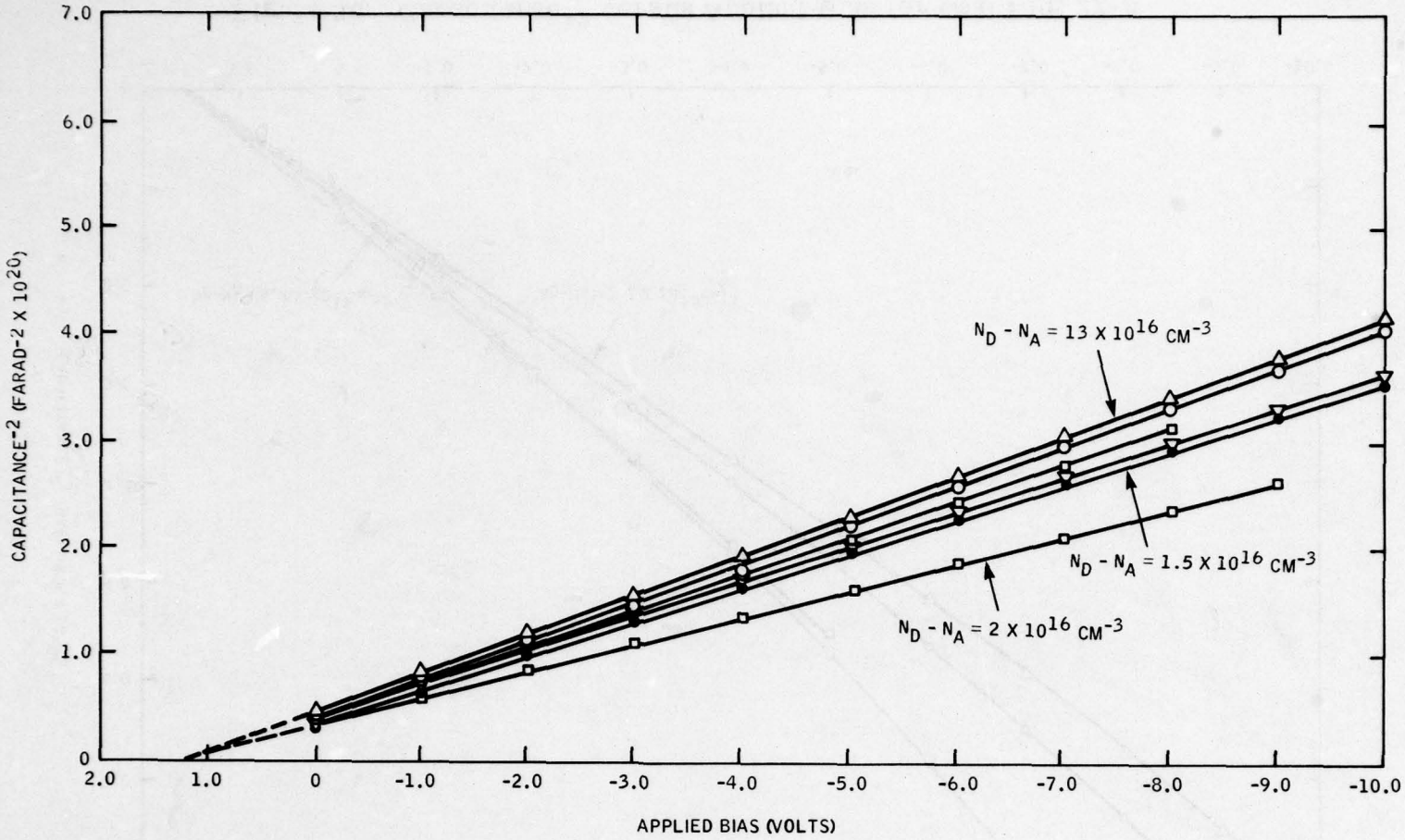

Figure 37. Capacitance^{-2} versus Applied Bias for Schottky Barriers on GaP LPE 30-A

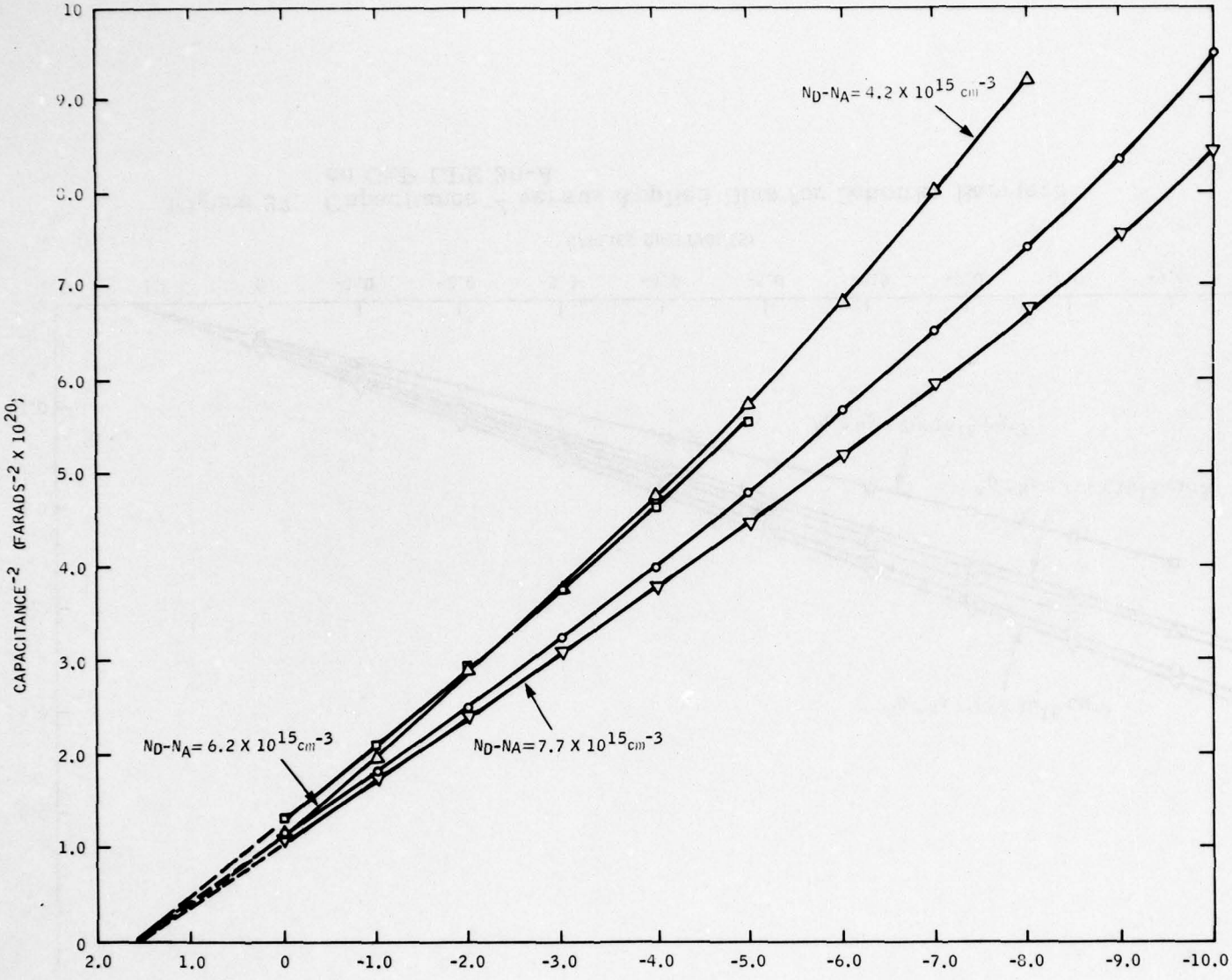

Figure 38. Capacitance^{-2} versus Applied Bias for GaP LPE 22-A

the surface. Figure 39 shows the $1/C^2$ - V characteristic for Schottky barriers fabricated on the surface of this converted material. Near the surface, the carrier concentration is heavily p-type ($\sim 1.6 \times 10^{18}$ cm^{-3}), but according to these data it decreases to $\sim 7.7 \times 10^{16}$ within a few hundred angstroms.

Photocapacitance Spectroscopy

Deep levels in semiconductors can significantly influence device operation and performance. For example, deep levels can act as majority carrier traps and, hence, increase the response time. They can also affect the minority carrier lifetime and, consequently, influence the luminescence efficiency of light emitters. They are also detrimental to charge transfer action in CCDs and can act as sensitizing centers in photoconductors. Recently, deep-level-transient-spectroscopy (DLTS) has been developed by Lang[22] and many others for investigating deep levels in semiconductors. This technique requires a rather elaborate set-up and detailed mathematical analysis to obtain results. In addition, as discussed by Lang, the DLTS technique may not be able to detect all of the important recombination centers.

We decided to develop a modification of the photocapacitance technique which was advanced by White, Dean and Porteous[23]. This technique (Figure 40) requires that the sample be cooled to a temperature sufficiently low (77K in our case) so that thermal processes can be neglected. The deep levels are detected by observing the changes in the depletion layer capacitance of a Schottky barrier, which are induced by photon illumination.

---

[22] D. V. Lang, J. Appl. Physics, 45, 3023 (1974)

[23] A. M. White, P. J. Dean, and P. Porteous, J. Appl. Phys., 47, 3230 (1976)

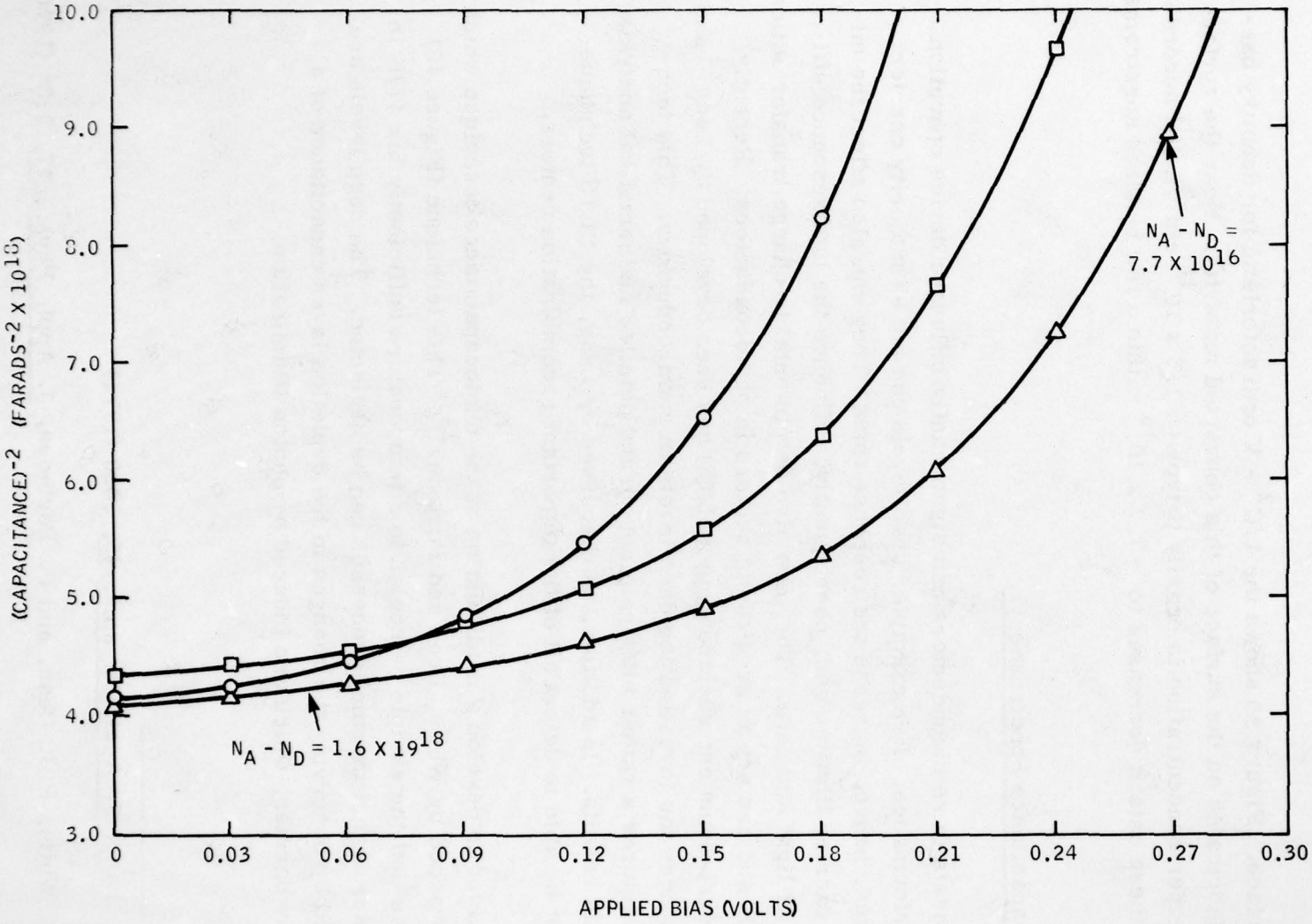

Figure 39. Capacitance^{-2} versus Applied Bias for Samples from LPE 33-B Following the 900°C Anneal

AD-A075 065 HONEYWELL CORPORATE TECHNOLOGY CENTER BLOOMINGTON MN F/G 20/2
GROWTH OF SINGLE CRYSTAL GALLIUM PHOSPHIDE BY LIQUID PHASE EPIT--ETC(U)
APR 79 P E PETERSEN , R G SCHULZE F33615-77-C-5043
UNCLASSIFIED HR-47108 AFML-TR-79-4049 NL

2 OF 2
AD
A075065

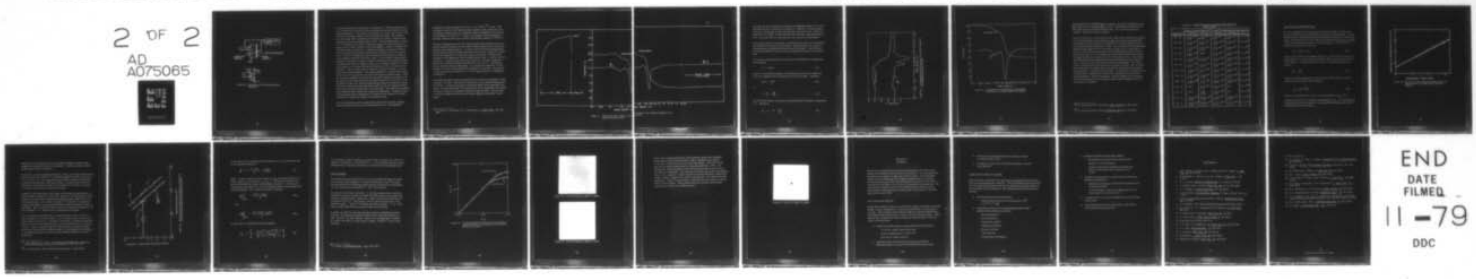

END
DATE FILMED
11-79
DDC

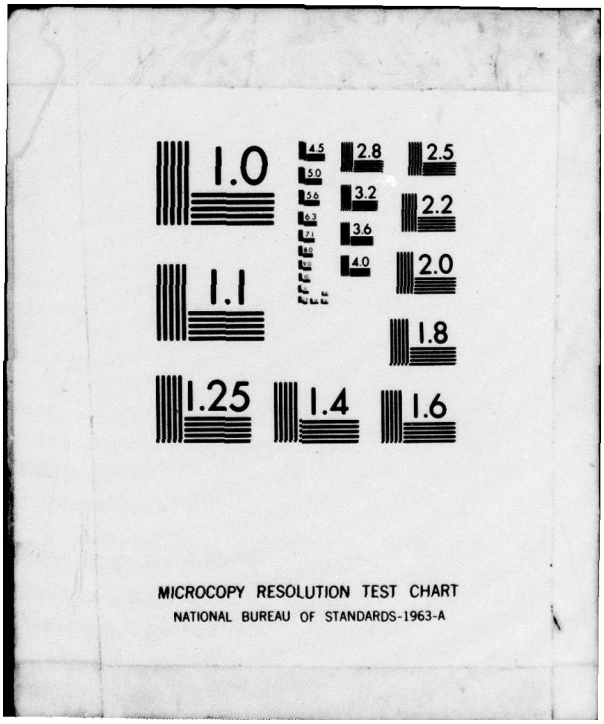
1.0
1.1
1.25
1.4
1.6
1.8
2.0
2.2
2.5
2.8
3.2
3.6
4.0
4.5
5.0
5.6
6.3
7.1
MICROCOPY RESOLUTION TEST CHART
NATIONAL BUREAU OF STANDARDS-1963-A

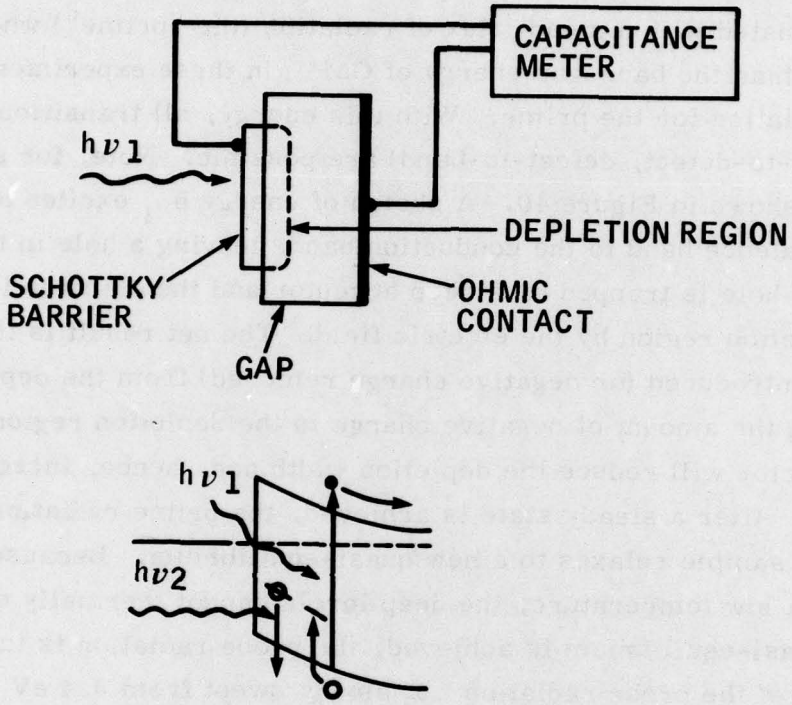

Figure 40. Schematic of the Photocapacitance Technique

In this photocapacitance technique, a transparent (~ 75Å) gold Schottky barrier is fabricated on the GaP surface using the process described in the preceeding subsection. The sample is then placed in a dewar and cooled to 77K. The diode is forward-biased to fill all the electron states. The sample is then illuminated with a steady flux of radiation (the "prime") whose energy is greater than the band-gap energy of GaP. In these experiments, we used 2.7 eV radiation for the prime. With this energy, all transitions (band-to-band, band-to-defect, defect-to-band) are possible. Note, for example, the transition shown in Figure 40. A photon of energy $h\nu_1$ excites an electron from the valence band to the conduction band, leaving a hole in the valence band. The hole is trapped by a deep acceptor and the electron is swept out of the depletion region by the electric field. The net result is that positive charge is introduced (or negative charge removed) from the depletion region. Decreasing the amount of negative charge in the depletion region of a n-type semiconductor will reduce the depletion width and, hence, increase the capacitance. After a steady state is achieved, the prime radiation is turned off and the sample relaxes to a new quasi-equilibrium. Because the sample is held at a low temperature, the deep levels cannot thermally empty. After the new quasi-equilibrium is achieved, the probe radiation is turned on and the energy of the probe radiation $h\nu_2$ slowly swept from 0.4 eV up to 2.0 eV. As shown in Figure 40, when the probe energy equals or exceeds the energy difference between the band edge and the defect level, the trapped electron/hole can be optically excited back to the band edge. This alters the magnitude of the depletion layer charge and changes the capacitance. Therefore, measuring depletion layer capacitance as a function of the energy of the probe radiation can identify the position of the defect levels.

For this technique to work, the absorption depth of the incident radiation must be greater than the width of the depletion layer. The absorption

coefficient for photon energies <2.8 eV is $<5 \times 10^3 cm^{-1}$[24] in GaP. This technique is valid for GaP samples whose depletion width is less than 2 μm. According to Equation 13 a 2 μm depletion width corresponds to an impurity concentration of $4 \times 10^{14} cm^{-3}$. Hence, the technique under discussion is useful for material whose net impurity concentration exceeds $4 \times 10^{14} cm^{-3}$.

We have investigated several LPE unintentionally doped samples which were grown during this program and two copper-doped samples which were grown during the preceeding program. A typical result from this photocapacitance spectroscopic probe of the deep level structure is shown in Figure 41, where we plot the capacitance C versus the energy of the probe. With the prime radiation on the capacitance of the Schottky barrier rose to ~260 pf, and then decayed to ~208 pf when the prime was turned off. The probe radiation is then turned on and the radiation scanned from 0.4 eV to 2.0. During this probe, several levels are observable. To increase the resolution, we constructed a circuit to differentiate the capacitance in real time. Four levels, 1 donor (A) and three acceptor (B, C, D) are readily detected in the $\frac{dc}{dt}$ scan in Figure 41.

Two additional experiments were performed to improve our confidence in this technique. Firstly, a second probe sweep was run immediately following the first probe. As seen in the figure, this had no effect on the capacitance and, hence, we conclude that the C-F characteristic is not dependent on the source, and that the levels are completely emptied by the first scan. The scan was run slowly enough so that the spectral shape of $\frac{dc}{dt}$ was independent of scan speed.

---

[24] P. J. Dean, G. Kaminsky, R. B. Zietterstrom, J. Appl. Phys., 33, 3551 1967.

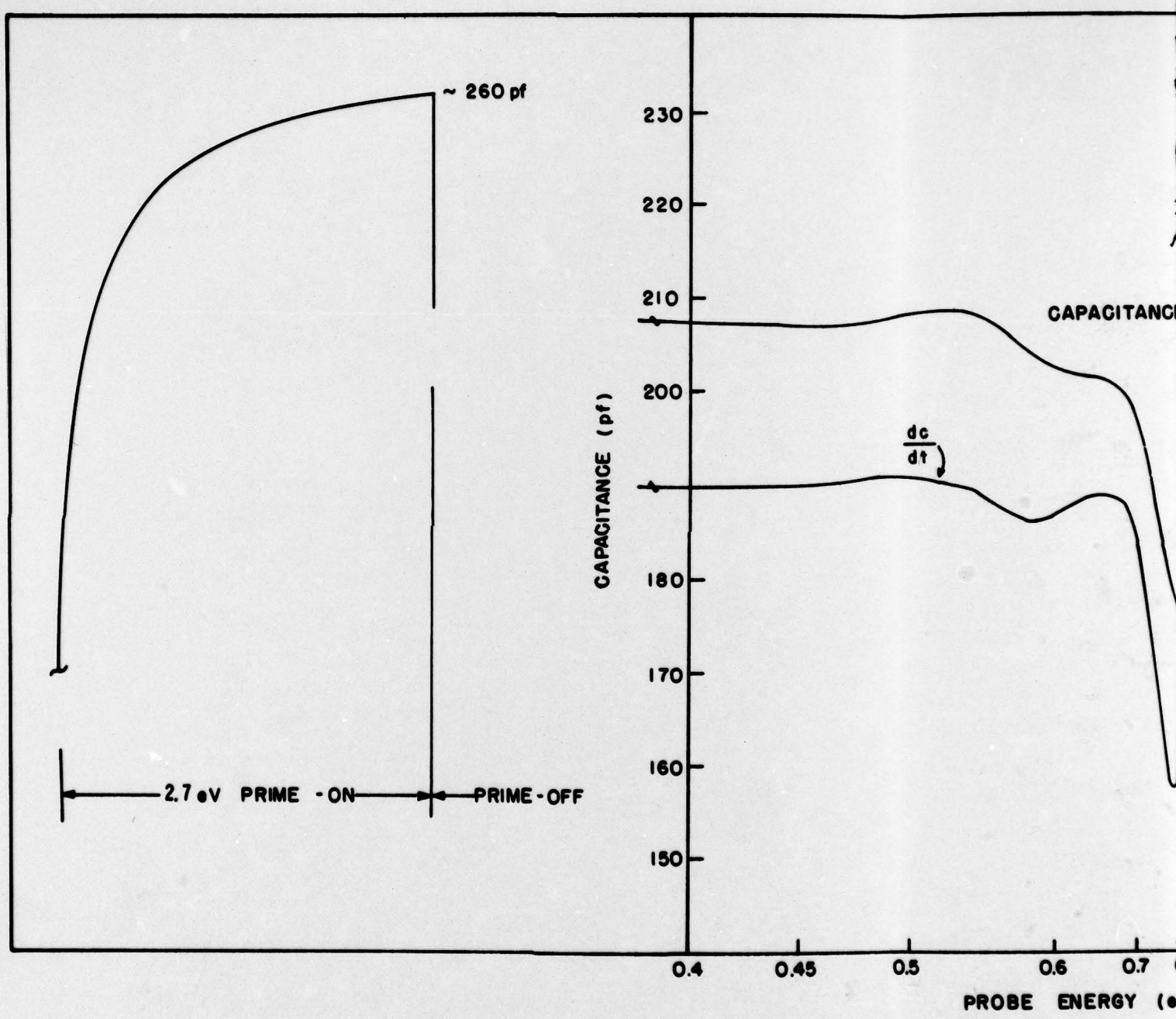

Figure 41. Capacitance versus Energy of the Schottky Barrier on LPE.

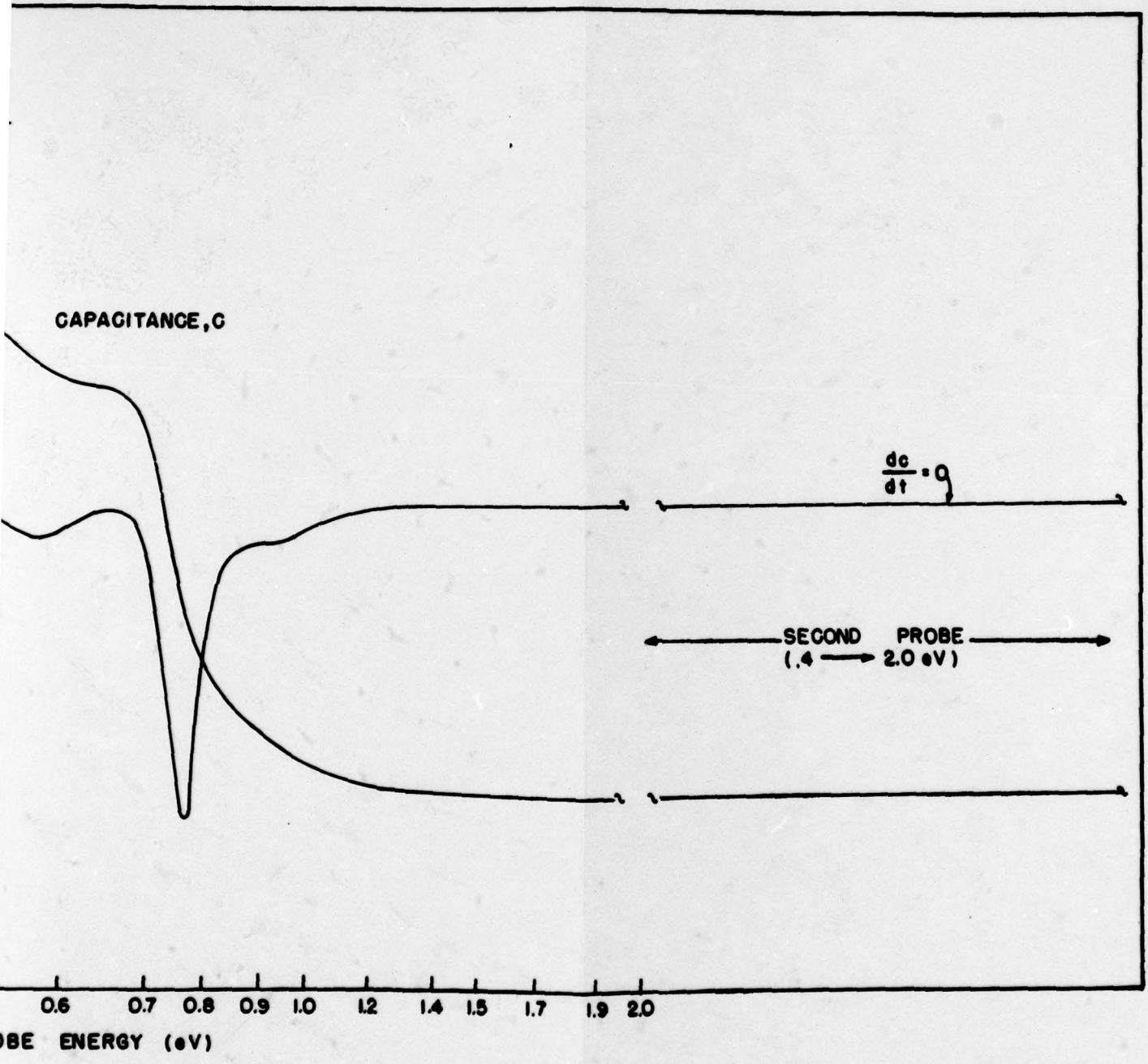

us Energy of the Incident Radiation for a
on LPE.

The majority of the undoped LPE samples investigated exhibited a C-E characteristic similar to that shown in Figure 41. However, in a few samples (9-B is an example) the D-level was dominant over the C-level. Figure 42 shows the C-E and $\frac{dc}{dt}$ - E characteristics for a Schottky diode fabricated on 9-B. (Note also that, for this particular run, level B is undetectable.)

In an earlier program concerning photoconductivity in GaP, we had intentionally doped some LPE layers with copper. Figure 43 shows the results of measurements on sample intentionally doped with copper. Levels B and C are readily detectable, level D is barely detectable and level A is undetectable.

The impurity concentration for each level can be obtained by a straight forward analysis:

$$C^2 = A\,(N^+), \tag{14}$$

where N^+ is the charge density in the depletion layer and A is constant as long as the applied bias and temperature are held constant. Therefore,

$$2CdC = AdN^+ \tag{15}$$

or

$$2\,\frac{\Delta C}{C} = \frac{\Delta N^+}{N^+}\,, \tag{16}$$

but ΔN^+ is the density of the level N_i associated with the change in capacitance ΔC. Therefore,

$$N_i = 2\,N^+\,\frac{\Delta C_i}{C}\,. \tag{17}$$

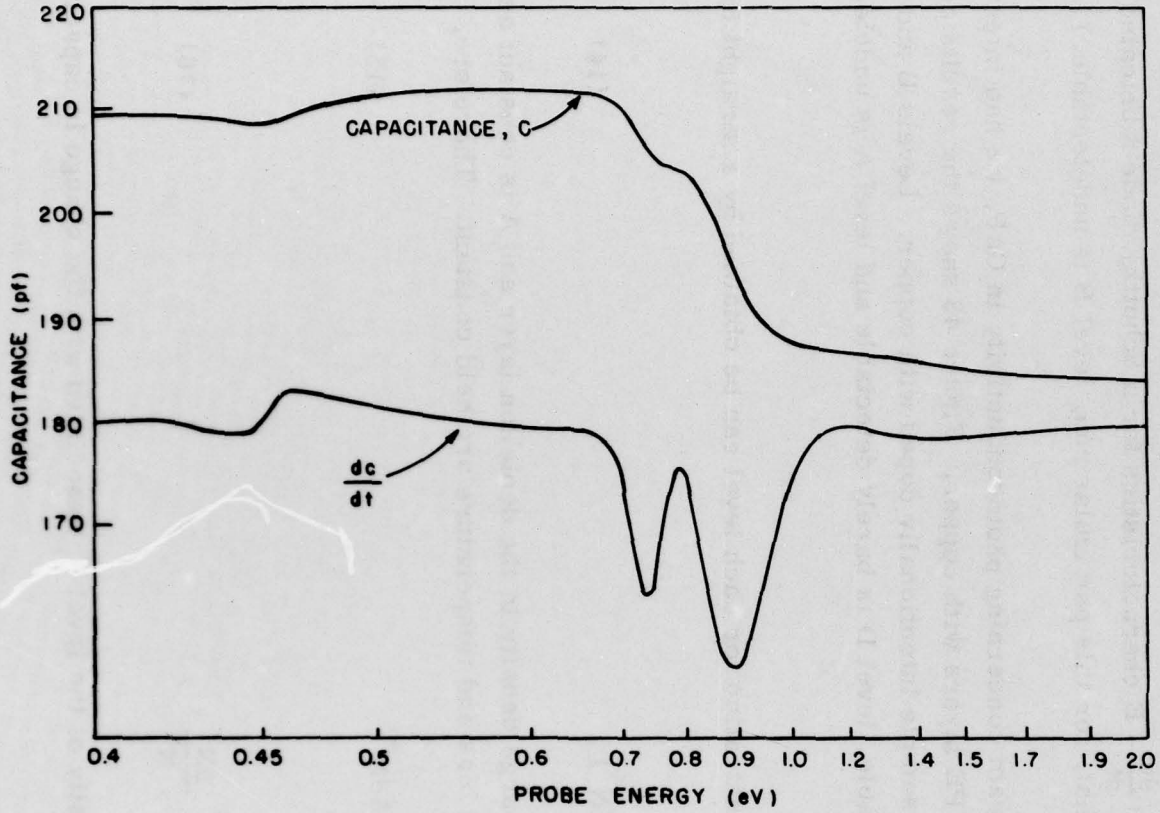

Figure 42. Capacitance versus Energy of the Incident Radiation for a Schottky Barrier on LPE

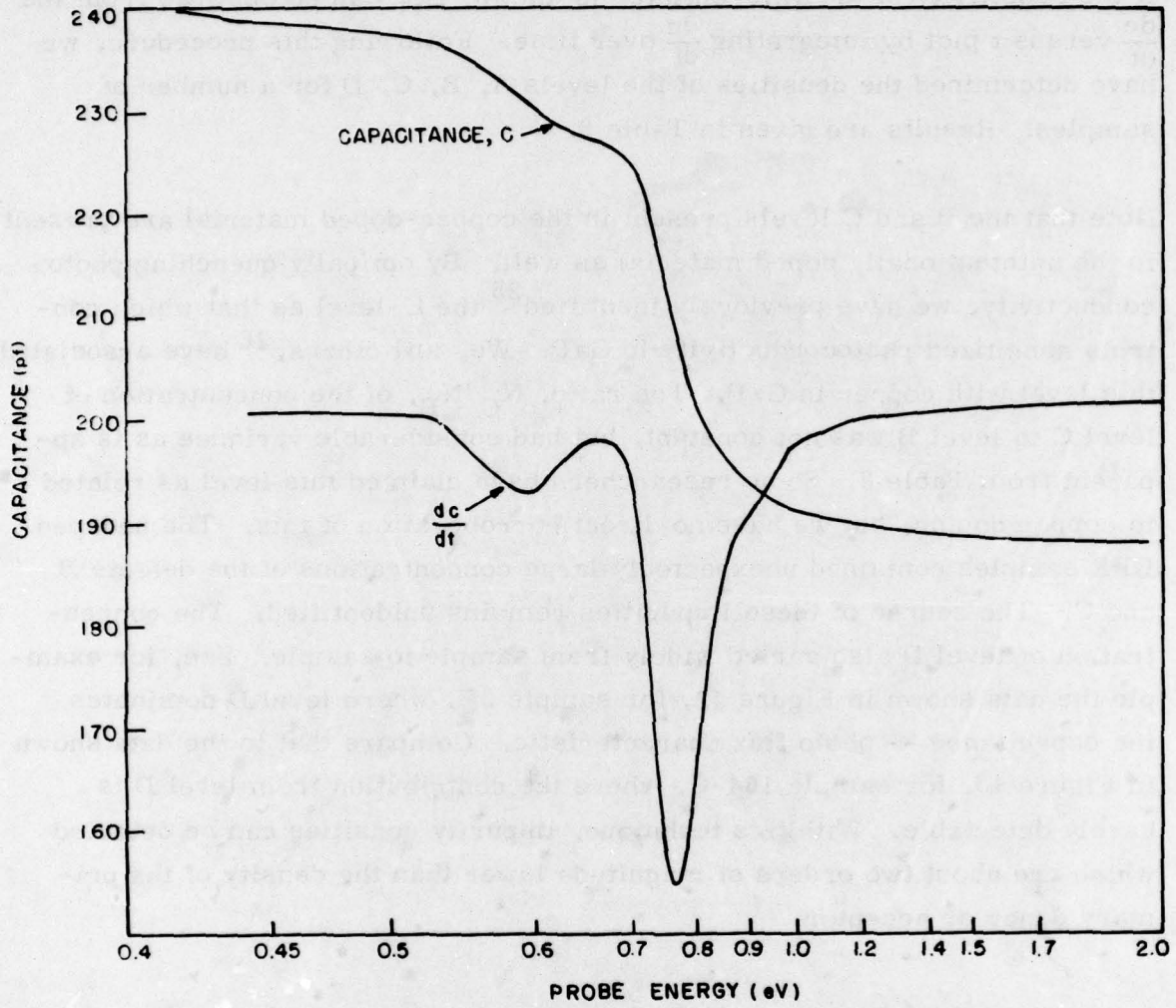

Figure 43. Capacitance versus Energy of the Incident Radiation for a Copper Doped LPE Sample

If the sensitivity of the differentiator is known, ΔC_i can be obtained from the $\frac{dc}{dt}$ versus t plot by integrating $\frac{dc}{dt}$ over time. Following this procedure, we have determined the densities of the levels A, B, C, D for a number of samples. Results are given in Table 8.

Note that the B and C levels present in the copper-doped material are present in the unintentionally doped material as well. By optically quenching photoconductivity, we have previously identified[25] the C-level as that which controls sensitized photoconductivity in GaP. We, and others,[26] have associated this level with copper in GaP. The ratio, N_C/N_B, of the concentration of level C to level B was not constant, but had considerable variance as is apparent from Table 8. Some researchers have claimed this level as related to copper doping, but we have no direct corroboration of this. The undoped LPE samples contained unexpectedly large concentrations of the defects B and C. The source of these impurities remains unidentified. The concentration of level D also varied widely from sample to sample. See, for example the data shown in Figure 42, for sample 9B, where level D dominates the capacitance -- photo flux characteristic. Compare that to the data shown in Figure 43, for sample 164-C, where the contribution from level D is barely detectable. With this technique, impurity densities can be detected which are about two orders of magnitude lower than the density of the primary donor or acceptor.

---

[25] R. G. Schulze and P. E. Petersen J. Appl. Physics 45, 5307 (1974)

[26] H. G. Grimmeiss and H. Scholz Philips Res Rpts, 20, 107 (1965)

TABLE 8. EXPERIMENTALLY DETERMINED IMPURITY STRUCTURE

Sample No.	Impurity Level Density (cm^{-3}) and 10^{15} and Density Normalized to N+				
	Level A	Level B	Level C	Level D	N+
9A - 3A	1.3×10^{15} 0.063	1.0×10^{15} 0.048	6.9×10^{15} 0.33	4.6×10^{15} 0.22	2.1×10^{16}
9A - 3B	1.7×10^{15} 0.043	2.2×10^{15} 0.057	14.0×10^{15} 0.36	6.6×10^{15} 0.17	3.9×10^{16}
9A - 5A	1.2×10^{15} 0.039	2.0×10^{15} 0.065	9.6×10^{15} 0.31	6.8×10^{15} 0.22	3.1×10^{16}
9B - 3B	3.25×10^{15} 0.065	undet.	3.5×10^{15} 0.07	11.0×10^{15} 0.22	5.0×10^{16}
9B - 4B	2.0×10^{15} 0.033	0.7×10^{15} 0.011	11.4×10^{15} 0.19	13.2×10^{15} 0.22	6.0×10^{16}
9B - 5B	1.6×10^{15} 0.031	1.1×10^{15} 0.021	10.2×10^{15} 0.20	10.2×10^{15} 0.20	5.1×10^{16}
12B - 1B	$.76 \times 10^{15}$ 0.020	4.2×10^{15} 0.11	14.4×10^{15} 0.38	5.3×10^{15} 0.14	3.8×10^{16}
12B - 2A	4.3×10^{15} 0.053	3.5×10^{15} 0.043	17.2×10^{15} 0.21	17.2×10^{15} 0.21	8.2×10^{16}
12B - 2C	0.42×10^{15} 0.011	6.1×10^{15} 0.16	22.0×10^{15} 0.58	39.3×10^{15} 0.077	3.8×10^{16}
164 - A	undet.	5.4×10^{15} 0.12	21.1×10^{15} 0.47	det.	4.5×10^{16}
164 - C	undet.	1.84 0.099	16.7×10^{15} 0.37	det.	4.5×10^{16}
167 - A	2.0×10^{15} 0.080	0.43×10^{15} 0.017	8.5×10^{15} 0.34	6.2×10^{15} 0.25	2.5×10^{16}
167 - B	0.81×10^{15} 0.032	0.33×10^{15} 0.013	8.5×10^{15} 0.14	6.8×10^{15} 0.27	2.5×10^{16}

Minority Carrier Diffusion Length

We have investigated the minority carrier diffusion length in n-type LPE grown GaP layers, using the Schottky diode photocurrent technique. The apparatus used for these experiments was described in Section II. In this technique, a Schottky barrier is illuminated with radiation whose energy is slightly less than the band-gap energy of the semiconductor. The short circuit photocurrent density Jp is given by

$$J_p = (eF)(w + L_p) \tag{18}$$

where w is the width of the depletion region, L_p is the minority carrier diffusion length, F = carrier density generation rate, and e is the unit of electronic charge. The capacitance per unit area of the Schottky barrier is given by

$$\frac{C}{A} = \frac{\kappa\varepsilon_o}{w} \quad . \tag{19}$$

Hence, according to Equation 18, J_p will vary linearly with 1/C, and the minority carrier lifetime will be given by

$$L_p = (\kappa\varepsilon_o A)\left(\frac{J_{p_o}}{m}\right) \quad , \tag{20}$$

where m is the slope of the J_p vs. 1/C characteristic and J_{p_o} is the value of the J_p for 1/C = 0 found by extrapolating the J_p - 1/C characteristic. Figure 44 is a plot of the data for a representative Schottky barrier which was fabricated on an LPE layer.

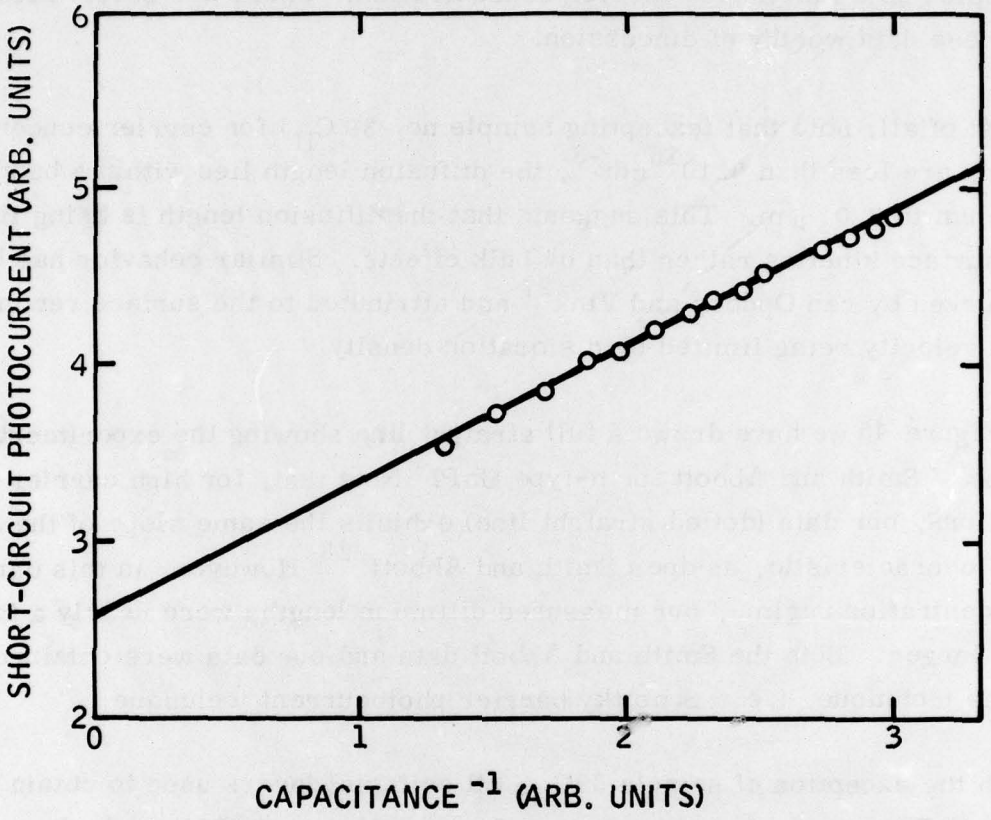

Figure 44. Short Circuit Photocurrent versus Reciprocal Capacitance for an LPE GaP/Au Schottky Barrier

Figure 45 is a composite plot of the hole diffusion length for several LPE samples as a function of carrier concentration. There are several features of these data worthy of discussion.

First of all, note that (excepting sample no. $39\,C_{II}$) for carrier concentrations which are less than $8 \times 10^{16} cm^{-3}$, the diffusion length lies within a band from 1.2 μm to 2.0 μm. This suggests that the diffusion length is being limited by surface kinetics rather than by bulk effects. Similar behavior has been observed by van Opdorp and Vink[27] and attributed to the surface recombination velocity being limited by dislocation density.

In Figure 45 we have drawn a full straight line showing the experimental results of Smith and Abbott for n-type GaP. Note that, for high carrier concentrations, our data (dotted straight line) exhibits the same slope of the J_p vs $1/C$ characteristic, as does Smith and Abbott.[28] However, in this carrier concentration regime, our measured diffusion lengths were nearly a factor of two larger. Both the Smith and Abbott data and our data were obtained by the same technique, i.e., Schottky barrier photocurrent technique.

With the exception of sample $39C_{II}$, all epitaxial layers used to obtain the data in Figure 45 were thicker than 5 μm. In sample $39C_{II}$, the layer thickness varied from 2 to 4 μm. As shown in Figure 45, the measured diffusion length in the 2 μm thick material was 1.9 μm while that in the 4 μm layer as 3.65 μm. Hence, it appears that, for these samples, the layer thickness limited the minority carrier diffusion length. To substantiate this hypothesis, we calculated the effective minority carrier diffusion length for a thin epitaxial layer.

---

[27] C. van Opdorp, A. T. Vink C. Werkhoven, Sixth International Symposium on GaAs and Related Compounds, Conf Series No. 336, 317, 1977.

[28] B. L. Smith and M. Abbott, Solid State Electronics, 15 361 (1972).

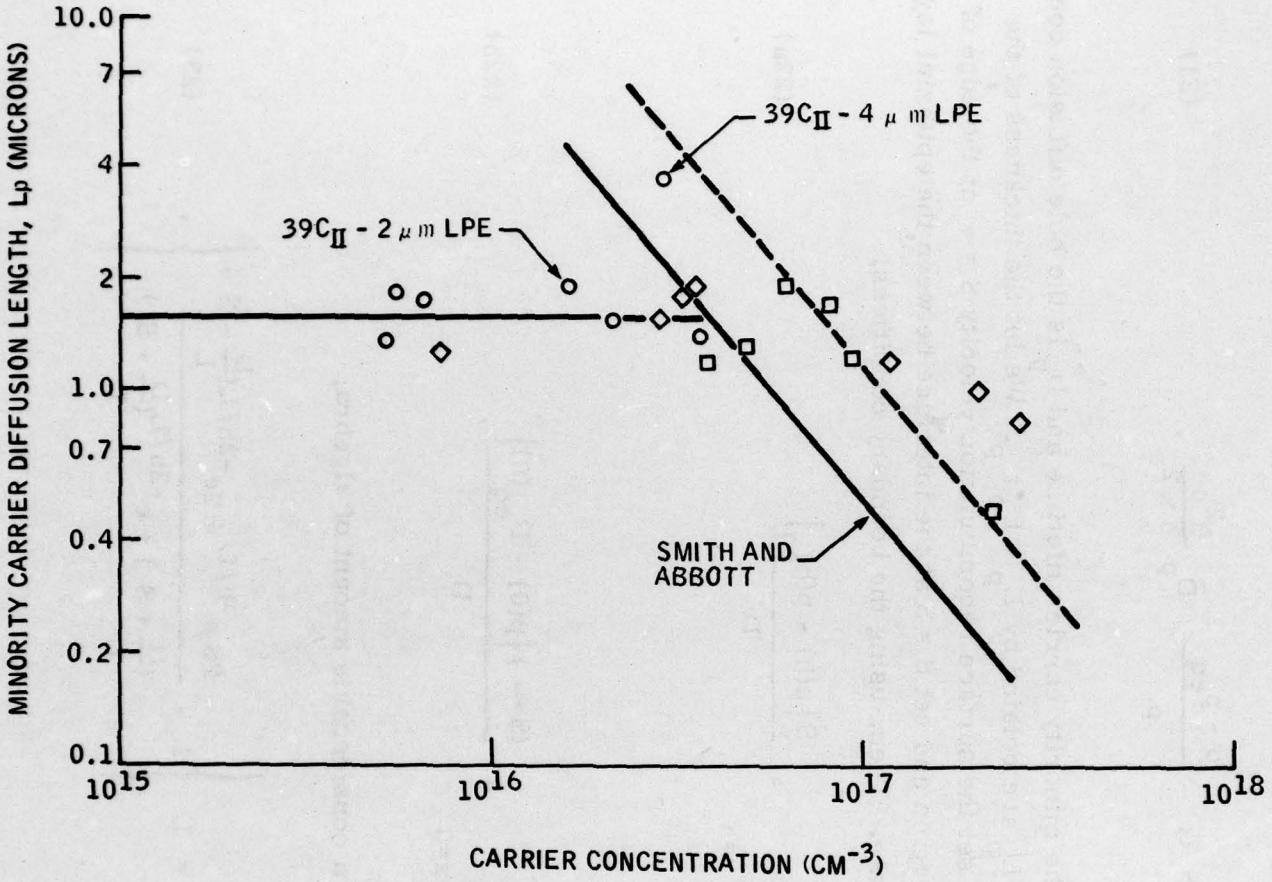

Figure 45. Minority Carrier Diffusion Length as a Function of Carrier Concentration for Several LPE Layers

In the presence of an external source resulting in a volume generation rate G, the continuity equation is

$$\frac{\partial p}{\partial t} = G - \frac{p - p_{eq}}{\tau_p} \quad D_p \frac{\partial^2 p}{\partial x^2} , \tag{21}$$

where τ_p is the minority carrier lifetime and D_p is the hole diffusion constant. D_p and L_p are related by $L_p = D_p \tau_p$. We let the thickness of the layer be h and set the surface recombination velocity $S = \infty$ at the edge of the depletion region and set $S = S$ at the interface between the epitaxial layer and the substrate. Then, using the boundary conditions,

$$\left.\frac{\partial p}{\partial x}\right|_{x=h} = \frac{S\left|p(h) - p(h)_{eq}\right|}{D} \tag{22a}$$

and

$$\left.\frac{\partial p}{\partial x}\right|_{x=0} = \frac{(S\to\infty)\left|p(0) - P_{eq}(0)\right|}{D} , \tag{22b}$$

we find, after a considerable amount of algebra,

$$L_{eff} = L \left\{ 1 - \frac{2S\, e^{-h/L} + 2e^{-2h/L}\left(\frac{D}{L} - S\right)}{\left(\frac{D}{L} + S\right) + e^{-2h/L}\left(\frac{D}{L} \cdot S\right)} \right\} . \tag{23}$$

As an example, Figure 46 plots L_{eff} versus L for two values of S and for an epilayer of thickness h. Note that, for $L \gtrsim h$, the measured minority carrier diffusion length is strongly influenced by the thickness of the epitaxial layer.

Etch Pit Density

We measured the etch pit density in the bulk grown SSD GaP using the standard etch and reveal technique. We used the modified RC etch[29] to reveal the dislocations and a Normarski phase contrast microscope for examination. All of the studies were performed on $\langle \bar{1}\bar{1}\bar{1} \rangle$ GaP surfaces.

We observed three types of behavior. In the early growth runs in which the material was grown in carbon cruicibles, the SSD material had a rather high density of small-diameter, etched pits. Figure 47 shows the etched pits on a sample for SSD C-4. This sample, which is typical of these early runs, showed a density $\sim 2 \times 10^5 cm^{-2}$ of etched pits with a diameter $\sim 2 \mu m$. They have a D-like shape and are sometimes referred to as D pits.

In growth run SSD C-6, the seed was held in place by dimpling the growth crucible. The dimpling introduced strain into the boule and resulted in an EPD $\sim 2 \times 10^4 cm^{-2}$ in this material. Figure 48 is a photograph of a portion of a wafer from SSD C-6, which shows a density $\sim 2 \times 10^4 cm^{-2}$ of the D-like etch pits.

[29] T. Iizuka, J. Electrochem Soc., 118, 1190 (1971)

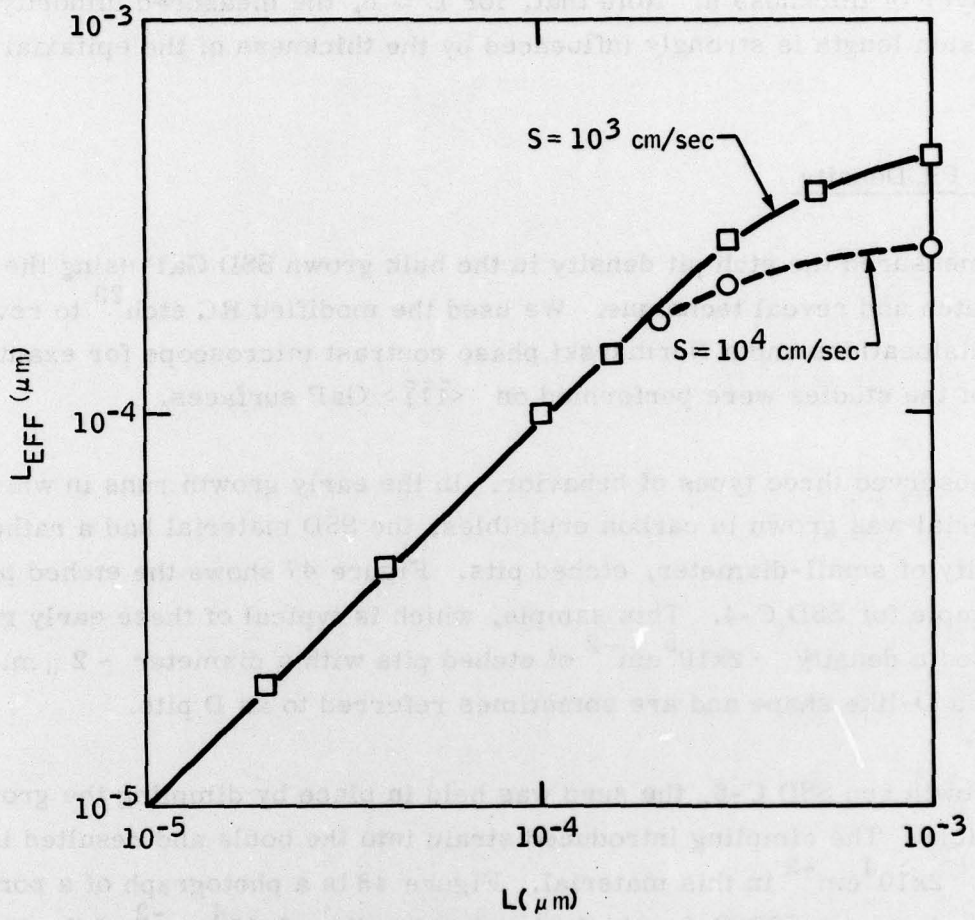

Figure 46. Calculated Effective Minority Carrier Diffusion Length for Surface Recombination Velocities of 10^3 and 10^4 cm/sec

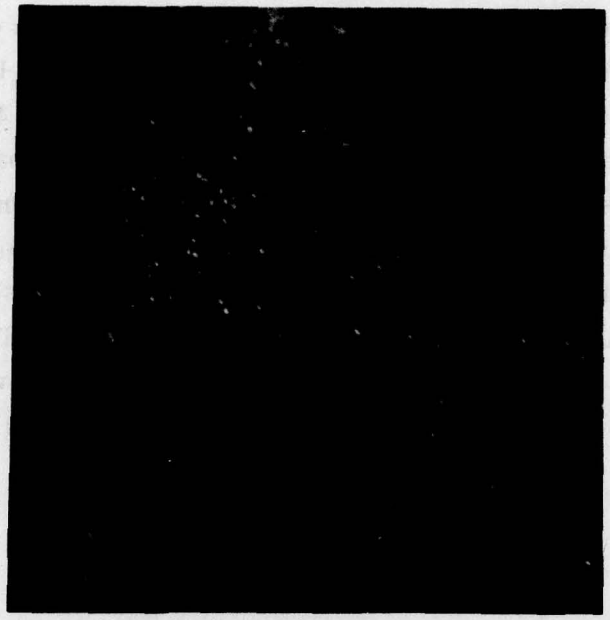

Figure 47. Etch Pit Density in SSD C-4 (400X)

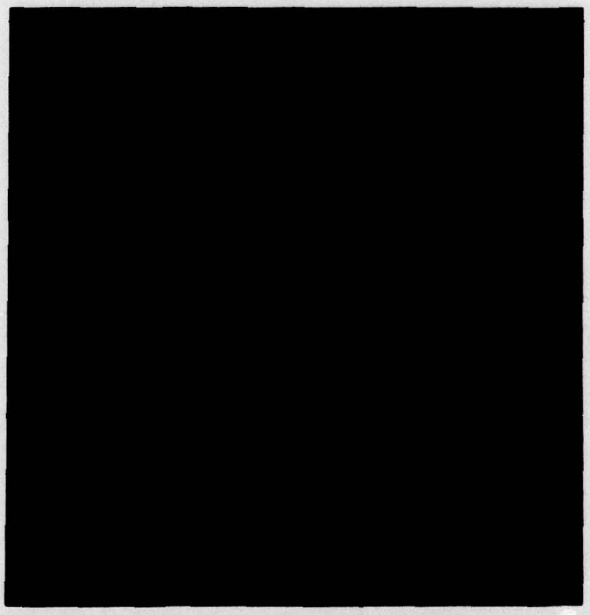

Figure 48. Etch Pit Density in SSD C-6 (160X)

Some of the material grown later in the program, which used a graphite-coated quartz insert to hold the seed in place, exhibited large regions (~ sq. mm.) which were free of the above two defects. Since the RC etch may not be a good revealing etch for orientation other than $\langle \bar{1}\bar{1}\bar{1} \rangle$, we checked the crystal orientation of this low dislocation density material by x-ray diffraction techniques. We found that the surface was within a few degrees of the < 111 > direction. Figure 49 shows such a low dislocation region from a wafer of SSD C-8 which had a single D-like etch pit. The density of D-like defects was $<10 cm^{-2}$ on this sample. Note there is a low density of surface defects on this sample. These results show that low-dislocation-density material can be grown by the SSD technique.

Figure 49. Etch Pit in SSD C-8 (400X)

SECTION IV
SUMMARY

This section summarizes the major accomplishments of the GaP crystal growth and evaluation work performed in this project. Two techniques were developed for the growth of high-quality GaP crystals. The liquid phase epitaxy technique using specially designed equipment and very carefully monitored growth parameters was developed for the growth of low-carrier concentration GaP layers ~2 to ~50 μm in thickness on GaP substrates. The bulk solution technique in the form of synthesis-solute-diffusion growth, used equipment and procedures developed under this program for growing high-quality ingots of GaP.

BULK-SOLUTION GROWTH

Bulk-solution growth experiments examined the effects of crucible and ampule design, furnace configuration, materials and procedures on crystal purity and size. Both synthesis-solute-diffusion (SSD) and random nucleated solution (RNS) growth experiments in a variety of forms were performed. These experiments, coupled with material evaluation measurements, resulted in major accomplishments:

- Refined process for growth of high quality bulk GaP achieved:
  - 1.3 cm dia. single crystal GaP boules
  - Carrier concentration ~2 x 10^{16} cm^{-3}
  - Low-etch pit density material
- Identified source-and-incorporation mode of carbon into SSD grown GaP by a series of controlled growth experiments

- Developed new growth apparatus for growing of single-crystal bulk GaP by SSD
- Identified a primary hole-scattering mechanism in carbon-doped SSD GaP.

LIQUID PHASE EPITAXY GROWTH

This work used a completely new LPE apparatus designed and built specifically for growing high-purity LPE GaP. The growth experiments performed with this apparatus iteratively improved the process by using the results of accompanying material evaluation. The following major accomplishments resulted:

- Achieved high purity GaP LPE layers
  - Eleven layers with electron concentration in 10^{15} to 10^{16} cm^{-3} range
- Developed a process for the reproducible growth of GaP epitaxy which controls and monitors:
  - H_2O contamination
  - O_2 contamination
  - Temperature profile
  - Substrate preparation
  - H_2 purity and flow
  - Cool-down rate
  - Growth system cleanliness

- Designed new slider system which enabled:
  - Identification of benefits of thin melt technique
  - Growth of 1 cm^2 area layers
  - Growth of layers with thickness variations of as little as three percent over a distance of up to 14 mm
- Identified and eliminated two major factors in LPE layer thickness nonuniformity:
  - Determined temperature profile which minimized melt convection currents
  - Converted slider to thin-melt configuration to minimize convection current cell size
- Verified silicon as the major residual donor in the GaP epitaxial layers
- Determined energy levels of deep states in LPE GaP by photocapacitance measurements.

REFERENCES

1. A.S. Jordan, R. Caruso, A.R. VonNeida and M.E. Weiner, J. Appl. Phys. 45, 3472 (1974).

2. P.D. Sudlow, A. Mottram, and A.R. Peaker, J. Mat. Sci. 7, 168 (1972).

3. R.J. Chicotka, Method of Polishing GaP, U.S. Patent 3,679,501.

4. E. Hajkova and R. Fremunt, Phys. Stat. Sol. (a) 10, K35 (1972).

5. L.R. Plauger, J. Electrochem Soc. 121, 455 (1974).

6. J.S. Blakemore, Semiconductor Statistics, Pergamon Press, New York (1962).

7. J.A.W. van der Does de Bye and R.C. Peters, Phillips Res. Repts., 24, 210 (1969).

8. M. Neuberger, III-V Semiconducting Compounds IFI/Plenum (1971).

9. H.C. Casey Jr., F. Ermanis and K.B. Wolfstirn, J. Appl. Phys. 40, 2945.

10. J. Bardeen and W. Shockley, Phys. Rev. 80, 72 (1950).

11. H. Ehrenreich, J. Phys. Chem. Solids, 8, 130 (1959).

12. Technical Report AFML-TR-77-37.

13. J.D. Wiley, M. DiDomenico, Jr. Phys. Rev. B., 2, 427 (1970).

14. F.J. Blatt, Solid State Phys., 4, 344 (1957).

15. C. Erginsoy, Phys. Rev. 79, 1013 (1950).

16. Montgomery, J. Appl. Phys. 39, 2002 (1968).

17. Pearson and Bardeen, Phys. Rev. 75, 865 (1949).

18. See reference 12.

19. M. Toyama, M. Naito, A. Kasami, Japanese Journal of Applied Physics, 8, 358 (1969).

20. S.M. Sze, Physics of Semiconductor Devices, John Wiley, New York (1969).

21. M. Cowley and H. Heffner, J. Appl. Phys. 35, 255 (1964).

22. D.V. Lang, J. Appl. Physics, 45, 3023 (1974).

23. A.M. White, P.J. Dean, and P. Porteous, J. Appl. Phys., 47, 3230 (1976).

24. P.J. Dean, G. Kaminsky, R.B. Zietterstrom, J. Appl. Phys., 33, 3551 (1967).

25. R.G. Schulze and P.E. Petersen, J. Appl. Physics, 45, 5307 (1974).

26. H.G. Grimmeiss and H. Scholz, Philips Res. Rpts., 20, 107 (1965).

27. C. van Opdorp, A.T. Vink, C. Werkhoven, Sixth International Symposium on GaAs and Related Compounds, Conf. Series No. 336, 317 (1977).

28. B.L. Smith and M. Abbott, Solid State Electronics, 15, 361 (1972).

29. T. Iizuka, J. Electrochem Soc., 118, 1190 (1971).

*U.S.Government Printing Office: 1979 — 657-002/71